DK and $\pi\pi$ Scattering from Lattice QCD

DISSERTATION ZUR ERLANGUNG DES DOKTORGRADES DER NATURWISSENSCHAFTEN
(DR. RER. NAT.) DER FAKULTÄT FÜR PHYSIK
DER UNIVERSITÄT REGENSBURG

vorgelegt von

Antonio Cox

aus

London, Vereinigtes Königreich

im Jahr 2018

Promotionsgesuch eingereicht am: 15.12.2017
Arbeit wurde angeleitet von: Prof. Dr. A. Schäfer

Prüfungsausschuss:	Vorsitzender:	Prof. Dr. F. Gießibl
	1. Gutachter:	Prof. Dr. A. Schäfer
	2. Gutachter:	Prof. Dr. V. Braun
	weiterer Prüfer:	PD Dr. J. D. Urbina

Termin Promotionskolloquium: 19.12.2018

Contents

Introduction

Lattice QCD simulations have the capability to render precious information about various non-perturbative aspects of QCD which would otherwise be unknown to us. Among these aspects, the properties of scattering of relativistic particles - namely phase shifts, scattering lengths, resonance couplings etc. - play a central role.

At first sight, lattice QCD may not seem a suitable framework to handle scattering. As the theory is defined on a finite discrete Euclidean space-time, it is not possible to introduce the notion of asymptotic states. Particles can never be isolated and will always feel the effect of each other due to the presence of the boundary. Consequently, a scattering formalism together with the features that result cannot be introduced. No scattering happens on the lattice.

Fortunately, the lack of a scattering formalism in Lattice QCD does not prevent us from accessing, from lattice simulations, the collision properties of particles of our real world. The outstanding relations introduced by Lüscher and subsequently generalised by others, determine a connection between the energies on the lattice and the scattering matrix of the infinite volume quantum field theory. If the systematics are kept under control, results can be compared to experiment.

The task of this work is to employ Lüscher's method for studying the elastic scattering in four different channels, DK, D^*K, $\pi\pi$ and $K\pi$, in the $J^P = 0^+$, 1^+, 1^- and 1^- sectors, respectively. In the first two channels the enigmatic $D_{s0}^*(2317)$ and $D_{s1}(2460)$ bound states are respectively present, while the last two couple to the ρ and K^* resonances.

The thesis is presented in an approximately self-contained fashion. Many of the formulae and features which are concretely applied in chapters (3) and (4) to the channels under consideration are defined and discussed in general in the supporting chapters (1) and (2). Specifically, relativistic scattering theory is the topic of chapter (1). Starting from basic principles, as Poincaré invariance, asymptotic completeness and analyticity of the S-matrix, the whole theory can be constructed in a general way. Concepts such as phase shifts and

resonances in the relativistic setting appear as a consequence and are also treated. In chapter (2) some general features of continuum QCD and lattice QCD are discussed. The way Lüscher's formalism connects lattice data to physical scattering information is presented in detail at the end of the chapter. The scattering parameters of the DK and D^*K system as well as the mass, the coupling and the decay constants of the $D_{s0}^*(2317)$ and $D_{s1}(2460)$ states are calculated and discussed in Chapter (3). Finally, in chapter (4), the results for the masses and widths of the ρ and K^* resonances and their coupling to the channels $\pi\pi$ and $K\pi$ are presented.

Chapter 1

Relativistic scattering

Since Lüscher has extended the window of applications of lattice simulations from isolated particles to scattering states, many of the notions inherent to scattering theory have become widely used in the lattice community. It is today possible to address on the lattice questions such as "what is the decay width of the ρ resonance?", or "what is the threshold behaviour of neutron-proton scattering and is this behaviour compatible with the existence of a bound state?". Due to the significant role played for the lattice, this chapter is dedicated to the theory of relativistic scattering and to some of its notions relevant for this work.

Relativistic scattering theory is based on general, non-perturbative and model independent principles which are shared by any reasonable relativistic quantum field theory. A rigorous treatment is not required here and the assumptions listed in the following by no means constitute a formal set of mathematical postulates[1]. With this clarification, we require that:

- The space of states is a separable Hilbert space $\mathcal{H}$ in which the laws of quantum mechanics apply.
- The Hamiltonian is such that the system behaves freely at asymptotic times $t \to \pm\infty$ and the space enjoys the property of asymptotic completeness.
- The Poincaré group is a symmetry of the theory, i.e., the Hilbert space carries a unitary representation $U(a, \Lambda)$ of the Poincaré group. The spectrum of the four-momentum operator P^μ spans the space and lies in the forward light cone, $P^2 \geq 0$ and $P^0 \geq 0$.
- There exists a unique state, the vacuum $|0\rangle$, which has unit norm and is invariant under Poincaré transformations, $U(a, \Lambda)|0\rangle = |0\rangle$, as well as a set of stable particles (m_i, s_i)

[1]Readers interested in a formal definition may refer to those applications of constructive quantum field theory where a rigorous axiomatic formulation is attempted.

which transform irreducibly from which, the whole Hilbert space can be constructed by tensor products.

- A field theoretical description on Minkowski spacetime can be given. In particular, observables commute for space-like distances (causality),

$$[O_1(x), O_2(y)] = 0, \qquad (x-y)^2 < 0.$$

The first two assumptions are at the base of a general scattering theory and are discussed in Sec. (1.1). The second two specialise to relativistic scattering and introduce the concept of relativistic particle states. These will be discussed in Sec. (1.2). The field description is actually not required in this chapter but was added for completeness. Instead, in Sec. (1.4), the additional assumption of analyticity of the S-matrix - in the sense that will be explained - will be added.

The topics covered in this chapter can be found in several textbooks, see e.g. Refs. [1–5].

1.1 The S-matrix

As quantum field theory is a particular case of a quantum mechanical theory, the same laws of quantum mechanics apply. In particular, a Hamiltonian operator is present in the Hilbert space $\mathcal{H}$ of the theory. The dimensionality of the latter is not finite, although the notion of separability is required, i.e. a countable orthonormal basis is present. Nevertheless, we will not be concerned with mathematical formalities and non-normalisable states will be extensively considered.

Concerning time evolution, we will work in the Heisenberg picture, where operators are time-dependent and state vectors are constant. The second condition above assumes that at asymptotic times $t \to \pm\infty$ the Hamiltonian of the quantum theory is such that the system behaves freely. In ordinary quantum mechanics, the existence of this freedom can be proved for potentials (in the coordinate representation) going to zero fast enough as the coordinate tends to infinity. In a quantum field theory, such a behaviour must be postulated. We are in the setting of a scattering experiment: at time $t \to -\infty$, long before the collision, a system of isolated and non-interacting particles are prepared and will undergo scattering at finite times. Similarly, long time after the collision takes place, the particles no longer interact and behave freely. At this stage, it is irrelevent whether the states have a particle interpretation and the content of this subsection can be applied in general.

Due to the freedom at asymptotic times, "in" states and "out" states can be naturally introduced: $|\phi, \text{in}\rangle$ and $|\psi, \text{out}\rangle$ are states which are non-interacting in the infinite past and infinite future, respectively. As the Heisenberg picture is being considered, please note that e.g. the state $|\phi, \text{in}\rangle$ describes the whole history of the system, also when the interaction is over, and the label "in" just reminds one that at $t \to -\infty$ the system was free.

The asymptotic completeness assumption states that in-states and out-states both span the physical Hilbert space. This means that it is possible to find in $\mathcal{H}$ two complete orthogonal bases[2]

$$\sum_a \frac{1}{f_a} |a, \text{in}\rangle \langle a, \text{in}| = \mathbb{1}, \qquad \langle a, \text{in}|a', \text{in}\rangle = \sqrt{f_a f_{a'}}\delta_{aa'}, \tag{1.1.1}$$

$$\sum_a \frac{1}{f_a} |a, \text{out}\rangle \langle a, \text{out}| = \mathbb{1}, \qquad \langle a, \text{out}|a', \text{out}\rangle = \sqrt{f_a f_{a'}}\delta_{aa'}. \tag{1.1.2}$$

The sums run over the eigenvalues of a complete set of commuting operators. $|a, \text{in}\rangle$ is a state such that a simultaneous measurement of such operators performed at $t \to -\infty$, when the system is free, will result in the set of values "a". At a later time, the measurament of the same observables will lead in general to a different result, as the eigenstates of the evolving operators corresponding to the eigenvalues a will have evolved. Similarly, the state $|a, \text{out}\rangle$ is labelled by the result of a measurement performed at $t \to \infty$.

The S-matrix, or the scattering matrix, is defined to be the operator S that maps the out-states onto the in-states,

$$|\psi, \text{in}\rangle \quad = \quad S\,|\psi, \text{out}\rangle\,. \tag{1.1.3}$$

It is unitary,

$$SS^\dagger = S^\dagger S = \mathbb{1}, \tag{1.1.4}$$

as it can be seen using Eqs. (1.1.1) and (1.1.2):

$$\mathbb{1} = \sum_a \frac{1}{f_a} |a, \text{in}\rangle \langle a, \text{in}| = S \sum_a \frac{1}{f_a} |a, \text{out}\rangle \langle a, \text{out}|\, S^\dagger = SS^\dagger. \tag{1.1.5}$$

The unitarity of the S-matrix will have profound consequences, as we will see.

Suppose that the physical state is $|a, \text{in}\rangle$. By the laws of quantum mechanics, the probability amplitude that a measurement at time $t \to \infty$ will result in "a'" is given by $(f_a f_{a'})^{-\frac{1}{2}}$

[2]The annoying normalisation factors $f_a = \langle a|a\rangle$ are shown to make contact to the relativistic normalisation that will be used.

times

$$\langle a', \text{out}|a, \text{in}\rangle = \langle a', \text{in}|S|a, \text{in}\rangle = \langle a', \text{out}|S|a, \text{out}\rangle = S_{a'a},$$

which are the matrix elements of the operator S in either basis. The unitarity of S is just a conservation of probability - the probability that at time $t \to \infty$ $|a, \text{in}\rangle$ will be found to be in any state is one:

$$\begin{aligned}\sum_{a'} \frac{1}{f_{a'} f_a} |S_{a'a}|^2 &= \sum_{a'} \frac{1}{f_{a'} f_a} |\langle a', \text{in}|S|a, \text{in}\rangle|^2 = \sum_{a'} \frac{1}{f_{a'} f_a} \langle a, \text{in}|S^\dagger|a', \text{in}\rangle \langle a', \text{in}|S|a, \text{in}\rangle \\ &= \frac{1}{f_a} \langle a, \text{in}|S^\dagger S|a, \text{in}\rangle = \frac{1}{f_a} \langle a, \text{in}|a, \text{in}\rangle = 1. \end{aligned} \tag{1.1.6}$$

If $S = \mathbb{1}$, no interaction takes place in the theory, or $|a, \text{out}\rangle = |a, \text{in}\rangle$ for any a. It is customary to separate the non-trivial part of S from the T-matrix term which is due to interaction:

$$S = 1 + iT, \qquad \frac{S_{a'a}}{\sqrt{f_{a'} f_a}} = \delta_{a'a} + i \frac{T_{a'a}}{\sqrt{f_{a'} f_a}}. \tag{1.1.7}$$

Unitarity $SS^\dagger = 1$ implies

$$\frac{1}{i}\left(T - T^\dagger\right) = TT^\dagger, \qquad \frac{1}{i}\left(T_{a'a} - T^*_{aa'}\right) = \sum_{a''} \frac{1}{f_{a''}} T_{a'a''} T^*_{aa''}. \tag{1.1.8}$$

The lhs is called the absorptive part and would be twice the imaginary part of $T_{a'a}$ if, for some reason, $T_{a'a} = T_{aa'}$. This happens for instance for elastic scattering of spinless particles or if time reversal is a symmetry of the theory. In this case,

$$2\text{Im}T_{a'a} = \sum_{a''} \frac{1}{f_{a''}} T_{a'a''} T^*_{aa''}. \tag{1.1.9}$$

In particular, taking $a = a'$,

$$2\text{Im}T_{aa} = \sum_{a''} \frac{1}{f_{a''}} |T_{aa''}|^2. \tag{1.1.10}$$

These formulas are different versions of what in the literature is known as the optical theorem.

1.1.1 Symmetries of the S-matrix

Suppose there is an observable X that commutes with the S-matrix, $[X, S] = 0$. Then clearly, if the initial state $|a, \text{in}\rangle$ is an eigenstate of X with eigenvalue x, $X|a, \text{in}\rangle = x|a, \text{in}\rangle$,

so will be $S\,|a,\mathrm{in}\rangle$:

$$X\left(S\,|a,\mathrm{in}\rangle\right) = SX\,|a,\mathrm{in}\rangle = x\left(S\,|a,\mathrm{in}\rangle\right). \tag{1.1.11}$$

Thus, final states $|a',\mathrm{out}\rangle$ should be looked for only in the subspace relative to the eigenspace x and the latter is referred to as a good quantum number. In terms of scattering of particles, the collision will not alter the result of the measurement of the observable X. From now on, the labels "in/out" will be dropped with the understanding that all considerations are valid for both cases.

Suppose now that there is a group G and a representation D acting on the Hilbert space such that $[D_g, S] = 0$ for all g in G. By Schur's lemma, the S-matrix is diagonal if sandwiched by elements of an irreducible representation of the group and does not depend on the particular elements of the representation space. To be specific, suppose we choose our basis as $a = (x, c_x, \mu)$, where x identifies the irreducible representation of G, c_x labels its vectors and μ are the remaining indices to completely identify the state. Then, the S-matrix simplifies to

$$\langle\, x'\, c'_x\, \mu'\,|S|\, x\, c_x\, \mu\,\rangle = S_{x'c'_x\mu',xc_x\mu} = \delta_{xx'}\delta_{c_xc'_x}S^x_{\mu'\mu}, \tag{1.1.12}$$

where the non trivial part $S^x_{\mu'\mu}$ is a function of the irreducible representation labelled by x. Thus, to exploit this symmetry, it is convenient to choose a basis for the Hilbert space according to irreducible representations of the symmetry group. If we had chosen another basis, labelled say by $b = (y, \mu)$, a change of basis could have been performed,

$$|b\rangle = |\, y\, \mu\,\rangle = \sum_{xc_x} g^y_{xc_x}\,|\, x\, c_x\, \mu\,\rangle \tag{1.1.13}$$

and the S-matrix element with respect to the original basis could have be expanded,

$$\begin{aligned}
\langle\, y'\, \mu'\,|S|\, y\, \mu\,\rangle &= \sum_{xx'}\sum_{c_xc'_x} g^{y'*}_{x'c'_x} g^y_{xc_x}\,\langle\, x'\, c'_x\, \mu'|S|\, x\, c_x\, \mu\rangle \\
&= \sum_{xx'}\sum_{c_xc'_x} g^{y'*}_{x'c'_x} g^y_{xc_x}\delta_{xx'}\delta_{c_xc'_x}S^x_{\mu'\mu} = \sum_x\left(\sum_{c_x} g^{y'*}_{xc_x} g^y_{xc_x}\right)S^x_{\mu'\mu} \\
&= \sum_x h^{y'y}_x S^x_{\mu'\mu}.
\end{aligned} \tag{1.1.14}$$

For fixed $\mu\mu'$, the S-matrix element $\langle\, y'\, \mu'\,|S|\, y\, \mu\,\rangle$ is a sum over irreducible components $S^x_{\mu'\mu}$. Partial wave decompositions, both in ordinary quantum mechanics and in quantum field theory, are typical examples of Eq. (1.1.14). In our context, the symmetry groups will include the Poincaré group as well as internal symmetries as isospin.

1.2 Particle states

Up to this point we have considered a quantum mechanical theory equipped with a unitary S-matrix operator in the Hilbert space. We now want to add the condition of relativistic invariance, i.e., we want to implement in the theory the well established fact that physics is the same in all inertial frames of reference. The transformation between frames is enforced by the Poincaré action $x \to \Lambda x + a$ on Minkowski spacetime, leaving the distance $ds^2 = \eta_{\mu\nu} dx^\mu dx^\nu$ invariant.

In the quantum mechanical setting, this symmetry is represented by requiring that the action of the Poincare transformation on the Hilbert space $\mathcal{H}$ via an operator $U(g) \equiv U(a, \Lambda)$ is such that measurable quantities are unchanged,

$$|\langle \psi' | \phi' \rangle| = \left| \langle \psi | U^\dagger(g) U(g) | \phi \rangle \right| = |\langle \psi | \phi \rangle| . \tag{1.2.1}$$

This means that, for any g, $U^\dagger(g) U(g) = e^{i\phi} \mathbb{1}$ for some phase ϕ. Moreover, any subsequent transformation should imply $U(g'g) = e^{i\phi} U(g') U(g)$. The phase factors can be set to ± 1 without loss of generality, so that the operators are either unitary or anti-unitary and representations may be double-valued. Quantum-mechanically, one considers the universal cover of the Poincaré group so that operators are unitary and representations are single-valued.

Then, the Hilbert space $\mathcal{H}$ must carry a (reducible) unitary representation

$$U(a, \Lambda) = e^{i a_\mu P^\mu} e^{-\frac{i}{2} \omega_{\mu\nu} M^{\mu\nu}}, \tag{1.2.2}$$

where P^μ and $M^{\mu\nu}$ are meant to be operators on $\mathcal{H}$ satisfying the Poincaré algebra, Eqs. (A.1.15) and (A.1.21). The Hamiltonian operator H is identified with P^0, $\boldsymbol{P}$ is the three-momentum operator and the $M^{\mu\nu}$ includes the angular momentum $\boldsymbol{J}$ operator. Let us now look at the states in the Hilbert space.

1.2.1 Vacuum and one-particle states

First of all, we assume the existence of a unique vacuum state $|0\rangle \equiv |0, \text{in}\rangle = |0, \text{out}\rangle$ with unit norm which is associated to the trivial irreducible representation and which is invariant under $U(a, \Lambda)$, $U(a, \Lambda) |0\rangle = |0\rangle$. This implies that $|0\rangle$ is annihilated by the generators, $P^\mu |0\rangle = 0$ and $M^{\mu\nu} |0\rangle = 0$ and hence has zero energy.

Secondly, we require that there are subspaces of $\mathcal{H}$, say N of them, that transform

irreducibly under the Poincaré group. More precisely, for each $i = 1, ..., N$ there is a positive[3] number m_i and a non-negative integer or semi-integer s_i which identify the smallest subspace $\mathcal{H}_{(m_i,s_i)} \subset \mathcal{H}$ made of all those states $|\, m_i\, s_i\, ;\, \psi \,\rangle$ on which the Casimir operators P^2 and W^2, built from the algebra in Eq. (1.2.2), assume the same value m_i^2 and $-m_i^2 s_i\,(s_i+1)$, respectively. A basis $|\, m_i\, s_i\, ;\, \boldsymbol{p}_i\, \sigma_i \,\rangle$ of $\mathcal{H}_{(m_i,s_i)}$, with scalar product given by (A.1.38), is labelled by the eigenvalues $\boldsymbol{p}_i \in \mathbb{R}^3$ and $\sigma_i = -s, ..., s$ of respectively $\boldsymbol{P}$ and Σ, where Σ is some operator constructed from the algebra and commuting with P^2, W^2 and $\boldsymbol{P}$. As discussed in App. (A.1.4), $\mathcal{H}_{(m_i,s_i)}$ is an irreducible space of the Poincaré group and the action of the general element Eq. (1.2.2) on $\mathcal{H}_{(m_i,s_i)}$ is given by Eq. (A.1.36).

We see that the concept of relativistic particle emerges automatically once we include the Poincaré group in our quantum mechanical theory. Indeed to the couple (m_i, s_i) we associate a particle with mass m_i and spin s_i, which are identified simply by the constant eigenvalues of P^2 and W^2 respectively when acting on $\mathcal{H}_{(m_i,s_i)}$. The degrees of freedom of the particle are instead provided by the operators $\boldsymbol{P}$, $P^0 = H$ (redundant) and Σ, whose eigenvalues on $\mathcal{H}_{(m_i,s_i)}$ identify respectively the three-momentum $\boldsymbol{p}_i$, the energy $E_i = \sqrt{m_i^2 + |\boldsymbol{p}_i|^2}$ and the spin degeneracy σ_i of the particle. Σ can be chosen such that it reduces to J_3 in the centre of mass frame (the standard or canonical basis), the component of the angular momentum along the z-axis, leading to the usual non-relativistic interpretation of spin[4]. Another common choice is to take $\Sigma = \frac{\boldsymbol{J}\cdot\boldsymbol{P}}{|\boldsymbol{P}|}$, so that its eigenvalue σ_i represents the helicity of the particle[5] (the helicity basis).

Due to the particle interpretation, the states $|\, m_i\, s_i\, ;\, \psi \,\rangle$ considered are referred to as one-particle states. Just as for the vacuum, the *in* and *out* states for one-particle states coincide: if only one particle is present before the scattering, the same particle will emerge after, with unit probability.

1.2.2 n-particle states

Starting from the N one-particle states (m_i, s_i) in the theory we can identify n-particle systems by tensor products. The label (m_i, s_i) generalises to $\alpha = (m_{i_1} s_{i_1}, ..., m_{i_n} s_{i_n})$ where

[3]Massless representations are not considered here.

[4]The knowledge of Σ for an arbitrary frame is not important. For a relativistic particle it is enough to define the spin component in an arbitrary frame by its value in the centre of mass frame, where the Pauli-Lyubanski three-vector satisfies the spin algebra and $W_3 = mJ_3$.

[5]Usually one considers helicity only if the particle is massless, for which the representation space structure is different than the one discussed. Nevertheless, it can be defined for massive particles also. In this case, helicity is frame-dependent although some formulae are particularly simple if this basis is considered.

each index can be any in $\{1, 2, ..., N\}$[6]. We assume that the tensor product space, $\mathcal{H}_\alpha$, is still in the Hilbert space $\mathcal{H}$ of the theory. When acting on this space, $U(a, \Lambda)$ in Eq. (1.2.2) is a tensor product representation operator and the generators are the (Kronecker) sums of the one-particle correspondents, $M^{\mu\nu} = M^{\mu\nu}_{i_1} + ... + M^{\mu\nu}_{i_n}$ and $P^\mu = P^\mu_{i_1} + ... + P^\mu_{i_n}$, the latter being the total four-momentum of the system. The values in $\alpha = (m_{i_1} s_{i_1}, ..., m_{i_n} s_{i_n})$ are the eigenvalues of $P^2_{i_1}, W^2_{i_1}, ..., P^2_{i_n}, W^2_{i_n}$ (assumed fixed for now) and a basis in $\mathcal{H}_\alpha$ can be specified by the eigenvalues of $\boldsymbol{P}_{i_1}, ..., \boldsymbol{P}_{i_n}, \Sigma_{i_1} ... \Sigma_{i_n}$,

$$|a\rangle = |\alpha\,;\, \boldsymbol{p}_{i_1} ... \boldsymbol{p}_{i_n}\, \sigma_{i_1} ... \sigma_{i_n}\rangle\,. \tag{1.2.3}$$

The quantities referring to each particle,

$$\begin{aligned} p_{i_1} &= \left(E_{i_1}, \boldsymbol{p}_{i_1}\right), \qquad m^2_{i_1} = E^2_{i_1} - |\boldsymbol{p}_{i_1}|^2, \\ &\vdots \\ p_{i_n} &= \left(E_{i_n}, \boldsymbol{p}_{i_n}\right), \qquad m^2_{i_n} = E^2_{i_n} - |\boldsymbol{p}_{i_n}|^2, \end{aligned} \tag{1.2.4}$$

can be expressed in terms of the quantities of the whole system,

$$p = p_{i_1} + ... + p_{i_n} \quad \text{or} \quad E = E_{i_1} + ... + E_{i_n},\ \boldsymbol{p} = \boldsymbol{p}_{i_1} + ... + \boldsymbol{p}_{i_n}, \tag{1.2.5}$$

with

$$p = (E, \boldsymbol{p})\,, \qquad s \equiv m^2 = E^2 - |\boldsymbol{p}|^2. \tag{1.2.6}$$

The Mandelstam variable s is the invariant mass squared and is the energy squared of the n-particle system in the centre of mass frame. It is an eigenvalue of the operator $P^2 = (P_{i_1} + ... + P_{i_n})^2$ which, unlike the four-momenta, is not additive. Then, the n-particle states can be alternatively labelled in terms of the total four-momenta or in terms of $\sqrt{s}$ and $\boldsymbol{p}$:

$$|a\rangle = |\alpha\,;\, \sqrt{s}\,\boldsymbol{p}\,\rho_\alpha\rangle \quad \text{or} \quad |a\rangle = |\alpha\,;\, p\,\rho_\alpha\rangle\,. \tag{1.2.7}$$

ρ includes all the relative momenta variables ($3n-4$ variables, for $n > 1$) as well as the spin component indices $\sigma_1 ... \sigma_n$.

The n-particle Hilbert space $\mathcal{H}_\alpha$ is not an irreducible space for the Poincaré group. In other words, the Casimir operators P^2 and W^2 do not assume a unique value in this space. For instance, the eigenvalues s of P^2 can take any value $s \geq s_{\text{th}} = (m_{i_1} + ... + m_{i_n})^2$, where

[6]The same particle may appear more than once. In this case a symmetrisation or anti-symmetrisation in the relevant indices is understood, according to the spin-statistics theorem.

$s_{\rm th}$ is referred to as the threshold of the n-particle system. The relabelling of the states Eq. (1.2.3) in terms of Eq. (1.2.7) already identifies, fixing $\sqrt{s}$, an invariant subspace[7], but an exhaustive decomposition requires a change of basis in terms of the eigenvalues $-sj\,(j+1)$ of the other Casimir operator $W^2 = (W_{i_1} + ... + W_{i_n})^2$. The transformed basis has the form

$$|a\rangle = |\alpha\,;\,\sqrt{s}\,j\,\boldsymbol{p}\,\sigma_j\,\mu_\alpha\,\rangle\,, \tag{1.2.8}$$

on which Eq. (1.2.2) acts just as Eq. (A.1.36),

$$U\,(a,\Lambda)\,|\alpha\,;\,\sqrt{s}\,j\,\boldsymbol{p}\,\sigma_j\,\mu_\alpha\,\rangle \sim |\alpha\,;\,\sqrt{s}\,j\,\boldsymbol{p}'\,\sigma'_j\,\mu_\alpha\,\rangle \tag{1.2.9}$$

without leaving the space $\mathcal{H}_{\left(\sqrt{s},j\right)}$. The symbol j labels the total angular momentum of the system, σ_j is the eigenvalue of Σ[8] and μ_α identifies the copy of the decomposition of $\mathcal{H}_\alpha$ in terms of $\mathcal{H}_{\left(\sqrt{s},j\right)}$[9]. For a one-particle system, $\alpha = (m_i, s_i)$, $\sqrt{s}$ and j assume just one value, m_i and s_i respectively, and μ_α is empty.

Two-particle states As a practical example, we consider a two particle system and denote $\alpha = (m_{i_1}s_{i_1}, m_{i_2}s_{i_2}) = (m_A s_A, m_B s_B)$. The six variables $\boldsymbol{p}_A$ and $\boldsymbol{p}_B$ in Eqs. (1.2.3) and (1.2.4) can be traded off by the energy in the centre of mass frame $\sqrt{s}$ and by the direction of the relative momentum $\boldsymbol{k} = \frac{1}{2}\,(\boldsymbol{p}_B - \boldsymbol{p}_A)$, eigenvalue of $\frac{1}{2}\,(\boldsymbol{P}_B - \boldsymbol{P}_A)$. Then, Eq. (1.2.7) becomes ($\rho = \left(\hat{\boldsymbol{k}}, \sigma_A, \sigma_B\right)$)

$$|a\rangle = |\,\alpha\,;\,\sqrt{s}\,\boldsymbol{p}\,\hat{\boldsymbol{k}}\,\sigma_A\,\sigma_B\,\rangle \quad \text{or} \quad |a\rangle = |\alpha\,;\,p\,\hat{\boldsymbol{k}}\,\sigma_A\,\sigma_B\,\rangle \tag{1.2.10}$$

Let us explicitly look at the ranges of the variables in the first equation of (1.2.10). The energy in the centre of mass, $\sqrt{s}$, starts at the threshold of the two-particle system, $\sqrt{s} \geq \sqrt{s_{\rm th}} = m_A + m_B$. It can be parametrised in terms of one parameter $k = |\boldsymbol{k}| \geq 0$,

$$\sqrt{s} = \sqrt{m_A^2 + k^2} + \sqrt{m_B^2 + k^2}, \tag{1.2.11}$$

[7] $|\alpha\,;\,\sqrt{s}\,\boldsymbol{p}\,\rho_\alpha\,\rangle \to |\alpha\,;\,\sqrt{s}\,\boldsymbol{p}'\,\rho'_\alpha\,\rangle$ under $U\,(a,\Lambda)$.

[8] If we choose to use the standard basis, then, in the centre of mass frame, Σ reduces to the z-axis component J_3 of the total angular momentum J.

[9] We can write

$$\mathcal{H}_\alpha = \bigoplus_{\sqrt{s},j.} c_{\sqrt{s},j}\mathcal{H}_{\left(\sqrt{s},j\right)}$$

where the direct integral and sum run over $\sqrt{s} \geq \sqrt{s_{\rm th}}$ and $j = 0, \frac{1}{2}, 1, ...$.

and, the energy in any frame can be obtained from (1.2.11) by $E^2 = s + |\boldsymbol{p}|^2$. The total three momentum $\boldsymbol{p}$ varies in $\mathbb{R}^3$, $\hat{\boldsymbol{k}}$ varies in all directions and $\sigma_i = -s_i, ..., s_i$. The inverse relation of Eq. (1.2.11), which will be useful later, is

$$k^2 = \frac{\left(s - (m_A + m_B)^2\right)\left(s - (m_A - m_B)^2\right)}{4s}. \tag{1.2.12}$$

The decomposition into irreducible spaces is a partial-wave decomposition and affects the variables $\rho = \left(\hat{\boldsymbol{k}}, \sigma_A, \sigma_B\right)$ so that $\sqrt{s}$ and $\boldsymbol{p}$ can be kept fixed. Recall that according to the basis chosen (helicity basis or canonical basis), σ_i may refer either to the helicity of the particle or to the spin component in the z direction. In the first case the expansion is simple and has the form

$$|\,\alpha\,;\,\sqrt{s}\,\boldsymbol{p}\,\hat{\boldsymbol{k}}\,,\,\sigma_A\,\sigma_B\,\rangle = \sum_j \sum_{\sigma_j=-j}^{j} \sqrt{\frac{2j+1}{4\pi}} D^{\sigma_A\sigma_B}\left(\hat{\boldsymbol{k}}; j\,\sigma_j\right) |\,\alpha\,;\,\sqrt{s}\,j\,,\,\boldsymbol{p}\,\sigma_j\,,\,\sigma_A\,\sigma_B\,\rangle\,. \tag{1.2.13}$$

The degeneracy label μ in Eq. (1.2.8) represents the helicities of the two particles themselves, $\mu = (\sigma_A, \sigma_B)$. Alternatively, the canonical basis is the most common in non-relativistic quantum mechanics, although the expansion is much more complicated as it involves products of several Clebsch-Gordan coefficients. In the l-s coupling scheme, one first adds the spins of the two particles $(\sigma_A, \sigma_B) \to (s, \sigma_s)$, then expands $\hat{\boldsymbol{k}}$ in partial waves for definite orbital angular momenta, $\hat{\boldsymbol{k}} \to (l, \sigma_l)$ and finally adds s and l to obtain j, $(s, \sigma_s, l, \sigma_l) \to (s, l, j, \sigma_j)$. The basis obtained, $|\,\alpha\,;\,\sqrt{s}\,j\,\boldsymbol{p}\,\sigma_j\,l\,s\,\rangle$, has well defined total spin and orbital angular momentum and the degeneracy label in (1.2.8) is $\mu = (l, s)$.

The formulas simplify greatly for spinless particles, where $\alpha = (m_A 0, m_B 0)$. In this case, the total angular momentum coincides with the orbital angular momentum and the partial wave decomposition reads simply

$$|\,\alpha\,;\,\sqrt{s}\,\boldsymbol{p}\,\hat{\boldsymbol{k}}\,\rangle = \sum_{j=0}^{\infty} (2j+1)\, P_j\left(\hat{\boldsymbol{k}} \cdot \hat{\boldsymbol{u}}_z\right) |\,\alpha\,;\,\sqrt{s}\,j\,,\,\boldsymbol{p}\,\rangle\,, \tag{1.2.14}$$

where P_j are the Legendre polynomials.

1.2.3 The full space

We claim now that the whole Hilbert space can be spanned by an arbitrary number of tensor products of one-particle states, i.e., the N spaces $\mathcal{H}_{(m_i,s_i)}$ serve as a building blocks for the

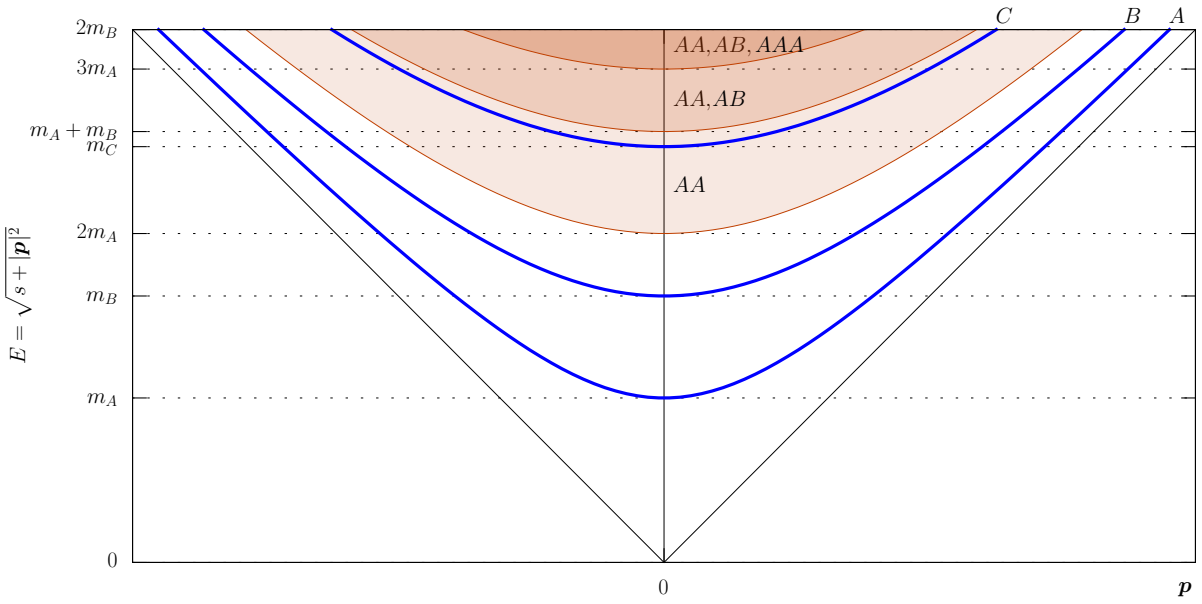

Figure 1.2.1: The low-energy spectrum of a typical theory. The horizontal axis represents the three-dimensional total momentum $\boldsymbol{p}$. One particle systems are represented in blue.

full space. In other words, in the Hilbert space there is nothing else than particles or combinations of them (or the absence of them). Hence we vary the label $\alpha = (m_{i_1} s_{i_1}, ..., m_{i_n} s_{i_n})$ and obtain, in addition to the vacuum and to the one-particle states $1, 2, ..., N$, the so called scattering states, i.e. two-particle states $11, 12, ..., 1N, 22, ..., NN$, three-particle states $111, 112, ..., NNN$ and so on, a Fock space.

In Fig. (1.2.1) we can visualise the spectrum in terms of $(\boldsymbol{p}, E(\boldsymbol{p}))$ of a a typical arbitrary theory which exhibits, within the range shown, three particles with positive masses m_A m_B and m_C. A central vertical line $(\mathbf{0}, E(\mathbf{0}) \equiv \sqrt{s})$ represents the energy in the centre of mass. Let's follow this line from bottom to top, as all other points in the the corresponding hyperboloid are obtained by Eq. (1.2.6). The origin $(0, \mathbf{0})$ represents the vacuum and has zero energy and momentum. The next energy value, which is followed by a mass gap, is obtained at $(\mathbf{0}, m_A)$ from which all A-particle states can be obtained by Lorentz transformations. Particle A is the lightest in the theory and all other one-particle states appear at higher energies. The point $(\mathbf{0}, 2m_A)$ represents the threshold of the AA-particle production, i.e. the starting point of a continuous spectrum of hyperboloids each identified by Eq. (1.2.11) as k increases from zero to infinity. A new threshold AB appears at $(\mathbf{0}, m_A + m_B)$ from which, a new set of continuous states superimposes on that of AA. At even higher energies we have three particle production AAA, the states of the BB system and so on.

Spacetime symmetries are not the only ones we see in our world. The theory can be adapted to include internal symmetries, as isospin, charge conjugation etc., collectively implemented by some group G, by enlarging the Hilbert space to be a representation of the direct product group $\mathcal{P} \times G$. Poincaré and internal symmetries commute so that each can be handled separately. Additional labels will be added to $|\, m_i\, s_i\, ,\, \boldsymbol{p}_i\, \sigma_i \,\rangle$ to identify irreducible states of $\mathcal{P} \times G$ and consequently, additional labels will be added to the tensor product Eq. (1.2.3) and will be included in ρ and μ in Eqs. (1.2.7) and (1.2.8).

The particle states discussed in this section determine a relativistic particle realisation of the abstract *in* and *out* states described in Sec. (1.1). We remind the reader that, with the exception of the vacuum and of one-particle states, the specification *in* and *out* is always understood for the particle states - Eqs. (1.2.3),(1.2.7) and (1.2.8) - in order to specify if their labels refer to the infinite past or to the infinite future. Unlike the four-momentum of each particle, the total four-momentum, as well as the total angular momentum, commutes with the Hamiltonian and does not evolve with time. The labels $p\ j$ and σ_j then refer to the eigenvalue of the corresponding operator at any time. The bases Eqs. (1.2.3), (1.2.7) and (1.2.8) are Heisenberg asymptotic states, free[10] only at asymptotic times, eigenstates of the Hamiltonian and span the whole (interacting) Hilbert space. In terms of states Eq. (1.2.7), the completeness relation Eqs. (1.1.1) and (1.1.2) reads, for either *in* or *out* states,

$$\mathbb{1} = \sum_a \frac{1}{f_a} \,|a\rangle\, \langle a| = \sum_\alpha \int \frac{d^4p}{(2\pi)^4} d\Phi_\alpha \,|\, \alpha\,;\, p\,\rho_\alpha\rangle\, \langle\, \alpha\,;\, p\,\rho_\alpha \,|\,. \tag{1.2.15}$$

The sum is over all sets of particles α, over all total four-momenta p and over the whole phase space $d\Phi_\alpha$. For economy of notation, also the sum over all spin components and internal symmetry indices are understood in $\int d\Phi_\alpha$. The scalar product in $\mathcal{H}$ is

$$\langle\, \alpha'\,;\, p'\,\rho'_{\alpha'} \,|\, \alpha\,;\, p\,\rho_\alpha\,\rangle = \sqrt{\mathcal{N}_\alpha \mathcal{N}_{\alpha'}}\, \delta_{\alpha\alpha'}\, (2\pi)^4\, \delta^{(4)}\,(p - p')\, \delta_{\rho'_{\alpha'}\rho_\alpha}, \tag{1.2.16}$$

where the normalisation $\mathcal{N}$ is a phase space factor that must be compatible with the denominator of (1.2.15) once $d\Phi$, for a given α, is expressed in terms of the variable ρ, symbolically $d\Phi = \frac{d\Phi}{d\rho} d\rho = \frac{1}{\mathcal{N}} d\rho$.

The notion of asymptotic completeness would fail in the presence of bound states: the interaction survives in the infinite future when two particles form a bound state. Asymptotic completeness can be safely retained by simply including all possible bound states in the

[10] The energies in the tensor products are additive and do not contain an interaction term.

spectrum of the stable one-particle states. We do not question, in this context, whether a stable particle is formed by other particles or not. For instance, in Fig. (1.2.1), particle C may be referred to as a bound state of A and B, but the system, as a whole, is free at asymptotic times. For QCD, the one-particle spectrum includes the pions, protons, the nucleus of the carbon atom, etc. On the contrary, resonances are unstable and do not appear in this spectrum but, as we shall see, have a different origin.

Fields The construction outlined in this section is particle-oriented and does not require the existence of field operators. Indeed, apart from these few lines, no mention of them will be made in this chapter. On the other hand, it is hard to imagine a quantum *field* theory without fields. If we were to build a Lagrangian (which may be an effective Lagrangian) in terms of some fields defined on Minkowski spacetime and which is capable to represent the physical spectrum, then the quantities that connect the field and particle description are given by the overlaps of general operators $\mathcal{O}(x)$, built from the fields of the Lagrangian, and the particle states. Examples of these which involve one-particle states are the overlaps of the form $\langle 0|\mathcal{O}(x)\,|\,m\,s\,;\,\boldsymbol{p}\,\sigma\,\rangle$ or more general matrix elements $\langle\, m\,s\,;\,\boldsymbol{p}'\,\sigma'\,|\mathcal{O}(x)\,|\,m\,s\,;\,\boldsymbol{p}\,\sigma\,\rangle$ which identify decay constants and form factors, respectively. There does not need to be an operator associated to each one-particle state or vice versa, all that matters are the non-zero overlaps. The operators $\mathcal{O}(x)$ can be combined in time-ordered correlation functions and the S-matrix elements, described in detail in the following sections, are obtained from these via the LSZ reduction formula.

1.3 Relativistic scattering

1.3.1 Poincaré invariance of the S-matrix

Except for the vacuum and for one-particle states, the connection between the *in* and *out* variants of the particle states is absolutely non trivial and the knowledge of this connection is exactly the aim of scattering theory. The number of independent S-matrix elements can be reduced by the fact that the S matrix commutes with $U(a,\Lambda)$, or equivalently, the S-matrix is invariant under a Poincaré transformation,

$$[S, U(a,\Lambda)] = 0, \qquad U(a,\Lambda)\, S U^{-1}(a,\Lambda) = S. \tag{1.3.1}$$

This implies that, for each generator:

$$[S, P^\mu] = 0, \qquad [S, M^{\mu\nu}] = 0. \tag{1.3.2}$$

Therefore, based on our considerations in Sec. (1.1), the S or T matrix elements are diagonal with respect to the total four-momentum and the total angular momentum. Moreover, they are independent of $\boldsymbol{p}$ and σ_j. In the three bases Eqs. (1.2.3), (1.2.7) and (1.2.8) we can write

$$\langle \alpha' \,;\, \boldsymbol{p}'_{i_1} ... \boldsymbol{p}'_{i_n}\, \sigma'_{i_1} ... \sigma'_{i_n} \,|\, T \,|\, \alpha \,;\, \boldsymbol{p}_{i_1} ... \boldsymbol{p}_{i_m}\, \sigma_{i_1} ... \sigma_{i_m} \rangle = (2\pi)^4\, \delta^4 (p' - p)\, T\, (\alpha' \leftarrow \alpha)\,, \tag{1.3.3}$$

$$\langle \alpha' \,;\, p'\, \rho' \,|\, T \,|\alpha \,;\, p\, \rho\rangle = (2\pi)^4\, \delta^4 (p - p')\, T^{[\alpha'\alpha]}_{\rho'\rho}\, (s)\,, \tag{1.3.4}$$

$$\langle \alpha' \,;\, p'\, j'\, \sigma'_{j'}\, \mu' \,|T|\alpha \,;\, p\, j\, \sigma_j\, \mu \rangle = (2\pi)^4\, \delta^4 (p - p')\, \delta_{jj'} \delta_{\sigma'_{j'}\sigma_j} T^{[\alpha'\alpha]\; j}_{\mu'\mu}\, (s)\,, \tag{1.3.5}$$

where $s = p^2$. The indices $[\alpha'\alpha]$ identify the channel in which the T-matrix elements are taken and will be dropped only when no confusion can arise. The conservation of the total angular momentum is exploited in the last relation which uses the basis Eq. (1.2.8).

It was previously mentioned that indices of internal symmetries were included in ρ and μ. Namely, say that the vectors at the lhs of Eq. (1.3.5) have well defined total isospin I, $\mu = (I, c_I, \overline{\mu})$ and $\mu' = (I', c'_I, \overline{\mu}')$ where c_I labels the particular vector in the I subspace and $\bar{\mu}$ all remaining indices. Then, if isospin is a symmetry of the theory, the Kronecker deltas $\delta_{II'}\delta_{c_I c'_I}$ can be extracted from the T-matrix element at the rhs,

$$T^{[\alpha'\alpha]\; j}_{\mu'\mu}\, (s) = \delta_{II'} \delta_{c_I c'_I} T^{[\alpha'\alpha]\; jI}_{\overline{\mu}'\overline{\mu}}\, (s)\,, \tag{1.3.6}$$

resulting in a T-matrix independent of c_I and with an explicit label I.

1.3.2 Two particle scattering

Two-particle states were explicitly discussed in Sec. (1.2.2) and we focus now on the scattering of these, i.e., we focus on the particular case of Sec. (1.3.1) where $AB \to CD$. The masses and the spins of the i-th particle are denoted by (m_i, s_i) and, in some frame of reference, the four-momenta are

$$p_i = (E_i, \boldsymbol{p}_i) \quad \text{with} \quad p_i^2 = m_i^2 \;\Rightarrow\; E_i^2 = m_i^2 + |\boldsymbol{p}_i|^2, \qquad i = A, B, C, D. \tag{1.3.7}$$

The process is described by the T-matrix element Eq. (1.3.3) with $\alpha = (m_A s_A, m_B s_B)$ and $\alpha' = (m_C s_C, m_D s_D)$. Apart from the spin variables, there are sixteen degrees of freedom for the four-particle system, $p_i = (E_i, \boldsymbol{p})$. Four are constrained by the masses which are fixed and an additional restriction comes from the four-momentum conservation:

$$p_A + p_B = p_C + p_D \quad \Longleftrightarrow \quad \begin{cases} E_A + E_B = E_C + E_D \\ \boldsymbol{p}_A + \boldsymbol{p}_B = \boldsymbol{p}_C + \boldsymbol{p}_D \end{cases}$$

Finally, Lorentz invariance adds six further restrictions, so that a $2 \to 2$ scattering can be described by just two variables. Hence, multiple kinematic situations in terms of p_i lead to the same value for the T matrix and only two variables have to be considered. We can choose these variables to be Lorentz invariant, so that the scattering formulae are the same in any frame. In particular, any two of the following Mandelstam variables is a possible choice

$$s = (p_A + p_B)^2 \equiv (p_C + p_D)^2 , \tag{1.3.8}$$

$$t = (p_A - p_C)^2 \equiv (p_B - p_D)^2 , \tag{1.3.9}$$

$$u = (p_A - p_D)^2 \equiv (p_B - p_C)^2 , \tag{1.3.10}$$

as their sum is fixed by

$$s + t + u = m_A^2 + m_B^2 + m_C^2 + m_D^2. \tag{1.3.11}$$

The variable s, already introduced in Sec. (1.2.2), is the square of the centre-of-mass energy and t is the momentum transfer squared. Then, Eq. (1.3.3) can be written as

$$\langle\, CD\,;\, \boldsymbol{p}_C\, \boldsymbol{p}_D\,,\, \sigma_C\, \sigma_D\, |T|\, AB\,;\, \boldsymbol{p}_A\, \boldsymbol{p}_B\,,\, \sigma_A\, \sigma_B\,\rangle = (2\pi)^4\, \delta^{(4)}\,(p_A + p_B - p_C - p_D)\, T_{\sigma_C \sigma_D, \sigma_A \sigma_B}\,(s,t)\,. \tag{1.3.12}$$

We have a set of $(2s_A + 1)\,(2s_B + 1) \times (2s_C + 1)\,(2s_D + 1)$ functions. Further symmetries, as parity or time reversal may reduce this number. The physical domain of definition of $T_{\sigma_C \sigma_D, \sigma_A \sigma_B}\,(s,t)$ depends on the masses of the particles. It is clear that

$$s \geq s_{th} = \max\left\{(m_A + m_B)^2\,, (m_C + m_D)^2\right\}, \tag{1.3.13}$$

where s_{th} is the threshold for the scattering to occur. The condition on t is more complicated and for general masses it can be found in Ref. [6].

An alternative choice of variables is the absolute value of the relative momentum of the

particles and the scattering angle. These quantities depend on the frame of reference and hence we choose one, the CM frame. Here, relations Eq. (1.3.7) are simplified and the relative momenta become $\boldsymbol{p}_A = -\boldsymbol{p}_B \equiv \boldsymbol{k}$ and $\boldsymbol{p}_C = -\boldsymbol{p}_D \equiv \boldsymbol{k}'$. We denote $k = |\boldsymbol{k}|$ and $k' = |\boldsymbol{k}'|$ (not to be confused with four-vectors). The Lorentz invariant Mandelstam variables can be expressed in terms of these CM quantities via

$$\sqrt{s} = \sqrt{m_A^2 + k^2} + \sqrt{m_B^2 + k^2} = \sqrt{m_C^2 + k'^2} + \sqrt{m_D^2 + k'^2}, \tag{1.3.14}$$

$$t = \frac{\left(m_A^2 - m_C^2 + m_B^2 - m_D^2\right)^2}{4s} - \left(k^2 + k'^2\right) + 2kk'\cos\theta. \tag{1.3.15}$$

For spinless particles, the decomposition Eq. (1.2.14) of the two bases imply a similar decomposition (the partial wave decomposition) for the T-matrices appearing in the rhs of Eqs. (1.3.4) and (1.3.5). We have

$$T(s,t) = \sum_{j=0}^{\infty} (2j+1) P_j(x) T^j(s), \tag{1.3.16}$$

$$T^j(s) = \int_0^1 dx T(s, t(s,x)) P_j(x). \tag{1.3.17}$$

where $x = \cos\theta$ is the scattering angle of the two particles in the centre of mass frame.

Elastic scattering For elastic scattering, $m_C = m_A$ and $m_D = m_B$, the kinematical formulas simplify. It is clear from Eq. (1.3.14) that in this case $k = k'$ so that Eqs. (1.3.14) and (1.3.15) imply

$$\sqrt{s} = \sqrt{m_A^2 + k^2} + \sqrt{m_B^2 + k^2}, \tag{1.3.18}$$

$$t = 2k^2(\cos\theta - 1). \tag{1.3.19}$$

The physical ranges $-1 \leq \cos\theta \leq 1$ and $k > 0$ imply physical ranges of the Mandelstam variables,

$$s \geq (m_A + m_B)^2, \qquad -4k^2 \leq t \leq 0. \tag{1.3.20}$$

1.3.3 Crossing

Of course, all energies of the four scattering particles are positive, i.e. the positive solution to the rhs of Eq. (1.3.7) is taken. Let us suppose instead that we had taken the unphysical negative solution for particles B and C, i.e. $E_B, E_C < 0$[11]. If we denote $p_{\overline{B}} = -p_B$ and $p_{\overline{C}} = -p_C$, then $p_A + p_B = p_C + p_D$ implies

$$p_A + (-p_C) = (-p_B) + p_D \qquad \text{or} \qquad p_A + p_{\overline{C}} = p_{\overline{B}} + p_D.$$

$p_{\overline{C}}$ and $p_{\overline{B}}$ are four-momenta with physical positive energy but are on the opposite side of the conservation relation. This corresponds to another channel, $A\overline{C} \to \overline{B}D$, where the physical four-momenta of particles $\overline{B}$ and $\overline{C}$ can be identified from the unphysical four-momenta of $AB \to CD$ via $p_{\overline{B}} = -p_B$ and $p_{\overline{C}} = -p_C$. In other words, the unphysical domain of the $AB \to CD$ scattering corresponds to the physical domain of the scattering $A\overline{C} \to \overline{B}D$. The particles $\overline{B}$ and $\overline{C}$ are identified as the anti-particles of B and C, respectively.

Similarly, if $E_B, E_D < 0$ then the channel $A\overline{D} \to C\overline{B}$ is identified. If we refer to $AB \to CD$ as the s-channel, then $A\overline{C} \to \overline{B}D$ and $A\overline{D} \to C\overline{B}$ are the t-channel and u-channel, respectively. In summary, in terms of the energy variables E_i of the s-channel, we have

$$\begin{aligned}
s-\text{channel} \quad & AB \to CD \quad E_A, E_B, E_C, E_D \geq 0 \\
t-\text{channel} \quad & A\overline{C} \to \overline{B}D \quad E_A, E_D \geq 0, \quad E_B, E_C \leq 0 \\
u-\text{channel} \quad & A\overline{D} \to C\overline{B} \quad E_A, E_C \geq 0, \quad E_B, E_D \leq 0 \\
\text{decay-channel} \quad & A \to \overline{B}CD \quad E_A, E_C, E_D \geq 0, \quad E_B \leq 0
\end{aligned}$$

Allowing for negative s-channel energies corresponds to allowing the s-channel Mandelstam variables for unphysical regions. The physical regions Σ_s, Σ_t and Σ_u for the corresponding channels can be visualised collectively in a symmetric way in the Mandelstam plane and are shown (blue shaded area) in Fig. (1.3.1) for a given fixed choice of the particle masses. The variables s, t and u in the figure refer to those of the s-channel[12] (bottom-right region) and every point (s, t, u) in the plane satisfies the condition Eq. (1.3.11), whose constant

[11] In the language of App. (A.1.3), we are considering the backward hyperboloid orbits for particles B and C. The representations of the Poincaré group associated to these orbits are absolutely analogous to the physical ones.

[12] If the channels $A\overline{C} \to \overline{B}D$ or $A\overline{D} \to C\overline{B}$ are to be referred to as the s-channel, we rotate the figure clockwise by 120° or 240°, respectively.

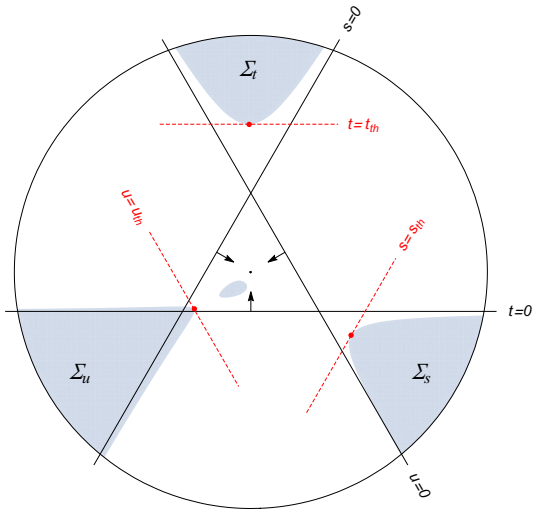

Figure 1.3.1: The physical regions of the crossed channels in the Mandelstam plane for some given particle masses. The arrows indicate the direction of increasing variables and the red dashed lines indicate the threshold value for each channel. In the case of all degenerate masses, as in $\pi^+\pi^+ \to \pi^+\pi^+$ scattering, the red dots would have been placed on the vertices of the triangle and the region boundaries would have been determined simply by the $s = 0$, $t = 0$ and $u = 0$ axes.

value is the height of the equilateral triangle appearing in the middle. Inside this triangle, the decay channel is present, as m_A is chosen to be $m_A > m_B + m_C + m_D$. Each point (s, t) in the physical regions correspond to an independent kinematical situation to which the scattering amplitude $T(s, t)$ is associated.

In summary, we have seen that enlarging the domain on which the kinematic variables assume values allows one to consider all three channels at once by using the same variables. The usefulness of this approach would be limited just to this statement if it wasn't for crossing symmetry. As it will be discussed in the next section, each region can be accessed from the others by the analytic properties of $T(s, t)$. In Fig. (1.3.1), the function $T(s, t)$ can be analytically continued to the white regions and indeed also to complex values of s and t, identifying therefore a unique analytic function for all crossed channels.

1.4 Causality, analyticity, unitarity

1.4.1 Causality implies analyticity

Causality, the concept that cause always precedes effect, is at the base of any physical theory. In several physical theories it is demonstrated that causality implies the analyticity of a function describing the physical system. Unlike for the case of non-relativistic scattering, a formal proof connecting causality and analyticity is missing in relativistic quantum field theory and must be postulated. An analytic S-matrix (or T-matrix), as a consequence of causality, has very powerful implications: once the S-matrix is known in a small region, it is known on all the domain of analyticity and dispersion relations can be formulated. To see the basic concept underlying the causality-analyticity connection, let us consider a general physical system which responds linearly to an input function $h(t)$ with an output function $f(t)$ via the response function $G(t,t')$:

$$f(t) = \int_{-\infty}^{\infty} G(t-t')\, h(t')\, dt. \tag{1.4.1}$$

Here time translation invariance is assumed, i.e. $G(t,t')$ depends only on the difference of its arguments. Applying the convolution theorem, in the Fourier transform space Eq. (1.4.1) becomes

$$\tilde{f}(\omega) = \tilde{G}(\omega)\, \tilde{h}(\omega). \tag{1.4.2}$$

We add now the causality assumption: the response function $f(t)$ in Eq. (1.4.1) receives contributions from the input function $h(t')$ only at times $t' < t$, i.e. $G(t-t')$ is zero for $t' > t$. Then,

$$\tilde{G}(\omega) = \int_{-\infty}^{\infty} d\tau e^{i\omega\tau} G(\tau) = \int_{0}^{\infty} d\tau e^{i\omega\tau} G(\tau). \tag{1.4.3}$$

This relation can be used to analytically extend $\tilde{G}(\omega)$ in the upper-half complex plane. Indeed, letting $\omega = \omega_R + i\omega_I$:

$$\tilde{G}(\omega) = \int_{0}^{\infty} d\tau e^{i(\omega_R + i\omega_I)\tau} G(\tau) = \int_{0}^{\infty} d\tau e^{i\omega_R\tau} e^{-\omega_I\tau} G(\tau). \tag{1.4.4}$$

The factor $e^{-\omega_I\tau}$ can only improve the convergence so that $\tilde{G}(\omega)$ is well defined on the whole upper half ω plane. It is clear that this is possible only because of causality, as negative values of τ would have introduced a non-converging factor $e^{\omega_I|\tau|}$.

By a similar reasoning, the T matrix is considered to be an analytic function in the s-variable in all the upper Im$s > 0$ plane. We will see in the next section that the analyticity can be extended also to the lower Im$s < 0$ plane.

1.4.2 Unitarity

Analyticity, when combined with unitarity, pose strong restrictions on the dynamics. In this section, the unitarity condition Eq. (1.1.8) and its powerful implications for the elastic scattering of two particles, $AB \to AB$ will be investigated. Here, the kets $|a\rangle$ and $|a'\rangle$ are more explicitly denoted by the basis Eq. (1.2.7) with $\alpha = (m_A s_A, m_B s_B)$ and ρ_α contains the direction of the relative momentum, $\hat{\boldsymbol{k}}$, as well as spin components and internal quantum numbers:

$$\begin{aligned} |a\rangle &= |\,\alpha\,;\,p\,\rho_\alpha\,\rangle \\ |a'\rangle &= |\,\alpha\,;\,p'\,\rho'_\alpha\,\rangle\,. \end{aligned}$$

The left hand side of Eq. (1.1.8) is

$$2\mathrm{Im}\,\langle\,\alpha\,;\,p'\,\rho'_\alpha\,|\,T\,|\,\alpha\,;\,p\,\rho_\alpha\,\rangle \;=\; (2\pi)^4\,\delta^{(4)}\,(p'-p)\,2\mathrm{Im}T^{\alpha\alpha}_{\rho'_\alpha\rho_\alpha}\,(s) \tag{1.4.5}$$

Inserting the completeness relation Eq. (1.2.15), for the right hand side we have

$$\begin{aligned} \langle\,\alpha\,;\,p'\,\rho'_\alpha\,|\,TT^\dagger\,|\,\alpha\,;\,p\,\rho_\alpha\,\rangle &= \sum_\beta \int \frac{d^4q}{(2\pi)^4} d\Phi_\beta\,\langle\,\alpha\,;\,p'\,\rho'_\alpha\,|T|\,\beta\,;\,q\,\rho_\beta\,\rangle\,\langle\,\beta\,;\,q\,\rho_\beta\,|T^\dagger|\,\alpha\,;\,p\,\rho_\alpha\,\rangle \\ &= \sum_\beta \int \frac{d^4q}{(2\pi)^4} d\Phi_\beta\,(2\pi)^4\,\delta^{(4)}\,(p'-q)\,T^{\alpha\beta}_{\rho'_\alpha\rho_\beta}\,(s')\,(2\pi)^4\,\delta^{(4)}\,(p-q)\,T^{\alpha\beta}_{\rho_\alpha\rho_\beta}\,(s)^* \\ &= (2\pi)^4\,\delta^{(4)}\,(p-p')\sum_\beta \int d\Phi_\beta T^{\alpha\beta}_{\rho'_\alpha\rho_\beta}\,(s)\,T^{\alpha\beta}_{\rho_\alpha\rho_\beta}\,(s)^*\,. \end{aligned}$$

Then, "simplifying" the Dirac delta $\delta^{(4)}\,(p-p')$ we obtain the generalised optical theorem

$$2\mathrm{Im}T^{\alpha\alpha}_{\rho'_\alpha\rho_\alpha}\,(s) = \sum_\beta \int d\Phi_\beta T^{\alpha\beta}_{\rho'_\alpha\rho_\beta}\,(s)\,T^{\alpha\beta}_{\rho_\alpha\rho_\beta}\,(s)^*\,. \tag{1.4.6}$$

For each s, the imaginary part of the T-matrix for the elastic $\alpha \to \alpha$ channel is given by the T-matrices of all channels $\alpha \to \beta$ allowed by the symmetries of the underlying theory. For

instance, if $\alpha = \pi^- p$, then $\beta = \pi^- p, \pi^0 n, K^0\Lambda, \pi^0 K^0\Lambda, \ldots$. We see now what terms on the rhs can contribute to the lhs as we vary s and keeping μ'_α and μ_α fixed.

Below threshold, $s < s_{th} = (m_A + m_B)^2$, there are no states on the rhs that can contribute and thus $\mathrm{Im}T^{\alpha\alpha}_{\rho'_\alpha\rho_\alpha}(s) = 0$[13]. This is true apart for possible one-particles states (e.g. bound states of AB or the particles A and B themselves if allowed by the theory) with mass $m_1, m_2, \ldots$ which couple to AB. These will give isolated contributions to $\mathrm{Im}T^{\alpha\alpha}_{\rho'_\alpha\rho_\alpha}(s)$ at $s = \sqrt{m_1}, \sqrt{m_2}, \ldots$ which are proportional to $\delta(s - m_1^2), \delta(s - m_2^2), \ldots$. As s increases and reaches the threshold s_{th}, the same AB states suddenly appear on the rhs, i.e., the term $\beta = \alpha$ appears. This leads to an abrupt increase of $\mathrm{Im}T^{\alpha\alpha}_{\rho'_\alpha\rho_\alpha}(s)$, which starts varying continuously. The AB states will provide the only contributions to the rhs of Eq. (1.4.6) until s has increased enough, above inelastic threshold s^{in}_{th}, to allow new states with $\beta \neq \alpha$ which couple to AB to appear. Once again, the opening of the new channel results in an abrupt increase to $\mathrm{Im}T^{\alpha\alpha}_{\rho'_\alpha\rho_\alpha}(s)$ which adds to the still present AB contribution. This behaviour continues as more and more inelastic thresholds are reached.

More explicitly, for the case of AB being spinless (and neglecting other quantum numbers) we have $T^{\alpha\alpha}_{\rho'_\alpha\rho_\alpha}(s) \equiv T^{\alpha\alpha}_{\hat{\boldsymbol{k}}'\hat{\boldsymbol{k}}}(s) \equiv T^{\alpha\alpha}(s,t)$ and $d\Phi_\alpha = \frac{k}{16\pi^2\sqrt{s}} d^2\Omega_{\boldsymbol{k}}$ with $k = |\boldsymbol{k}|$. Dropping the $\alpha\alpha$ label, Eq. (1.4.6) reads

$$\begin{aligned} 2\mathrm{Im}T(s,t) &= -\pi \sum_i g_i^2 \delta\left(s - m_i^2\right) + \theta(s - s_{th}) \int d^2\Omega_{\boldsymbol{k}} \left(\frac{16\pi^2\sqrt{s}}{k}\right)^{-1} T(s,t)\, T^*(s,t') \\ &\quad + \theta\left(s - s^{in}_{th}\right) \sum_{\beta\neq\alpha} \ldots \end{aligned} \tag{1.4.7}$$

In the range $s_{th} \leq s \leq s^{in}_{th}$, Eq. (1.4.7) is a closed relation in $T(s,t)$ which in principle can be solved. Unitarity provides the imaginary part while the real part depends on the particular dynamics for the theory under consideration. The isolated terms can be seen to be proportional to $\delta(s - m_i^2)$ when inserting a one-particle state in $\langle\, \alpha\,;\, p'\, \rho'_\alpha \,|\, TT^\dagger \,|\, \alpha\,;\, p\, \rho_\alpha \,\rangle$. The coefficient g_i^2 is the coupling of AB to the i-th one-particle state.

In terms of Fig. (1.3.1), we are looking at the values of $2\mathrm{Im}T(s,t)$ along an horizontal line representing a fixed t. This line is chosen to be negative but above the intersection point of the $s = s_{th}$ and $u = u_{th}$ lines, so that the u-channel contribution to $2\mathrm{Im}T(s,t)$, present in the region $s \in\,]-\infty, u_0]$ with $u_0 = \sum_{i=1}^4 m_i^2 - t - u_{th}$, does not overlap with the physical s-channel contributions displayed in Eq. (1.4.7).

[13] Indeed, $T^{\alpha\alpha}_{\mu'_\alpha\mu_\alpha}(s)$ is initially defined only for $s \geq s_{th}$ but it is extend to unphysical regions.

Now, let us make use of the analyticity of $T(s,t)$. Since below threshold s_{th} there is a region where $\mathrm{Im}T(s,t)=0$, apart from possible isolated points, we can apply the Schwartz reflection principle[14] to $T(s,t)$ as a function of s and analytically continue it for $\mathrm{Im}s<0$ with the relation

$$T(s^*,t)=T^*(s,t)\,. \tag{1.4.8}$$

For $s=s_R+i\epsilon$, Eq. (1.4.8) implies

$$\mathrm{Re}T(s_R-i\epsilon,t) = \mathrm{Re}T(s_R+i\epsilon,t)\,, \tag{1.4.9}$$

$$\mathrm{Im}T(s_R-i\epsilon,t) = -\mathrm{Im}T(s_R+i\epsilon,t)\,, \tag{1.4.10}$$

or, equivalently, it provides a formula for the the discontinuity along the real axis:

$$T(s_R+i\epsilon,t)-T(s_R-i\epsilon,t)=2i\mathrm{Im}T(s_R+i\epsilon,t)\equiv 2i\mathrm{Im}T(s_R,t)\,. \tag{1.4.11}$$

Unitarity requires that the discontinuity is zero below threshold (since here $\mathrm{Im}T(s_R,t)=0$) and non zero for $s\geq s_{th}$. The point $s=s_{th}$ is thus a branch point in the complex plane. At the opening of a new threshold, the rhs of Eq. (1.4.11) is itself going through a discontinuous change and a new branch point is identified. Conventionally all branch cuts are taken along the real axis in the positive direction (up to infinity). It is clear then that the analytic structure of $T(s,t)$ is involved, as it is made of an infinite number of Riemann sheets.

Due to the discontinuity, a specification must be made to identify from which side the physical region is reached. The convention usually adopted assumes that the physical region is reached from above,

$$T(s,t)=\lim_{\epsilon\to 0}T(s+i\epsilon,t)\,,\qquad s \text{ real},$$

and the physical sheet is defined to be the Riemann sheet which contains the physical region. In this context, adding a small imaginary part $i\epsilon$ is equivalent to Feynman's prescription in perturbation theory .

The isolated δ terms for $\mathrm{Im}T(s,t)$ in Eq. (1.4.7) translates into simple poles for the full $T(s,t)$. Indeed, due to the well known relation

$$\frac{1}{s-m^2+i\epsilon}=P\frac{1}{s-m^2}-i\pi\delta\left(s-m^2\right),$$

[14] If a function $f(z)$ is analytic in a region containing a segment of the real axis and is real here, it can be continued to the complex conjugate region and satisfies $f^*(z)=f(z^*)$.

where P denotes the principal value, we have, close to the stable particle mass $s \approx m_i^2$,

$$T(s,t) = \frac{g_i^2}{s - m_i^2}. \tag{1.4.12}$$

Even though these pole contributions are located in the unphysical region of the scattering, particularly shallow bound states can be close enough to s_{th} to give a significant contribution to the physical region.

In the previous subsection we have seen that all crossed channel reactions can be reached in suitable regions of the same variables s and t. Since $T(s,t)$ is analytic, the same function $T(s,t)$ describes the scattering of the crossed channels. Then, for fixed t, $T(s,t)$ will also have a cut for $s \in]-\infty, u_0]$ as well as bound state poles of the u-channel.

1.4.3 Partial wave amplitudes, phase shifts

More explicit unitarity constraints can be derived when using the total angular momentum basis Eq. (1.2.8). This time, instead of implementing unitarity via the T-matrix, it will be more instructive to use the S-matrix, namely Eq. (1.1.6),

$$\sum_b \frac{1}{f_b} |\langle b|S|a\rangle|^2 = f_a. \tag{1.4.13}$$

The matrix element $\langle b|S|a\rangle$ cannot represent a probability amplitude, as the states are not normalised to one. Instead, one defines S matrix elements via

$$\langle \alpha' \,;\, p'\, j'\, \sigma'_{j'}\, \mu' \,|\, S \,|\alpha \,;\, p\, j\, \sigma_j\, \mu\rangle = \sqrt{\mathcal{N}_{\alpha'}\mathcal{N}_\alpha}\,(2\pi)^4\,\delta^{(4)}(p-p')\,\delta_{jj'}\delta_{\sigma_j\sigma'_j} S^{[\alpha'\alpha]\;j}_{\mu'_\alpha\mu_\alpha}(s) \tag{1.4.14}$$

where the $\mathcal{N}_\alpha$ compensate the normalisations in Eq. (1.4.13). Here, $|b\rangle$ runs over the whole total angular momentum basis while we take $|a\rangle$ to be a two-particle state with $\alpha = (m_A s_A, m_B s_B)$,

$$|a\rangle = |\alpha \,;\, p\, j\, \sigma_j\, \mu_\alpha\rangle\,.$$

Recall that μ_α could represent either the helicities of the particles or the orbital and spin angular momenta (l,s). Further labels due to internal symmetries may be fitted inside μ_α. Then, Eq. (1.4.13) reads

$$\sum_\beta \sum_{j'\sigma'_j} \int \frac{d^4p'}{(2\pi)^4} d\Phi_\beta |\langle \beta \,;\, p'\, j'\, \sigma'_j\, \mu'_\beta \,|\, S \,|\, \alpha \,;\, p\, j\, \sigma_j\, \mu_\alpha\rangle|^2 = \mathcal{N}_\alpha\,(2\pi)^4\,\delta^{(4)}(0) \tag{1.4.15}$$

The factor $(2\pi)^4 \delta^{(4)}(0)$ can be thought of as a large spacetime volume TV when putting the system in a large box.

Using Eq. (1.4.14), the expression simplifies to

$$\sum_\beta \int d\Phi_\beta \mathcal{N}_\beta |S^{[\beta\alpha]\, j}_{\mu'_\beta \mu_\alpha}(s)|^2 = 1. \tag{1.4.16}$$

There is a unitarity relation for each value of j and each value of s. The probability for particles α to be found after the scattering in any other set of particles β is unity. Of course, β runs also over α itself and moving all $\beta \neq \alpha$ terms to the rhs, we get

$$\int d\Phi_\alpha \mathcal{N}_\alpha |S^{[\alpha\alpha]\, j}_{\mu'_\alpha \mu_\alpha}(s)|^2 = 1 - \sum_{\beta\neq\alpha} \int d\Phi_\beta \mathcal{N}_\beta |S^{[\beta\alpha]\, j}_{\mu'_\beta \mu_\alpha}(s)|^2. \tag{1.4.17}$$

The phase space integral $\int d\Phi_\alpha$ acts on μ'_α which, for a two particle system, is just a spin index (there is no relative momentum label). The integration over the phase space can be trivially performed and cancels out with $\mathcal{N}_\alpha$. We are left with a sum over the spins[15],

$$\sum_{\mu'_\alpha} |S^{[\alpha\alpha]\, j}_{\mu'_\alpha \mu_\alpha}(s)|^2 = 1 - \sum_{\beta\neq\alpha} \int d\Phi_\beta \mathcal{N}_\beta |S^{[\beta\alpha]\, j}_{\mu'_\beta \mu_\alpha}(s)|^2. \tag{1.4.18}$$

The lhs represents the probability for elastic scattering $AB \to AB$ and, for a given j and s, it is in general smaller than one due to the possibility of the inelastic contributions at the rhs. Let us now suppose that, for some reason, the S-matrix at the lhs is diagonal in μ_α (or can be set to be so). This is always the case for spinless particles, where the index μ is just not there (apart for possible further internal symmetries). It is also the case for $N\pi$ scattering thanks to parity conservation. Then, the sum at the lhs is non-zero only for $\mu'_\alpha = \mu_\alpha$ and for each diagonal element we have (the α labels are dropped now)

$$|S^j_\mu(s)|^2 = \eta^2_{j\mu}(s). \tag{1.4.19}$$

$\eta^2_{j\mu}(s)$ is the rhs of Eq. (1.4.18) and of course, as a consequence of conservation of probability (unitarity), $0 \leq \eta_{j\mu} \leq 1$. Then $S^j_\mu(s)$ is a complex number whose amplitude is $\eta_{j\mu}(s)$,

$$S^j_\mu(s) = \eta_{j\mu}(s)\, e^{2i\delta_{j\mu}(s)}, \qquad 0 \leq \eta_{j\mu} \leq 1,\ \delta_{j\mu} \text{ real}. \tag{1.4.20}$$

[15]Recall that the sum over all spins and quantum number indices are included in $\int d\Phi_\alpha$ for economy of notation.

The real phase $\delta_{j\mu}$ is called the phase shift and $\eta_{j\mu}$ is called inelasticity. The unitarity condition is expressed in terms of the bounds for $\eta_{j\mu}$. Alternatively, one can write $\eta_{j\mu} = e^{-2Im\delta_{j\mu}}$ so that the phase shift gets complex and the unitarity restriction is exhibited by the non-negativity of the imaginary part of $\delta_{j\mu}$.

Now, if s is below the inelastic threshold, all terms in $\sum_\beta$ at the rhs of Eq. (1.4.18) will be zero since there is not enough energy to create intermediate states. This means that the probability to obtain the same state again after the scattering is one, or, in other words, $\eta_{j\mu} = 1$:

$$S_\mu^j(s) = e^{2i\delta_{j\mu}(s)}, \qquad \delta_{j\mu} \text{ real, elastic scattering.}$$

Below inelastic threshold, the dynamics of the elastic scattering is just expressed by a real function.

Alternatively, as done in the previous section, we could have used Eq. (1.1.9) to implement unitarity. Below inelastic threshold, the $d\Omega_{\hat{\boldsymbol{k}}}$-independent $T^j(s)$ amplitudes would have appeared in the integral of Eq. (1.4.7), leading to

$$\mathrm{Im}T^j(s) = \rho(s)\, T^j(s)\, T^{j*}(s), \tag{1.4.21}$$

where $\rho(s)$ is the two-particle phase space factor

$$\rho(s) = -\frac{k}{8\pi\sqrt{s}}. \tag{1.4.22}$$

Here, k is the three momentum modulus of either particle in the CM frame, related to s via Eq. (1.2.12).

In the total angular momentum basis, the complicated unitarity relation reduces to a simple algebraic relation. Including spins and additional quantum numbers, Eq. (1.4.21) is to be viewed as a matrix relation. Then, since

$$S^j(s) = e^{2i\delta_j(s)} = 1 + 2i\rho T^j(s),$$

we have an expression of T^j in terms of the phase shift,

$$T^j(s) = \frac{1}{\rho} e^{i\delta_j} \sin\delta_j \equiv \frac{1}{\rho}\frac{e^{2i\delta_j}-1}{2i} \equiv \frac{1}{\rho}\frac{1}{\cot\delta_j - i} \equiv -\frac{8\pi\sqrt{s}}{k\cot\delta_j - ik}. \tag{1.4.23}$$

From Eq. (1.4.23), it is clear that the imaginary part of T_j^{-1} is fully provided by unitarity,

$$\mathrm{Im}T_j^{-1}(s) = -\rho(s) \equiv \frac{k}{8\pi\sqrt{s}}. \tag{1.4.24}$$

1.4.4 Threshold behaviour, bound states, resonances

Previously we have studied the analytical properties of the scattering amplitude $T(s,t)$ for elastic scattering of two particles A and B. The function is analytic over the whole s complex plane, except for regions on the real axis which include a branch cut at $s > s_{th} = (m_A + m_B)^2$, possible poles due to one-particle states below threshold, and the u-channel cut and poles.

The partial wave amplitudes $T^j(s)$ are obtained from $T(s,t)$ by integrations over the t variable, Eq. (1.3.17) for spinless particles. In this section we are interested in the way the analytical properties of $T^j(s)$ are inherited from $T(s,t)$ via the integration and for simplicity we limit ourselves to elastic scattering of spinless particles. The detailed analysis requires dispersion relations and the reader is forwarded to textbooks like Ref. [3]. Here we briefly summarise the results:

- The physical cut $s > s_{th}$ survives the integration and is present in $T^j(s)$ for every j.
- A stable particle pole survives the integration only for one value of j, the spin of the particle.
- The t and u channel singularities lead to an unphysical cut for $s < 0$ and, if $m_A \neq m_B$, additional cuts are present in the circle $|s| = m_A^2 - m_B^2$ $(m_A > m_B)$ and along the real axis in the negative direction starting from $(m_A - m_B)^2$.

Threshold behaviour Partial wave amplitudes are particularly useful also thanks to the fact that close to the elastic threshold $\mathrm{Re}T^l(s) \sim k^{2l}$, where $k = |\boldsymbol{k}|$ is the modulus of the CM momentum of each particle, Eq. (1.2.12). This implies that, close to threshold, only the lowest partial waves contribute to $T(s,t)$. The function $k^{2l+1}\cot\delta_l(k)$, which explicitly appears at the denominator of Eq. (1.4.23) when $l = 0$, is real for real s or k and depends on k^2. The expansion around the threshold $k^2 = 0$,

$$k^{2l+1}\cot\delta_l(k) = \frac{1}{a_l} + \frac{1}{2}r_l k^2 + \mathcal{O}\left(k^4\right), \tag{1.4.25}$$

is called effective range expansion and defines the scattering length a_l and effective range r_l for the partial wave l. Dropping the $\mathcal{O}(k^4)$ term results in what is known as the effective range approximation. At the threshold $s_{th} = (m_A + m_B)^2$ (or $k^2 = 0$), Eq. (1.4.23) implies, for $l = 0$, the exact relation

$$T^{l=0}(s_{th}) = -8\pi a_0 (m_A + m_B). \tag{1.4.26}$$

Bound states Below elastic threshold, $\sqrt{s} < m_A + m_B$, k^2 becomes negative and k imaginary, $k = i|k|$, as it can be seen from Eq. (1.3.18) or its inverted relation Eq. (1.2.12). If in this region there is a bound state with spin l, mass m_B and coupling g, Eq. (1.4.12) implies the behaviour

$$T^l(s) = \frac{g^2}{s - m_B^2} \tag{1.4.27}$$

at $s \approx s_B = m_B^2$, corresponding to $k \approx k_B = i|k_B|$. The bound state pole can be identified by setting the denominator of Eq. (1.4.23) to zero,

$$k_B \cot \delta_l(k_B) = ik_B \equiv -|k_B| \tag{1.4.28}$$

and the coupling can be obtained by

$$g^2 = \lim_{s \to m_B^2} T^l(s)\left(s - m_B^2\right) = \lim_{s \to m_B^2} \frac{-8\pi\sqrt{s}\,(s - m_B^2)}{k \cot \delta_l(k) - ik}. \tag{1.4.29}$$

If the bound state is shallow enough such that the effective range approximation is still valid at $s = m_B^2$, then Eq. (1.4.28) and Eq. (1.4.29) become more explicit. For an s-wave channel we have

$$|k_B| = \frac{1}{2} r_0 |k_B|^2 - \frac{1}{a_0}, \tag{1.4.30}$$

$$g^2 = \frac{64\pi m_B |k_B|}{(1 - r_0 k_B)\left(1 - \left(\frac{m_A^2 - m_B^2}{m_B^2}\right)^2\right)}. \tag{1.4.31}$$

Resonances Resonances are "particles" whose instability is believed to be the only fundamental feature that distinguishes them from stable particles. Consequently, as for a stable particle, we expect a simple pole of the scattering amplitude to be associated to a resonance. However, while stable particle poles appear on the real axis of the physical sheet, resonances

are relagated to unphysical sheets[16]. Due to hermitian analyticity, resonance poles always come in complex conjugate pairs, s_R and s_R^*. The situation is sketched in Fig. 48.1 of the PDG review [7]: starting from the physical region of scattering (where s is real and above threshold), it is possible to smoothly cross the cut by decreasing Ims (entering the unphysical sheet) and to access the resonance pole s_R. The path in reaching the complex conjugate s_R^* is longer (one would have to go around the branch point s_{th}), hence this pole usually has negligible impact on the physical region and will not be considered here.

Starting from the pole position s_R, one may define the mass and the width of the resonance as[17]

$$s_R = \mathrm{Re}s_R + i\mathrm{Im}s_R = \left(m - i\frac{\Gamma}{2}\right)^2 = m_{BW}^2 - i\Gamma_{BW} m_{BW}. \tag{1.4.32}$$

The pole (m, Γ) and the Breit-Wigner (m_{BW}, Γ_{BW}) definitions are related by

$$\begin{cases} m_{BW} = m\gamma \\ \Gamma_{BW} = \Gamma/\gamma \end{cases} \qquad \gamma = \sqrt{1 - (\Gamma/2m)^2}, \tag{1.4.33}$$

and coincide for $\Gamma \ll 2m$. A low width resonance is very close to the physical region which will be then strongly influenced by its pole. Experimentally, the characteristic bump observed in the cross section on the real s-axis is reminiscent of the pole lying nearby in the complex plane.

The partial-wave T-matrix can be expressed via a function $f(s)$ which is regular at s_R,

$$T^l(s) = \frac{f(s)}{s - s_R}, \tag{1.4.34}$$

Explicitly, $f(s)$ can be expanded in a power series around s_R[18]

$$f(s) = f(s_R) + f'(s_R)(s - s_R) + \ldots \quad . \tag{1.4.35}$$

The positive power terms make up the background of the T-matrix, while the pure pole

[16] This is a consequence of the Mandelstam's maximal analyticity hypothesis.

[17] Numerous definitions of the mass of a resonance have been introduced in the literature. These definitions include the peak position of the cross section or the value of $\sqrt{s}$ at which the phase shift is $\frac{\pi}{2}$. What is model-independent and fundamental about a resonance is just the pole position, i.e. the couple $(\mathrm{Re}s_R, \mathrm{Im}s_R)$.

[18] The series converges in a disc centered on s_R and bounded by the nearest singularity. The boundary may be due to an additional resonance or to the threshold branch point. In the latter case, the circle includes part of the physical region.

contribution is given by the residue term $f(s_R) = -g^2$,

$$T_R^l(s) = \frac{-g^2}{s - s_R} = \frac{-g^2}{s - \left(m - i\frac{\Gamma}{2}\right)^2} \equiv \frac{-g^2}{s - (m_{BW}^2 - i\Gamma_{BW} m_{BW})}. \tag{1.4.36}$$

One may want to keep the background terms and parametrise the scattering amplitude in a way that the behaviour at the threshold (discussed earlier in this subsection) is reproduced. In the case of a single and narrow resonance generated by the elastic scattering of two particles (and with far away negligible inelastic thresholds), the common relativistic varying-width Breit-Wigner parametrisation is often accurate,

$$T_{BW}^l(s) = \frac{1}{\rho(s)} \frac{-\sqrt{s}\Gamma_l(s)}{s - (m_{BW}^2 - i\sqrt{s}\Gamma_l(s))}, \tag{1.4.37}$$

$$\Gamma_l(s) = \frac{g^2}{6\pi} \frac{k^{2l+1}}{s m_{BW}^{2l-2}} \tag{1.4.38}$$

and satisfies the unitarity condition Eq. (1.4.24). Comparing with Eq. (1.4.23), we easily get

$$\cot\delta_l(s) = \frac{m_{BW}^2 - s}{\sqrt{s}\Gamma_l(s)}. \tag{1.4.39}$$

It is clear that the value of s such that $\delta_l(s) = \frac{\pi}{2}$ is m_{BW}^2 which, as mentioned above, differs from m^2. For $l > 0$, the width Eq. (1.4.38) increases unrealistically with the energy and the effect of the resonance is felt far away from its position. This behaviour can be fixed by adding some damping factors to Eq. (1.4.38).

1.4.5 Potential

We have seen in the previous section that partial wave amplitudes $T^j(s)$ possess a physical right hand cut for s above the lowest threshold as well as unphysical left hand cuts which originate from the crossed channels. In the N/D method [8], the two sets of cuts are separated into two distinct functions $N^j(s)$ and $D^j(s)$ which in full generality form $T^j(s)$ through their ratio, $T^j(s) = N^j(s)/D^j(s)$. The numerator $N^j(s)$ carries all and only left hand cuts and the denominator $D^j(s)$ carries exclusively the physical cut. It was shown in Ref. [9] that if the unphysical cuts can be neglected, the numerator function can be set to one and the denominator assumes a simple form such that the two-body partial wave amplitude with masses $m_2 > m_1$ is (the index j is dropped and we are restricting to s-wave but the relation

is valid in general),

$$T(s) = \frac{1}{V^{-1}(s) - G(s)}. \tag{1.4.40}$$

$V(s)$ is called potential and is a real function well behaved at threshold which encodes the dynamics of the system. G is an infinite[19] loop function that can be either regularised with a cutoff Λ,

$$G^c(s,\Lambda) = \int_{|\boldsymbol{q}|<\Lambda} \frac{d^3q}{(2\pi)^3} I(s,\boldsymbol{q}), \tag{1.4.41}$$

$$I(s,\boldsymbol{q}) = \frac{1}{2E_1(\boldsymbol{q})E_2(\boldsymbol{q})} \frac{E_1(\boldsymbol{q}) + E_2(\boldsymbol{q})}{s + i\epsilon - (E_1(\boldsymbol{q}) + E_2(\boldsymbol{q}))^2}, \tag{1.4.42}$$

with $E_{1/2}(\boldsymbol{q}) = \sqrt{m_{1/2}^2 + |\boldsymbol{q}|^2}$, or alternatively, can be renormalised with a subtraction constant $\alpha(\mu)$ at scale μ,

$$G^D(s,\alpha) = \frac{1}{16\pi^2}\left[\alpha(\mu) + \log\frac{m_1 m_2}{\mu^2} + \frac{\delta m}{2s}\log\frac{m_2^2}{m_1^2} + \frac{k}{\sqrt{s}} l(s)\right], \tag{1.4.43}$$

$$\begin{aligned} l(s) = &+\log\left(2\sqrt{s}k + s + \delta m\right) + \log\left(2\sqrt{s}k + s - \delta m\right) \\ &- \log\left(2\sqrt{s}k - s + \delta m\right) - \log\left(2\sqrt{s}k - s - \delta m\right), \end{aligned} \tag{1.4.44}$$

where $\delta m = m_2^2 - m_1^2$ and k is related to s via Eq. (1.2.12).

The notation $G(s)$ in Eq. (1.4.40) can refer to either Eq. (1.4.41) or to Eq. (1.4.43). Of course, the potential $V(s)$ has the corresponding form $V^c(s,\Lambda)$ or $V^D(s,\alpha)$. The T-matrix $T(s)$ is a physical quantity and does not depend on the regularisation artefacts. In particular, in the cutoff form, $T^{-1}(s)$ is obtained as the infinite cutoff limit of the difference $V^c(s,\Lambda)^{-1} - G^c(s,\Lambda)$. In the dimensional notation, changes in G due to changes of μ are absorbed by changes in V^{-1}, such that the physical $T(s)$ is unchanged. Explicitly,

$$T(s) = \lim_{\Lambda\to\infty} \frac{1}{V^c(s,\Lambda)^{-1} - G^c(s,\Lambda)} = \frac{1}{V^D(s,\alpha)^{-1} - G^D(s,\alpha)}. \tag{1.4.45}$$

An explicit (non-integral) expression also for $G^c(s,\Lambda)$ can be found in the erratum [10] of Ref. [11]. The same work connects the renormalisation scale μ with the cutoff Λ via the relation $\mu = \frac{2}{\sqrt{e}}\Lambda \approx 1.2\Lambda$.

In both cases, the form Eq. (1.4.40) guarantees the analytic and unitary properties of the

[19] The real part is infinite, the imaginary part is trivial and dictated by unitarity, see Eq. (1.4.46).

partial wave. In particular, the function $G(s)$, viewed as a complex function, is equipped with the correct physical cut. For real values of s, its imaginary part is zero below threshold and is equal to $-k/(8\pi\sqrt{s})$ above, in agreement with Eq. (1.4.24):

$$G(s) = \mathrm{Re}G(s) - i\frac{k}{8\pi\sqrt{s}}, \quad s > s_{th}. \tag{1.4.46}$$

The derivative of G with respect to s, $\frac{\partial G}{\partial s}$, is independent of α in its dimensional renormalised form (which appears just as a constant in Eq. (1.4.43)) and coincides with the $\Lambda \to \infty$ limit of the cutoff regularised derivative counterpart, which is regular,

$$\frac{\partial G}{\partial s} = \frac{\partial G^D(s,\alpha)}{\partial s} \equiv \lim_{\Lambda\to\infty} \frac{\partial G^c(s,\Lambda)}{\partial s}. \tag{1.4.47}$$

Below threshold, $G(s)$ (real) is a decreasing function with respect to s, therefore the derivative Eq. (1.4.47) is negative.

Although the notation adopted follows that of Unitarised Chiral Perturbation theory, Eq. (1.4.40) is valid in general and the potential can be any function that describes the elastic scattering of the two particles.

In the notation Eq. (1.4.40), a possible bound state below threshold at $s = s_B = m_B^2$ is determined by setting the denominator of Eq. (1.4.40) to zero,

$$V(s_B)\, G(s_B) = 1. \tag{1.4.48}$$

The bound state s_B is a physical quantity and the solution(s) to Eq. (1.4.48) should be independent of renormalisation parameters.

Using Eq. (1.4.27), it is straightforward to obtain the sum rule

$$\underbrace{g^2\frac{\partial V^{-1}}{\partial s}}_{Z} + \underbrace{g^2\left(-\frac{\partial G}{\partial s}\right)}_{1-Z} = 1 \tag{1.4.49}$$

which is valid at $s = s_B$; $0 \le 1 - Z \le 1$ is known as the compositeness factor.

Interpretation of Z The interpretation of the factors Z and $1 - Z$ appearing in Eq. (1.4.49) was discussed in Ref. [12] (see also Ref. [13]) as a generalisation of Weinberg's work [14].

As explained in Sec. (1.2.3), the state $|B\rangle = |\, m_B\, s_B\, ;\, \boldsymbol{p}\, \sigma\, \rangle$ associated with a bound

state, as well as the scattering state[20] $|12\rangle$ that we are considering and all others $|1'2'\rangle, ...$ are asymptotic states and eigenstates of the interacting Hamiltonian H of the theory. The same Hilbert space may be spanned in terms of the eigenstates $|B_0\rangle$, $|12_0\rangle$, $|1'2'_0\rangle, ...$ of a bare Hamiltonian H_0 and the state $|B\rangle$ can be decomposed in terms of these,

$$|B\rangle = c_B\,|B_0\rangle + c_{12}\,|12_0\rangle + c_{1'2'}\,|1'2'_0\rangle + ... \,. \tag{1.4.50}$$

The state $|B_0\rangle$ is a "bare bound state", $|12_0\rangle$ is the bare version of the $|12\rangle$ scattering state that we are considering and $c_{1'2'}\,|1'2'_0\rangle + ...$ denote all other states. We say that the bound state $|B\rangle$ has an "elementary" or "genuine" component $|B_0\rangle$ with probability

$$c_B^2 = \left|\frac{\langle B_0|B\rangle}{\langle B_0|B_0\rangle}\right|^2, \tag{1.4.51}$$

as well as "molecular" components $c_{12}^2, c_{1'2'}^2, ...$ and all amplitudes squared sum up to one. Then,

$$1 - Z = c_{12}^2 \tag{1.4.52}$$

$$Z = c_B^2 + c_{1'2'}^2 + ... \tag{1.4.53}$$

$1 - Z$ represents the probability for the bound state $|B\rangle$ to be found in the 12 channel, and can be calculated from Eq. (1.4.49). Z represents all other possibilities, including "elementariness" and couplings to other channels. An approximately vanishing Z is associated with a strong 12 molecular component for the bound state. It is clear from Eq. (1.4.49) that an energy-independent potential can not allow couplings of the bound state to other states than the $|12\rangle$ scattering state in question.

The discussion of compositeness was introduced by Weinberg [14] in a non-relativistic setting. He considered the Hilbert space of two-particle states formed by a proton and a neutron, $|12\rangle = |pn\rangle$, as well as a state associated to the deuteron $|B\rangle = |\text{deuteron}\rangle$. With no other scattering states (the particle number is fixed in this non-relativistic formulation), $Z = c_B^2$ represents just the elementary contribution. In the low binding energy approximation, Weinberg linked Z to the measurable and known scattering length and effective range of the proton-neutron system, finding $Z \approx 0$ and thus stating that the deuteron is mainly a

[20] Momenta and spin component labels are hidden. For instance $|12\rangle = |\, m_1\, s_1\, m_2\, s_2\, ; \, ...\,\rangle$.

composite system of a proton and a neutron.

Chapter 2

QCD on the continuum and on the lattice

The introduction of QCD as a theory for strong interactions was revolutionary. Before its emergence, the theoretical world was living a period of confusion as it could not keep pace with all experimental phenomena that were being discovered in the laboratories, a situation which is basically the opposite of that of today. A number of isolated phenomenological models were being developed but a general field description which was so successful for QED seemed to be impossible to achieve for the strong interaction. S-matrix theory, based on the general symmetry considerations of the previous chapter could provide actual results only for a limited number of cases. Therefore it is no surprise that S-matrix theory was swamped by the advent of QCD and was almost forgotten. QCD was able to explain experimental evidence like colour and asymptotic freedom and furnished a calculative tool with predictive power via perturbation theory in the high energy limit.

Nevertheless, non-perturbative aspects like confinement are yet to be derived analytically from QCD. These are believed to be hidden behind the complicated mathematical structure of the theory. Placing the theory on the lattice and understanding the connection with the continuum version allows to numerically access its non-perturbative features.

This chapter is organised as follows. In Sec. (2.1) QCD and its dynamical fields and symmetries are introduced and the connection with the physical spectrum is discussed. In Sec. (2.2) how QCD can be implemented on a finite discretised lattice is explained. The Wilson action and the partition function are introduced and a quantum mechanical Hilbert space is identified. Sec. (2.3) collects some useful technical methods relevant to perform calculations in the next chapters and, finally, Sec. (2.4) shows how to access physical

quantities in the continuum from the lattice results.

2.1 Continuum QCD

2.1.1 The classical action

The dynamical fields of QCD are

$$\psi^f_{i\alpha}(x), \quad \overline{\psi}^f_{i\alpha}(x), \quad A^\mu_{ij}(x), \qquad f = 1, ..., N_f \quad i, j = r, g, b \quad \alpha = 1, 2, 3, 4$$

where ψ and $\overline{\psi}$ represent quarks and anti-quarks and A^μ represents the gauge bosons. Apart from spacetime variables, the former carry a flavour index f ($= u, d, c, s, t, b$ in the real world), a spin index α and a colour index i. With respect to the spin index α, they are Dirac fermions and transform under the $\left(\frac{1}{2}, 0\right) \oplus \left(0, \frac{1}{2}\right)$ representation of the Lorentz group. With respect to the colour index i, they are vectors that live in the **3** (quarks) and $\overline{\mathbf{3}}$ (antiquarks) representation of the gauge group $SU(3)$. The gauge fields A^μ carry a Lorentz index μ and transform as vectors under the Lorentz group, according to the $\left(\frac{1}{2}, \frac{1}{2}\right)$ representation. For each μ, they are traceless hermitian 3×3 matrices. Therefore they belong to the algebra of $SU(3)$, i.e. they are a linear combination of the generators t_a of $SU(3)$ with coefficients A^μ_a:

$$A^\mu = \sum_{a=1}^{8} A^\mu_a t_a. \tag{2.1.1}$$

The generators t_a are half the Gell-Mann matrices, $t_a = \frac{\lambda_a}{2}$, and satisfy the $SU(3)$ commutation and trace relations

$$[t_a, t_b] = i f_{abc} t_c, \tag{2.1.2}$$

$$\mathrm{Tr}\,[t_a t_b] = \frac{1}{2}\delta_{ab}, \tag{2.1.3}$$

where f_{abc} are the structure constants of $SU(3)$.

A local gauge transformation is defined to be

$$\psi^f_\alpha \rightarrow \Omega \psi^f_\alpha, \tag{2.1.4}$$

$$\overline{\psi}^f_\alpha \rightarrow \overline{\psi}^f_\alpha \Omega^{-1}, \tag{2.1.5}$$

$$A^\mu \rightarrow \Omega A^\mu \Omega^{-1} - i\Omega\left(\partial^\mu \Omega^{-1}\right), \tag{2.1.6}$$

where, for each spacetime x, Ω is a $SU(3)$ matrix,

$$\Omega(x) = e^{i\omega_a(x)t_a}. \tag{2.1.7}$$

The (classical) QCD Lagrangian is a locally gauge invariant quantity (flavour indices are summed)

$$\begin{aligned} \mathcal{L} &= -\frac{1}{2}\mathrm{Tr}\left[F^{\mu\nu}F_{\mu\nu}\right] + \overline{\psi}^f\left(i\gamma^\mu\partial_\mu - m^f\right)\psi^f - g\overline{\psi}^f\gamma_\mu A^\mu\psi^f, & (2.1.8)\\ F^{\mu\nu} &= \partial^\mu A^\nu - \partial^\nu A^\mu + ig\left[A^\mu, A^\mu\right]. & (2.1.9) \end{aligned}$$

The first term is purely bosonic and contains, besides the kinetic term $\mathrm{Tr}\left[\partial^\mu A^\nu \partial_\mu A_\nu\right]$, cubic and quartic self-interactions of the gauge field A^μ. The second term is the kinetic and mass term for the quarks[1] and the last term expresses the antiquark-gauge-quark interaction.

Depending on the quark masses, the QCD Lagrangian (2.1.8) enjoys, apart from gauge invariance, different flavour symmetries, i.e. symmetries under transformations that mix the flavour index f while keeping all others fixed:

	Classical symmetry
Massless quarks	$SU(N_f)_V \times U(1)_V \times SU(N_f)_A \times U(1)_A$
Degenerate quark masses	$SU(N_f)_V \times U(1)_V$
Arbitrary quark masses	$U(1)^{N_f}$

.

Here V stands for vector and A for axialvector. For massless quarks we have maximal chiral symmetry. $U(1)_V$ is the symmetry associated to baryon number conservation while the $U(1)_A$ symmetry does not survive quantisation due to the non-invariance of the path-integral measure (the axial anomaly). $SU(N_f)_V$ is the N_f-isospin symmetry and survives quantisation while the $SU(N_f)_A$ symmetry is spontaneously broken.

The mass term of the Lagrangian explicitly breaks chiral symmetry. The vector symmetries survive for degenerate masses. In particular, in the real world $m_u \approx m_d$ so $SU(2)_V$, isospin, is an good approximate symmetry which can be enlarged to $SU(3)_V$ if also the strange quark is considered degenerate. For generic masses, $U(1)^{N_f}$ is the remaining symmetry which is associated to the conservation of each flavour and includes $U(1)_V$.

In general, to each quark the baryon number $\mathcal{B} = \frac{1}{3}$ and the flavour quantum numbers

[1] a $\mathbb{1}_{4\times4}$ spin matrix is understood in the latter as well as an overall $\mathbb{1}_{3\times3}$ colour matrix

	u	d	s	c	b	t
I_z	$1/2$	$-1/2$	0	0	0	0
S	0	0	-1	0	0	0
C	0	0	0	$+1$	0	0
B	0	0	0	0	-1	0
T	0	0	0	0	0	$+1$

Table 2.1: Flavour quantum numbers of the quarks. I_z is the z-axis projection of the isospin, S the strangeness, C the charmness, B the bottomness and T the topness. Antiquarks carry the opposite signs.

of Tab. (2.1) are associated.

2.1.2 Quantisation and the QCD Hilbert space

The difference between a classical and a quantum system resides in the fact that, given a classical action S of variables ϕ, not only the $\delta S = 0$ solution will be the dynamical one but each variable contributes with a weight given by the exponential of the action. A naive application of this concept to QCD results in a partition function

$$Z = \int DA_\mu D\psi D\overline{\psi} e^{iS_{cl}\left[\psi,\overline{\psi},A_\mu\right]}, \tag{2.1.10}$$

where S_{cl} refers to the classical action of the previous subsection. As for general continuum gauge theories, some complications arise in this quantisation procedure. The presence of all gauge-equivalent degrees of freedom in Eq. (2.1.10) leads to an over-counting of the path-integral making it infinite. In light of the Faddeev-Popov procedure, after fixing a gauge it is possible to factor out from Eq. (2.1.10) the infinite contribution (which cancels out in the expectation values) leading to the partition function for QCD

$$Z = \mathcal{N} \int DA_\mu D\psi D\overline{\psi} DcDc^* e^{i\left(S_{cl}\left[\psi,\overline{\psi},A_\mu\right]+S_{gf}[A_\mu,c,c^*]\right)}, \tag{2.1.11}$$

which includes unphysical ghost fields, c and c^*. We end up with a general non-perturbative formalism from which all features of the strong interactions could in principle be derived. Correlator functions can be generated from Eq. (2.1.11) equipped with a source term and quark and gluon operators can be defined. In the high-energy limit a perturbative treatment can be performed and results can be compared to experiment.

Physical spectrum of QCD from quarks and gluons The set of physical states of QCD is highly complicated. These include all stable (under the strong interaction) particles, hadrons as pions and protons as well as stable atomic nuclei. Among the zoo of particles that have been discovered and that are listed on the particle data group [7], only a few are actually stable under the strong interaction, even fewer if considering also electromagnetism and weak interactions. The majority are instead resonances which can, however, be treated as stable in those contexts where the decay width is small enough to have no significant impact.

The classification of the physical spectrum derives from the symmetries of QCD. Apart from the Poincaré symmetry, which for QCD includes also parity and time-reversal and which results in the classification of states in terms of momenta and angular momenta (described in Sec. (1.2)), conservation of flavour is always valid in QCD. The spectrum is then separated into sectors of well defined flavour quantum numbers as strangeness and charmness.

On the other hand, the QCD Lagrangian is expressed in terms of quarks and gluons. The connection between the quark-gluon perspective and the physical spectrum is absolutely non trivial. When expressing the latter in terms of the former, in light of confinement which is a non-perturbative feature of QCD, only gauge-invariant combinations out of quarks and gluons are to be formed to match the colourless spectrum observed.

From quarks q and antiquarks $\overline{q}$ living respectively in the fundamental **3** and anti-fundamental $\overline{\mathbf{3}}$ representation of the $SU(3)$ gauge group, gauge-invariant combinations can be formed by tensor products $q\overline{q}$ and qqq, which are the (conventional) mesons and baryons, respectively. Gauge-invariant combinations are not limited to these, as any exotic aggregate of $q\overline{q}$ and qqq results in a singlet. We have tetraquarks $(qq)(\overline{q}\overline{q})$ made out of a diquark and an antidiquark, mesonic molecules $(q\overline{q})(q\overline{q})$, pentaquarks $(qq)(qq)\overline{q}$, molecules $(qqq)(\overline{q}q)$ and so on. In addition, gluons g living in the adjoint **8** representation can form colourless objects, either by themselves, creating e.g. glueballs gg, or in association with quarks, forming for instance hybrid mesons $q\overline{q}g$ or hybrid baryons $qqqg$.

Matrix elements between the gauge-invariant operators and the physical states and the resulting decay constants provide the bridge between the two aspects of the theory.

J^P	(s,l)
0^-	$(0,0)$
0^+	$(1,1)$
1^-	$(1,0)$ or $(1,2)$
1^+	$(0,1)$ or $(1,1)$
2^-	$(0,2)$ or $(1,2)$
2^+	$(1,1)$ or $(1,3)$
$\vdots$	$\vdots$

Table 2.2: Spin-orbital angular momentum combinations for a given J^P.

2.1.3 The quark model for mesons

In the quark model only the simplest gauge-invariant combinations, $q^f\overline{q}^{f'}$ for mesons and $q^{f_1}q^{f_2}q^{f_3}$ for baryons, are taken as the fundamental structure of the hadrons[2]. In this framework, $q^f\overline{q}^{f'}$ and $q^{f_1}q^{f_2}q^{f_3}$ define the mesons and hadrons, respectively.

Let us focus on the first. The flavour quantum numbers listed in Tab. (2.1) are additive so that a first classification of mesons, which have (additive) baryon number $\mathcal{B}=0$, is in terms of their flavour content. For instance, $\overline{c}s$ has zero flavour quantum numbers except for $C=S=-1$ while the non zero flavour quantum numbers of $\overline{s}d$ are $S=1$ and $I_z=-\frac{1}{2}$. No mesons are believed to be formed by the top quark as it decays too quickly to form one.

A second classification of the mesons is provided by their angular momentum. The addition of the $\frac{1}{2}$ spins of the quark and anti-quark results in a meson with either spin 1 or 0, $\frac{1}{2}\otimes\frac{1}{2}=1,0$. There is no limit on the orbital angular momentum of the quarks, which can be any $l=0,1,2,...$ with parity $P=(-1)^{l+1}=\pm1$ and charge conjugation $C=(-1)^{l+s}$ for unflavoured mesons $q^f\overline{q}^f$. Thus, combining spin and orbital angular momentum, mesons can by classified according to the total angular momentum, parity and charge conjugation[3], J^{PC}. As shown in Tab. (2.2), a given J^P does not identify a unique spin-orbital combination except for the $J=0$ case.

Mesonic states of the form $0^{+-},1^{-+},2^{+-}...$ as well as 0^{--} are legitimate states for QCD but are not allowed within the quark model.

The mesons states we obtained, in the form $q\overline{q}'$, can be rearranged in multiplets according to the representations of the vector special unitary group. In particular, in terms of the isospin group $SU(2)$, the light quarks u and d with $I_z=\pm\frac{1}{2}$ correspond to an isodoublet

[2]The notion of quark was introduced in this context before the advent of QCD as an attempt to classify and explain the zoo of hadrons which were relentlessly being discovered.

[3]Also radial excitations are present.

in the fundamental representation $\mathbf{2}$ with $I = \frac{1}{2}$. The corresponding antiquarks live in $\overline{\mathbf{2}}$ representation and the combination $\mathbf{2} \otimes \overline{\mathbf{2}} = \mathbf{3} \oplus \mathbf{1}$ leads to an isotriplet and an isosinglet. For $J^P = 0^-$ these are respectively associated to the $I = 1$ pions (π^+, π^0, π^-) and to the $I = 0$ η_0 state. Mesons with only one light quark carry the isospin of the light quark. For instance, Kaons are identified by two $I = \frac{1}{2}$ doublets, (K^+, K^0) and $\left(K^-, \overline{K}^0\right)$.

When isospin is considered as a true (or at least an approximate) symmetry, this arrangement becomes particularly useful as the degeneracy of the masses of the light quarks is reproduced in the degeneracies of the particles composing each multiplet. By extension, also the enlarged $SU(3)$ flavour group leads to degenerate multiplets when all u d and s quarks are treated with the same mass.

2.2 QCD on the lattice

The first step in constructing a formulation of QCD accessible for numerical simulations is to set up a discretised Euclidean spacetime. The relevant formulas can be found in App. (A.2).

Once a lattice is introduced, a discretised action has to be defined on it such that Euclidean QCD is reproduced in the continuum limit. The choice of the lattice action is not unique as any kind of discretisation which differs by irrelevant operators all lead to the same continuum limit. Some of them may be easier to simulate, others may lead to reduced discretisation errors. In any case, the lattice introduces a cutoff a which provides a non-perturbative regularisation of the continuum theory. In momentum space this becomes $\frac{\pi}{a}$ (see App. (A.2)) and therefore only low energy quantities, at momentum scales less than $\frac{\pi}{a}$, can be calculated.

While the identification of QCD in the continuum limit is mandatory for a lattice action, preserving gauge invariance also at finite a is strongly advisable in order to benefit from simplifying relations that this symmetry guarantees. In the next two subsections the simplest gauge-invariant actions will be introduced.

2.2.1 The pure gluonic action

We define the gauge fields as dimensionless elements $U_\mu(x)$ of $SU(3)$, where x denotes the space-time point and $\mu = 1, 2, 3, 4$ is the directional index. They are represented as links between two adjacent points and are thus referred to as link variables. The index μ can be

extended also to negative values, $\mu = -1, -2, -3, -4$, once the connection between opposite signs is defined:

$$U_{-\mu}(x) = U_{\mu}^{\dagger}(x - \hat{\mu}). \tag{2.2.1}$$

A local gauge transformation is implemented by a local $SU(3)$ matrix,

$$\Omega(x) = e^{i\omega_a(x)t_a}. \tag{2.2.2}$$

which, apart for the discontinuous range of x, it is exactly the same of the continuum counterpart Eq. (2.1.7).

The gauge transformation applied on the link variables is defined via

$$U_{\mu}(x) \rightarrow U_{\mu}^{'}(x) = \Omega(x) U_{\mu}(n) \Omega^{\dagger}(x + \hat{\mu}), \tag{2.2.3}$$

$$U_{\mu}^{\dagger}(x) \rightarrow U_{\mu}^{\dagger'}(x) = \Omega(x + \hat{\mu}) U_{\mu}^{\dagger}(x) \Omega^{\dagger}(x). \tag{2.2.4}$$

The gluon part of the action is to be constructed from gauge invariant combinations of the link variables. For this purpose, given a field configuration $U_{\mu}(x)$, we can build a "path" between two points x and y, which is a $SU(3)$ matrix defined as

$$P_C[U] = U_{\mu_0}(x) U_{\mu_1}(x + \hat{\mu}_0) ... U_{\mu_{N-1}}(y - \mu_{\hat{N}-1}), \tag{2.2.5}$$

where the directional indices are allowed to be negative. A closed path, where $y = x$, is called a loop. The shortest non trivial loop is a plaquette, and is denoted as

$$\begin{aligned} U_{\mu\nu}(x) &= U_{\mu}(x) U_{\nu}(x + \hat{\mu}) U_{-\mu}(x + \hat{\mu} + \hat{\nu}) U_{-\nu}(x + \hat{\nu}) \\ &= U_{\mu}(x) U_{\nu}(x + \hat{\mu}) U_{\mu}^{\dagger}(x + \hat{\nu}) U_{\nu}^{\dagger}(x). \end{aligned} \tag{2.2.6}$$

Under a gauge transformation acting on Eq. (2.2.5) all Ω terms lying between the fields cancel out, leaving just the endpoint terms:

$$P_C[U] \rightarrow P_C[U'] = \Omega(x) P_C[U] \Omega^{\dagger}(y). \tag{2.2.7}$$

It is clear that, due to the cyclic property of the trace, when C is a loop, the object $\mathrm{Tr} P_C[U]$ is gauge invariant and does not depend on the endpoint $y = x$.

For a given gluon configuration $U_{\mu}(x)$, the Wilson gauge action is defined to be [15]

$$S_G[U] = \frac{2}{g^2} \sum_{x \in \Lambda} \sum_{\mu<\nu} \mathrm{ReTr}\left[1 - U_{\mu\nu}(x)\right], \tag{2.2.8}$$

where the sum $\sum_{\mu<\nu}$ is over all positively oriented plaquettes, $1 \leq \mu < \nu \leq 4$ and g is the bare strong coupling.

The fact that this action reproduces the correct (naive) continuum limit is seen by expressing the link variables, elements of $SU(3)$, in terms of fields $A_\mu(x)$ that live in the algebra of the group,

$$U_\mu(x) = e^{iaA_\mu(x)} \equiv e^{iaA_{\mu a}(x)t_a}, \tag{2.2.9}$$

$$F_{\mu\nu}(x) = \partial_\mu A_\nu(x) - \partial_\nu A_\mu(x) + i\left[A_\mu(x), A_\nu(x)\right]. \tag{2.2.10}$$

Then, one can show that the action Eq. (2.2.8) when expressed in terms of $A_\mu(x)$ reads

$$S_G[A] = \frac{1}{2g^2} a^4 \sum_{x \in \Lambda} \sum_{\mu\nu} \mathrm{Tr}\left[F_{\mu\nu}(x) F_{\mu\nu}(x)\right] + \mathcal{O}\left(a^2\right). \tag{2.2.11}$$

When letting $a \to 0$, derivatives in $F_{\mu\nu}$ become continuous, $a^4 \sum_{x \in \Lambda} \to \int d^4x$ and $S_G[A]$ approaches the (Euclidean) continuum gauge action.

2.2.2 The Wilson fermionic action

Similarly to the continuum, fermionic fields representing quark and anti-quarks $\psi^f_{i\alpha}(x)$ and $\overline{\psi}^f_{i\alpha}(x)$ are introduced on the lattice. The flavour f, colour i and spin α indices are identical to the continuum, the difference being only the fact that the spacetime variables are discrete. Also, the dimensions are the same, $[\psi] = \left[\overline{\psi}\right] = \frac{3}{2}$. As in the continuum, the gauge transformation on the fermionic fields read

$$\psi^f_\alpha(x) \;\to\; \Omega(x)\,\psi^f_\alpha(x), \tag{2.2.12}$$

$$\overline{\psi}^f_\alpha(x) \;\to\; \overline{\psi}^f_\alpha(x)\,\Omega^\dagger(x), \tag{2.2.13}$$

where $\Omega(x)$ is the $SU(3)$ matrix Eq. (2.2.2). Introducing the covariant derivative operator D_μ and covariant Laplacian D_μ^2 by

$$D_\mu \psi(x) = \frac{1}{2a}\left[U_\mu(x)\,\psi(x+\hat{\mu}) - U_{-\mu}(x)\,\psi(x-\hat{\mu})\right], \tag{2.2.14}$$

$$D_\mu^2 \psi(x) = \frac{1}{a^2}\left[U_\mu(x)\,\psi(x+\hat{\mu}) + U_{-\mu}(x)\,\psi(x-\hat{\mu}) - 2\psi(x)\right], \tag{2.2.15}$$

the Wilson fermionic action can by defined (for $r=1$):

$$S_W\left[\psi,\overline{\psi},U\right] = a^4 \sum_x \overline{\psi}^f(x)\left(\gamma_\mu D_\mu - \frac{ar}{2}D_\mu^2 + m^f\right)\psi^f(x). \tag{2.2.16}$$

It is made up of three terms, with kernels $\gamma_\mu D_\mu$, $-\frac{ar}{2}D_\mu^2$ (a sum over μ is understood in both) and m^f. The first and last term resemble the continuum action. The correctness of the continuum limit and gauge invariance can be easily checked. A convenient way to express the Wilson action Eq. (2.2.16) is via the Dirac matrix $D_U(y;x)$,

$$S_W\left[\psi,\overline{\psi},U\right] = a^4 \sum_{yx} \overline{\psi}^f(y)\, D_U^f(y;x)\, \psi^f(x), \tag{2.2.17}$$

$$D_U^f(y;x) \equiv \left(m^f + \frac{4r}{a}\right)\delta_{y,x} - \sum_{\mu=1}^{4} \frac{(r-\gamma_\mu)\,U_\mu(y)\,\delta_{y+\hat{\mu},x} + (r+\gamma_\mu)\,U_{-\mu}(y)\,\delta_{y-\hat{\mu},x}}{2a}. \tag{2.2.18}$$

For each flavour f, it is a matrix $D^f_{i\alpha,j\beta}(y,x)$ in all spin, colour and spacetime indices. In terms of explicit spin-colour indices, the first term contains a $\delta_{ij}\delta_{\alpha\beta}$ factor and in the second we have $r\delta_{ij}$. Note that $\left[D_U^f(y;x)\right] = 1$ so that $[S_W] = 0$. It satisfies γ_5-hermiticity, i.e. $\gamma_5 D \gamma_5 = D^\dagger$ where the symbol $\dagger$ is applied to all indices, spin, colour and spacetime.

The Wilson term The inverse of the Dirac matrix for a given flavour f is the propagator of the corresponding quark. As we shall see, performing inversions of Dirac matrices is a central topic in Lattice QCD. For the free case, i.e. setting $U_\mu(x) = \mathbb{1}$ for each μ, x, an exact form of the propagator exists. For flavour f we have

$$D_0(x;0) = \left(m + \frac{4r}{a}\right)\delta_{x,0} - \frac{1}{2a}\sum_\mu \left[(r-\gamma_\mu)\,\delta_{x+\hat{\mu},0} + (r+\gamma_\mu)\,\delta_{x-\hat{\mu},0}\right] \tag{2.2.19}$$

and its Fourier transform can be shown to be

$$a^{-4}\tilde{D}_0(p) = \sum_x D_0(x;0)\, e^{-ipx} = m + \frac{r}{a}\left(4 - \sum_\mu \cos(p_\mu a)\right) + \frac{i}{a}\sum_\mu \gamma_\mu \sin(p_\mu a),$$

which has inverse

$$G_0(p) \equiv \tilde{D}_0^{-1}(p) = a^{-4}\frac{m + \frac{r}{a}\left(4 - \sum_\mu \cos(p_\mu a)\right) - \frac{i}{a}\sum_\mu \gamma_\mu \sin(p_\mu a)}{\left[m + \frac{r}{a}\left(4 - \sum_\mu \cos(p_\mu a)\right)\right]^2 + \frac{1}{a^2}\sum_\mu \sin^2(p_\mu a)}. \tag{2.2.20}$$

The importance of the factor r, deriving from the $-\frac{ar}{2}D_\mu^2$ term in Eq. (2.2.16) which was added by Wilson, can be seen here. Indeed, for $r = 0$ and for simplicity $m = 0$, we would have sixteen poles for $G_0(p)$ corresponding to the solutions of

$$\sin^2(p_1 a) + \sin^2(p_2 a) + \sin^2(p_3 a) + \sin^2(p_4 a) = 0. \tag{2.2.21}$$

Explicitly, the expression is zero when choosing $p_\mu a = 0, \pi$, i.e.,

$$pa = (0,0,0,0)\ ,\ (\pi,0,0,0)\ ,\ (0,\pi,0,0)\ ,...,\ (\pi,\pi,\pi,\pi) \tag{2.2.22}$$

This is a problem for the quantised theory as, apart from the physical pole at $(0,0,0,0)$, fifteen unphysical degrees of freedom, called doublers, survive the continuum limit. With the Wilson term, the doublers acquire a mass $m + \frac{2rl}{a}$ and thus become very heavy in the continuum ($a \to 0$) and decouple from the theory .

The inclusion of the Wilson term fixes the doublers problem but comes at a price as it introduces other issues. Firstly, chiral symmetry on the lattice is explicitly broken by the Wilson term. Although chiral symmetry is restored in the continuum, the presence of the Wilson term is unsettling when considering observables for which chiral symmetry plays a crucial role. The issue is solved by generalising the definition of chiral transformation on the lattice in terms of the Ginsparg-Wilson equation.

Secondly, the Wilson action has larger $\mathcal{O}(a)$ discretisation errors. We will now discuss how these errors can be removed.

Clover improvement The freedom in the choice of the lattice action that was mentioned at the beginning of this section is exploited by the Symanzik improvement programme [16] which, by adding irrelevant operators with suitable coefficients to a given action, identifies in a systematic way a new action with the same continuum limit but with reduced discretisation

errors. Specifically for the Wilson action, at leading order $\mathcal{O}(a)$, one can determine five operators with the same symmetries of the Wilson action which are reduced to three when imposing the Dirac field equation. Two of them have the same form of the existing action and their net effect consists in a redefinition of the mass and the coupling. The remaining term is explicitly added to the Wilson action, resulting in the so-called clover-improved action:

$$S_{WC} = S_W + c_{SW} a^4 \sum_x \sum_{\mu<\nu} \overline{\psi}(x)^f \sigma_{\mu\nu} \frac{a}{2} F_{\mu\nu}(x) \psi^f(x), \tag{2.2.23}$$

where $\sigma_{\mu\nu} = [\gamma_\mu, \gamma_\nu]/2i$ and

$$F_{\mu\nu}(x) = \frac{-i}{8a^2}(Q_{\mu\nu} - Q_{\nu\mu}), \tag{2.2.24}$$

$$Q_{\mu\nu} = U_{\mu\nu}(x) + U_{\nu,-\mu}(x) + U_{-\nu,\mu}(x) + U_{-\mu,-\nu}(x). \tag{2.2.25}$$

$Q_{\mu\nu}$ is a sum over four plaquettes Eq. (2.2.6) resulting in a shape that reminds one of a clover leaf, hence the name. If the coefficient c_{SW} is tuned non-perturbatively in a convenient way, the resulting action have discretisation errors of order $\mathcal{O}(a^2)$ [17].

2.2.3 Path integral quantisation on the lattice

We have seen how to build a gauge invariant action which reproduces QCD in the continuum. The quantisation of the classical system is obtained via the path integral

$$Z = \int \mathcal{D}[U] \mathcal{D}\left[\psi\overline{\psi}\right] e^{-\left(S_G[U] + S_F\left[U,\psi,\overline{\psi}\right]\right)}. \tag{2.2.26}$$

$S_G[U]$ and $S_F\left[U,\psi,\overline{\psi}\right]$ are the gauge and fermionic actions and the measure is

$$\mathcal{D}[U] = \prod_x \prod_\mu dU_\mu(x), \tag{2.2.27}$$

$$\mathcal{D}\left[\psi\overline{\psi}\right] \equiv \prod_x \prod_{f,i,\alpha} d\psi^f_{\alpha i}(x)\, d\overline{\psi}^f_{\alpha i}(x). \tag{2.2.28}$$

Recall that each link $U_\mu(x)$, for fixed μ and x, is an element of $SU(3)$ and each integration $\int dU_\mu(x)$ is performed over the whole group. The measure $dU_\mu(x)$ is the Haar measure of $SU(3)$ which, by definition, is gauge invariant and is normalised to one, $\int dU_\mu(x) = 1$.

As fermions obey the Fermi statistics, the quark fields appearing in Eq. (2.2.26) are Grassmann variables and anti-commute with each other. This implies that the product of

two fermions at the same spacetime point and with same flavour/spin/colour index vanishes.

Since on the lattice the number of degrees of freedom is finite, gauge-fixing is not mandatory and ghost-fields are not needed. The path-integral Eq. (2.2.26) is ready to go.

Expectation values Expectation values have the form

$$\langle A\rangle = \frac{\int \mathcal{D}\left[U\right]\mathcal{D}\left[\psi\overline{\psi}\right] e^{-\left(S_G[U]+S_F\left[U,\psi,\overline{\psi}\right]\right)} A\left[U,\psi,\overline{\psi}\right]}{\int \mathcal{D}\left[U\right]\mathcal{D}\left[\psi\overline{\psi}\right] e^{-\left(S_G[U]+S_F\left[U,\psi,\overline{\psi}\right]\right)}}, \tag{2.2.29}$$

where the denominator is the partition function Z, Eq. (2.2.26). The functional $A\left[U,\psi,\overline{\psi}\right]$ usually depends on a subset of indices of the fields, for instance on only those fields which have spacetime label x. An important simple example is

$$A\left[U,\psi,\overline{\psi}\right] = \psi^f_{\alpha i}\left(y\right)\overline{\psi}^f_{\beta j}\left(x\right), \tag{2.2.30}$$

a quadratic functional that depends only on the two fermionic fields at the lattice coordinates shown. Then, also the lhs of Eq. (2.2.29) will carry the labels $(f,\alpha\beta,ij,yx)$ [4].

The measure and the exponential in Eq. (2.2.29) are gauge invariant, so $\langle A\rangle$ will be so if $A\left[U,\psi,\overline{\psi}\right]$ is.

Let us introduce the fermionic partition function,

$$Z_F\left[U\right] = \int \mathcal{D}\left[\psi\overline{\psi}\right] e^{-S_F\left[U,\psi,\overline{\psi}\right]} = \prod_f \det D^f\left[U\right]. \tag{2.2.31}$$

The second equality can be shown using the Grassmann nature of the fermionic fields and reduces $Z_F\left[U\right]$ to a product of determinants of the Dirac matrix which are called fermion determinants. Then, keeping in mind this relation, Eq. (2.2.29) can be written as

$$\langle A\rangle \equiv \left\langle \langle A\rangle^U_F \right\rangle_G = \frac{\int \mathcal{D}\left[U\right] e^{-S_G[U]} Z_F\left[U\right]\langle A\rangle^U_F}{\int \mathcal{D}\left[U\right] e^{-S_G[U]} Z_F\left[U\right]}, \tag{2.2.32}$$

$$\langle A\rangle^U_F = \frac{\int \mathcal{D}\left[\psi\overline{\psi}\right] e^{-S_F\left[U,\psi,\overline{\psi}\right]} A\left[U,\psi,\overline{\psi}\right]}{\int \mathcal{D}\left[\psi\overline{\psi}\right] e^{-S_F\left[U,\psi,\overline{\psi}\right]}}. \tag{2.2.33}$$

The expectation value of A is viewed as the expectation value of $\langle A\rangle^U_F$ with respect to

[4] This is just like a standard expectation value $\langle A\rangle_{1,3,8} = Z^{-1}\int dx_1...dx_9 x_1^5 x_3^{11} x_8 e^{-S(x_1,...,x_9)}$ where each index $a = 1,...,9$ would correspond to space-spin-colour-flavour.

the gluonic weight $Z^{-1}\mathcal{D}[U]\,e^{-S_G[U]}Z_F[U]$; $\langle A\rangle_F^U$ is in turn the expectation value of A with respect to the fermionic weight $Z_F^{-1}[U]\,\mathcal{D}\left[\psi\overline{\psi}\right]e^{-S_F\left[U,\psi,\overline{\psi}\right]}$. The symbol U in $\langle A\rangle_F^U$ emphasises that $\langle A\rangle_F$ is a functional of U. This is the case also if $A\left[U,\psi,\overline{\psi}\right]$ does not depend on the link variables U as the latter explicitly appear in the fermionic action.

The fermionic part For a given link configuration U, the fermionic expectation value $\langle A\rangle_F^U$ can be calculated exactly due to the gaussian nature of the fermionic action. The basic object is the fermionic expectation value of Eq. (2.2.30) which is basically the propagator with flavour f,

$$\left\langle \psi_{\alpha i}^f(y)\,\overline{\psi}_{\beta j}^f(x)\right\rangle_F^U = a^{-4}\left(D_{U,f}^{-1}\right)_{\alpha i,\beta j}(y;x)\,. \tag{2.2.34}$$

The γ_5-hermiticity of the Dirac matrix, if valid, is inherited by its inverse.

More general functions are combinations of products of quarks-antiquarks $\psi_{a_1}\overline{\psi}_{b_1}...\psi_{a_n}\overline{\psi}_{b_n}$ with U-dependent coefficients[5]. Here all spin-colour-spacetime indices for quarks and antiquarks have been condensed to a_i and b_i, respectively. Then, Wick's theorem asserts that the fermionic expectation value of $\psi_{a_1}\overline{\psi}_{b_1}...\psi_{a_n}\overline{\psi}_{b_n}$ is a sum over all $n!$ possible ways to contract a quark with an antiquark, more explicitly

$$\begin{aligned}\left\langle \psi_{a_1}\overline{\psi}_{b_1}...\psi_{a_n}\overline{\psi}_{b_n}\right\rangle_F^U &= \frac{\int\mathcal{D}\left[\psi\overline{\psi}\right]e^{-S_F\left[U,\psi,\overline{\psi}\right]}\psi_{a_1}\overline{\psi}_{b_1}...\psi_{a_n}\overline{\psi}_{b_n}}{\int\mathcal{D}\left[\psi\overline{\psi}\right]e^{-S_F\left[U,\psi,\overline{\psi}\right]}} \\ &= (-1)^n\sum_{P(1,2,...,n)}\mathrm{sign}(P)\prod_{k=1}^{n}a^{-4}\left(D_U^{-1}\right)_{a_k b_{P_k}}\,,\end{aligned} \tag{2.2.35}$$

where $P(1,2,...,n)$ is a permutation of $(1,2,...,n)$. Eq. (2.2.35) refers to one flavour but it is generalisable to products of multiple flavours due to factorisation of Eq. (2.2.33) with respect to f.

The fermionic expectation value is reduced to the calculation of the Dirac matrix inverse. Please note that usually D is a sparse matrix (compare with Eq. (2.2.18) for the Wilson case) but its inverse is not. Even just storing $2\times12\times12\times N_L^3\times N_T\times N_L^3\times N_T$ real numbers in a RAM memory is today technologically prohibitive. How to by-pass this problem will be seen in the following sections.

The gluonic part Once the Wick contractions are performed, $\langle A\rangle_F^U$ is known. This is not the end of the story, as the integral Eq. (2.2.32) has still to be calculated to obtain our

[5]The coefficients can involve e.g. Dirac matrices, Levi-Civita symbols or Fourier-transforming exponentials.

desired answer $\langle A \rangle$. A direct numerical calculation is excluded due to the large number of degrees of freedom but a importance sampling Monte Carlo approach can be applied. N_C link configurations U_i are generated weighted on $Z^{-1}\mathcal{D}[U]\, e^{-S_G[U]} Z_F[U]$ and

$$\langle A \rangle = \frac{1}{N_C} \sum_{i=1}^{N_C} \langle A \rangle_F^{U_i} + \mathcal{O}\left(\frac{1}{\sqrt{N_C}}\right). \tag{2.2.36}$$

The integral Eq. (2.2.29) can be estimated at the price of introducing statistical errors which decrease with the reciprocal of the square root of the number of configurations. The link configurations are not independent as they form a Markov chain sequence $U_0 \to U_1 \to ....$ Selecting only configurations separated by enough steps or binning over the configurations are standard ways to deal with autocorrelation issues.

The generation of link configurations involves the calculation of fermion determinants Eq. (2.2.31) which is not an easy task. The fermion determinant for flavour f can be interpreted in a hopping parameter expansion as the exponential of a sum over closed fermionic loops. As $m_f \to \infty$, the contributions of the loops vanish, i.e. $\det D^f[U] \to 1$. Hence, setting the determinant to unity for higher mass flavours is a very reasonable approximation. Setting all determinants to unity, or quenching, is instead a crude approximation and yields reasonable results only for a limited number of cases. In present simulations, one distinguishes between $N_f = 2$ simulations, where the (degenerate) light quarks are fully simulated, $N_f = 2 + 1$ simulations which includes the strange quark and $N_f = 2 + 1 + 1$ which includes the charm.

2.2.4 The lattice Hilbert space and the spectral decomposition

The path integral we obtained and discussed in the previous section is Euclidean, an essential requirement in order to interpret the exponential of the action as a probability weight function and to perform a Monte-Carlo simulation. The resulting expectation values are therefore also Euclidean. However, our physical world is Minkowskian and there is no guarantee that, in the continuum limit, our Euclidean correlators can be analytically continued to Minkowski space and will correspond to a physical Hilbert space with a well-behaved Hamiltonian (positive norm, bounded by below spectrum, Poincaré invariance etc.).

The Osterwalder-Schrader theorem [18] provides conditions to which continuum Euclidean correlators should comply in order for this to be true. These include $SO(4)$ (Euclidean) covariance, reflection positivity and other technical conditions.

These requirements can be adapted for lattice Euclidean correlators [19]. Alternatively,

for the lattice, if we are clever enough to construct an explicit strictly positive, bounded, symmetric, unique transfer matrix $\hat{T} = e^{-a\hat{H}}$ and identify operators evolving in Euclidean time,

$$\hat{O}(t) = e^{t\hat{H}} \hat{O}(0) e^{-t\hat{H}}, \tag{2.2.37}$$

such that

$$\lim_{T\to\infty} \langle O_2(t) O_1(0)\rangle_T = \lim_{T\to\infty} \frac{\mathrm{Tr}\left[\hat{O}_2(t)\hat{O}_1(0) e^{-T\hat{H}}\right]}{\mathrm{Tr}\left[e^{-T\hat{H}}\right]} = \langle 0|\hat{O}_2(t)\hat{O}_1(0)|0\rangle, \tag{2.2.38}$$

then the resulting lattice Hamiltonian $\hat{H}$ is unique and enjoys the physical properties for the discretised theory. A continuum Hamiltonian can then be identified by the limit

$$\hat{H}_{\text{cont.}} = \lim_{a\to 0} \hat{H} = \lim_{a\to 0} -\frac{1}{a}\log \hat{T}. \tag{2.2.39}$$

Such an explicit construction was made by Lüscher for the Wilson action [20].

In Eq. (2.2.38) the quantity $\langle O_2(t) O_1(0)\rangle_T$ is the expectation value Eq. (2.2.29) of $A = O_2(t) O_1(0)$, a product of functionals of quarks and gauge fields at time t and 0 for respectively $O_2(t)$ and $O_1(0)$. A subscript T is appended to highlight the finite time extent. The traces are defined in an operatorial sense, i.e. for an operator $\hat{A}$, $\mathrm{Tr}\left[\hat{A}\right] = \sum_i \langle i|\hat{A}|i\rangle$, where the sum runs over an orthonormal basis of the Hilbert space. The denominator identifies the partition function of the previous section, $Z_T = \mathrm{Tr}\left[e^{-T\hat{H}}\right]$.

Eigenstates of the lattice Hamiltonian Since lattice QCD is defined on a finite volume, the energy spectrum is discrete and can be identified by a discrete index n

$$\hat{H}|n\rangle = E_n|n\rangle \qquad n = 0, 1, 2, \ldots \quad . \tag{2.2.40}$$

We assume normalised eigenvectors $|n\rangle$ and sort them according to $E_0 = 0 \leq E_1 \leq E_2 \leq \ldots$. The vacuum energy E_0, corresponding to the vacuum state $|0\rangle$, is set to zero.

The eigenstates $|n\rangle$, for fixed E_n, contain degeneracies ruled by the symmetries of the lattice Hamiltonian. To see these, let us recall from chapter (1) and App. (A.1.4) that in the continuum Minkowski theory, the Hamiltonian eigenstates can be expressed in the form $|\,E\,\boldsymbol{p}\,j\,\sigma_j\,\mu\rangle$, Eq. (1.2.8), with E and $\boldsymbol{p}$ being the total energy and momentum of the state, $j = 0, \frac{1}{2}, 1, \frac{3}{2}, \ldots$ the total angular momentum (defined for $\boldsymbol{p} = 0$ but extended for general

$\boldsymbol{p}$) and $\sigma_j = -j, ..., j$ its projection to the z-axis. This classification is a consequence of the Poincaré group and the spatial symmetries are dictated by its subgroup $\mathcal{T}^3 \rtimes O(3)$, formed by the semidirect product of spatial translations with the group of rotations in three dimensions. Spatial reflections I_S are being explicitely considered now, $O(3) = SO(3) \times \{e, I_s\}$, so that j carries the parity label, $j^{\pm}$. Moreover, the fermionic semi-integer representations should be thought as single-valued representations of the double covering group[6] $O^D(3)$ of $O(3)$.

Following Ref. [21], on the lattice the symmetry is reduced to the analogous $\mathcal{T}^3_{\text{latt}} \rtimes O_h$, the semidirect product of the group of lattice spatial translations with the group of lattice spatial rotations (the octahedral group) and reflections, $O_h = O \times \{e, I_s\}$, which has 24×2 elements. Analogously to the continuum, the double cover group O_h^D of O_h should be considered[7] and has 96 elements.

In a lattice Hamiltonian eigenstate we can add to the energy label a total momentum label $\boldsymbol{p} = \frac{2\pi}{L}\boldsymbol{d}$ which is, however, restricted to the 3d-integer values of $\boldsymbol{d}$. Let us now fix $\boldsymbol{p}$. In contrast to the Minkowski continuum, where the little groups for each $\boldsymbol{p}$ are all isomorphic to each other and isomorphic to the common rotational group (for massive states), on the lattice this is no longer true. The group that satisfies $g\boldsymbol{p} = \boldsymbol{p}$ for each g is a subgroup of O_h^D and depends on $\boldsymbol{p}$ or, less restrictively, on classes of $\boldsymbol{p}$. The eigenstates in Eq. (2.2.40) may be then expressed as

$$|n\rangle = |E\, \boldsymbol{p}\, \Lambda_{\boldsymbol{p}}\, \sigma_{\Lambda_{\boldsymbol{p}}}\, \mu\rangle\,, \tag{2.2.41}$$

where $\Lambda_{\boldsymbol{p}}$ identifies a representations of the little group of $\boldsymbol{p}$ (just as j labels the representations of the rotation group in continuum Minkowski), $\sigma_{\Lambda_{\boldsymbol{p}}}$ identifies a specific vector in that representation (a row) and, as usual, μ includes additional non-spatial symmetries. For each $\boldsymbol{p} = \frac{2\pi}{L}\boldsymbol{d}$, there is a finite number of irreps $\Lambda_{\boldsymbol{p}}$ (in contrast to the infinite span of the label j in the continuum) and, for each $\Lambda_{\boldsymbol{p}}$, there is a number of energies $E = E_m$ each degenerate in the remaining $\sigma_{\Lambda_{\boldsymbol{p}}}$ labels.

The little group for $\boldsymbol{p} = 0$ is the full group O_h^D itself. The 96 elements of O_h^D are distributed in sixteen classes, therefore there are sixteen (non-double-valued) irreducible representations $\Lambda_{\boldsymbol{0}}$,

[6] Just like $SU(2)$ being the double covering group of $SO(3)$.

[7] The notion of cover of a group presumes a topological structure which is absent for finite groups. Nevertheless, in this context, the notion can be transferred from the infinite topological counterpart.

	Bosonic					Fermionic			
Irreps of O_h^D	$A_1^\pm$	$A_2^\pm$	$E^\pm$	$T_1^\pm$	$T_2^\pm$	$G_1^\pm$	$G_2^\pm$	$H^\pm$	(2.2.42)
Dim.	1	1	2	3	3	2	2	4	

We distinguish between bosonic representations, which are the lattice analogous to the continuum representations identified by $j = 0^\pm, 1^\pm, 2^\pm, ...$ and fermionic representations, analogous to $j = \frac{1}{2}^\pm, \frac{3}{2}^\pm, \frac{5}{2}^\pm, ...$.

Let us consider now a continuum state $|\, E\, \boldsymbol{p}\, j\, \sigma_j\, \mu\rangle$ for simplicity at zero total momentum and focus on its rotational part $|\, j\, \sigma_j\, \rangle$. On the state $|\, j\, \sigma_j\, \rangle$, for fixed j, the irreducible representation $g \to D^{(j)}(g)$ of the continuous rotational group $O^D(3)$ acts. This action can be restricted to elements of $g \in O_h^D$. Being O_h^D a subgroup of $O^D(3)$, the resulting subduced representation $D^{(j)}(g)\Big|_{g\in O_h^D}$ is also a representation for O_h^D, although it is in general a reducible one. This means that the vector space $V^{(j)}$ associated to the j-th representation of $O^D(3)$ can be decomposed into vector spaces $V^{(\Lambda)}$ of the representation Λ,

$$V^{(j)} = \bigoplus_{\Lambda} m_{j\Lambda} V^{(\Lambda)}, \tag{2.2.43}$$

where $m_{j\Lambda}$ denotes the multiplicity in the decomposition. Correspondingly, an orthonormal basis $|\, j\, \sigma_j\, \rangle$ in $V^{(j)}$ can be decomposed into orthonormal bases $|\, \Lambda\, \sigma_\Lambda\, ;\, \eta\, \rangle$ of the η-th copy of $V^{(\Lambda)}$,

$$|\, j\, \sigma_j\, \rangle = \sum_{\Lambda} \sum_{\eta=1}^{m_{j\Lambda}} \langle\, \Lambda\, \sigma_\Lambda\, ;\, \eta\, |\, j\, \sigma_j\, \rangle\, |\, \Lambda\, \sigma_\Lambda\, ;\, \eta\, \rangle\, . \tag{2.2.44}$$

Under the action of $g \in O_h^D$, the state $|\, \Lambda\, \sigma_\Lambda\, ;\, \eta\, \rangle \to |\, \Lambda\, \sigma'_\Lambda\, ;\, \eta\, \rangle$ remains in the same subspace.

Integer representations j couple only to the bosonic representations and semi-integer only to fermionic. Explicitly, for j up to $\frac{9}{2}$, the decomposition reads

$$\begin{aligned}
V^{(0)} &= A_1 & V^{(\frac{1}{2})} &= G_1 \\
V^{(1)} &= T_1 & V^{(\frac{3}{2})} &= H \\
V^{(2)} &= E \oplus T_2 & V^{(\frac{5}{2})} &= G_2 \oplus H \\
V^{(3)} &= A_2 \oplus T_1 \oplus T_2 & V^{(\frac{7}{2})} &= G_1 \oplus G_2 \oplus H \\
V^{(4)} &= A_1 \oplus E \oplus T_1 \oplus T_2 & V^{(\frac{9}{2})} &= G_1 \oplus 2H \\
&\vdots
\end{aligned} \tag{2.2.45}$$

A $\pm$ symbol is understood in both sides of the equations, for instance $V^{(2)\pm} = E^\pm \oplus T_2^\pm$.

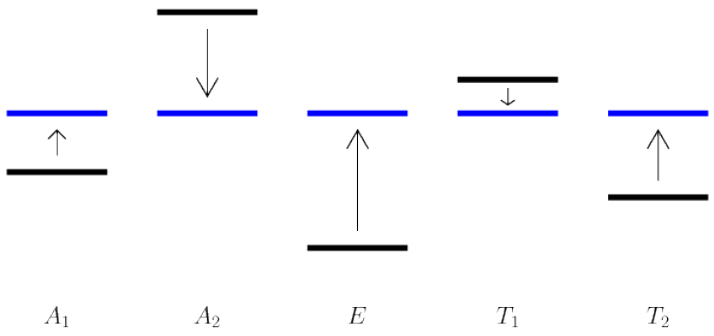

Figure 2.2.1: Lattice energy levels approaching the continuum value as $a \to 0$.

Of course, the dimensions $2j+1$ at the left-hand-sides are reproduced to the corresponding right-hand-sides, e.g. $2\frac{7}{2}+1 = 2+2+4$.

This discussion applies independently from the lattice theory - it is always possible to think of such a decomposition for states in the continuum. However, the relevance of the decomposition is based on the fact that the degeneracy of the continuum Hamiltonian in the whole $V^{(j)}$ is broken to a degeneracy for just each subspace $V^{(\Lambda)}$ for the lattice Hamiltonian. As the lattice spacing approaches zero, the discrete energy levels approach the common continuum value and the degeneracy of the whole $V^{(j)}$ is recovered. This is depicted schematically in Fig. (2.2.1). If we are able to access the lattice energy levels (and how this can be done will be shown in a while), simulations at multiple lattice spacings and an extrapolation to $a \to 0$ can often provide the correct identification of the continuum angular momentum.

We can invert the decompositions Eq. (2.2.45) to see to which j each Λ couples to,

Λ	j	Λ	j
A_1	$0, 4, 6, ...$	G_1	$\frac{1}{2}, \frac{7}{2}, \frac{9}{2}, ...$
A_2	$3, 6, 7, ...$	G_2	$\frac{5}{2}, \frac{7}{2}, \frac{11}{2}, ...$
E	$2, 4, 5, ...$	H	$\frac{3}{2}, \frac{5}{2}, \frac{7}{2}, ...$
T_1	$1, 3, 4, ...$		
T_2	$2, 3, 4, ...$		

and, as usual, a $\pm$ is understood. To a given irrep Λ corresponds an infinite number of continuum angular momenta.

We restricted ourselves to the sector of zero total momentum $\boldsymbol{p} = 0$, both on the lattice and on the continuum. For states with $\boldsymbol{p} = \frac{2\pi}{L}\boldsymbol{d} \neq 0$, the same assertions apply when replacing O_h^D and its irreducible representations $\Lambda \equiv \Lambda_{\mathbf{0}}$ with the little group of $\boldsymbol{p}$ and its

irreps $\Lambda_{\boldsymbol{p}}$.

The discussion in this paragraph is general and is relevant for any kind of state. In particular, the same considerations are valid for one-particle states for which the total angular momentum is simply its spin. For instance, a particle in the continuum with spin two in the centre of mass frame corresponds to two non-degenerate states (E and T_2) on the lattice.

Two-particle states In the continuum, we have seen that the energy spectrum of the Hamiltonian in the CM frame is made of discrete one-particle states, and continuum spectra for multi-particle states each starting from the threshold of their production. In particular, two particle states in the CM frame have their energies parametrised by the continuous parameter $k = |\boldsymbol{k}| \in [0, \infty[$ according to Eq. (1.2.11), starting from the threshold, at $k = 0$ or at $E = m_1 + m_2$. In the finite box instead, only a discrete number of k in the range $[0, \infty[$ are present and

$$E_n = \sqrt{m_1^2 + k_n^2} + \sqrt{m_2^2 + k_n^2} \tag{2.2.46}$$

$$= \sqrt{m_1^2 + q_n^2} + \sqrt{m_2^2 + q_n^2} + \Delta E_n, \qquad n = \sqrt{|\boldsymbol{n}|^2} = \sqrt{0}, \sqrt{1}, \sqrt{2}, \dots . \tag{2.2.47}$$

In Eq. (2.2.46), the momenta $\boldsymbol{k_n}$ do not have the form $\frac{2\pi}{L}\boldsymbol{n}$ valid for non-interacting particles, the 3d-integers $\boldsymbol{n}$ are instead replaced by an element of $\mathbb{R}^3$. Indeed, in contrast to the continuum case, at finite volume the two particles are always within interaction range and necessarily interact. The interaction is made explicit in the second line, where the energy is expressed in terms of "free" momenta $\boldsymbol{q_n} = \frac{2\pi}{L}\boldsymbol{n}$ ($\boldsymbol{n} \in \mathbb{Z}^3$ in a continuous box) added to a usually small interaction term ΔE_n that depends on L. Note that, although in a lower amount, the masses m_i themselves depend on L due to polarisation effects. As in the continuum case, the energy E_n is degenerate for a fixed $q = |\boldsymbol{q}|$. At finite-volume, there are θ_n momenta with same energy E_n, where θ_n is the theta series introduced in App. (A.2).

Spectral decomposition The relation Eq. (2.2.38) shows that it is possible to access the spectrum directly using our Euclidean correlators, even if these are unavoidably at non-zero

temperature. We insert a complete set of orthonormal eigenstates Eq. (2.2.40),

$$\begin{aligned}\langle O_2(t)\,O_1(0)\rangle_T &= \frac{\sum_m \langle m|e^{-(T-t)\hat{H}}\hat{O}_2 e^{-t\hat{H}}\hat{O}_1|m\rangle}{\sum_m \langle m|e^{-T\hat{H}}|m\rangle} = \frac{\sum_{nm}\langle m|\hat{O}_2 e^{-t\hat{H}}|n\rangle\langle n|\hat{O}_1|m\rangle\, e^{-(T-t)E_m}}{\sum_m e^{-TE_m}} \\ &= \frac{\sum_{nm}\langle m|\hat{O}_2|n\rangle\langle n|\hat{O}_1|m\rangle\, e^{-(T-t)E_m}e^{-tE_n}}{\sum_m e^{-TE_m}} \\ &= \sum_n \frac{\langle 0|\hat{O}_2|n\rangle\langle n|\hat{O}_1|0\rangle + \sum_{m\neq 0}\langle m|\hat{O}_2|n\rangle\langle n|\hat{O}_1|m\rangle\, e^{-(T-t)E_m}}{1+\sum_{m\neq 0}e^{-TE_m}} e^{-tE_n} \\ &\approx \sum_n \langle 0|\hat{O}_2|n\rangle\langle n|\hat{O}_1|0\rangle\, e^{-tE_n} \equiv \langle 0|\hat{O}_2(t)\,\hat{O}_1(0)|0\rangle \equiv C(t)\,. \end{aligned} \tag{2.2.48}$$

The terms $\sum_{m\neq 0}$ do not survive the $T\to\infty$ limit, resulting in a simple sum of exponentials.

The sum is restricted to all those states to which the operators $\hat{O}_2$ and $\hat{O}_1$ couple. For instance, operators with a well defined momentum, obtainable from a Fourier transform Eq. (A.2.14) of operators in coordinate space, identify only those states with the corresponding momentum. Translational invariance

$$\langle 0|\hat{O}_2(\boldsymbol{y},t)\,\hat{O}_1(\boldsymbol{x},0)|0\rangle = \langle 0|e^{i\boldsymbol{x}\cdot\hat{\boldsymbol{P}}}\hat{O}_2(\boldsymbol{y},t)\,e^{-i\boldsymbol{x}\cdot\hat{\boldsymbol{P}}}\hat{O}_1(\boldsymbol{0},0)\,e^{i\boldsymbol{x}\cdot\hat{\boldsymbol{P}}}|0\rangle = \langle 0|\hat{O}_2(\boldsymbol{y}-\boldsymbol{x},t)\,\hat{O}_1(\boldsymbol{0},0)|0\rangle$$

assures that $\langle 0|\hat{O}_2(\boldsymbol{p},t)\,\hat{O}_1(\boldsymbol{q},0)|0\rangle$, is non-zero only for $\boldsymbol{p}=\boldsymbol{q}$. Similarly, projecting the operators on a given lattice irrep furnish states which live only in the irrep considered.

As time increases, the lowest energy contribution in the sum Eq. (2.2.48) becomes the dominant one as long as the overlap $\langle 1|\hat{O}_{1/2}|0\rangle$ is not too small compared to the others. The dominance of the ground state and the quality of the signal can be inspected by calculating the effective mass

$$E_{\text{eff}}\left(t+\frac{a}{2}\right) = \log\frac{C(t)}{C(t+a)} \approx E_1. \tag{2.2.49}$$

For sufficiently large times, i.e. when the contribution from excited states no longer is significant, the effective mass exhibits a plateaux from which the ground state energy can be read off. Varying t in this region, a simple one-exponential fit furnishes the amplitude and a more accurate value for the energy. If the ground state corresponds to a one-particle state, E_1 is simply the mass of the particle when $\boldsymbol{p}=0$.

The choice of the operators depends on the sector of the spectrum we are interested in. In any case, to maximise overlap, it should resemble the physical state.

Mesonic operators For mesonic states, we can be inspired by the quark model to construct mesonic operators of the form

$$O(x) = \overline{\psi}^{f}(x)\,\Gamma\psi^{f'}(x)\,, \tag{2.2.50}$$

where f and f' are the quark flavours and Γ is a gamma matrix (or a derivative operator) with the quantum numbers of the meson under consideration. With the aid of the adjoint operator

$$\begin{aligned} O^{\dagger}(x) &= \left(\psi^{\dagger f}(x)\,\gamma_t\Gamma\psi^{f'}(x)\right)^{\dagger} = -\psi^{f'\dagger}(x)\,\Gamma^{\dagger}\gamma_t\psi^{f}(x) = -\psi^{f'\dagger}(x)\,\gamma_t\left(\gamma_t\Gamma^{\dagger}\gamma_t\right)\psi^{f}(x) \\ &= -\overline{\psi}^{f'}(x)\,\tilde{\Gamma}\psi^{f}(x)\,, \qquad (2.2.51) \\ \tilde{\Gamma} &= \gamma_t\Gamma^{\dagger}\gamma_t = \pm\Gamma, \qquad (2.2.52) \end{aligned}$$

it is then possible to build a correlator $C(y-x) = \langle O(y)\,O^{\dagger}(x)\rangle$ whose spectral decomposition runs over all states with the mesonic quantum numbers. The Wick contractions discussed in Sec. (2.2.3) are straightforward in this case ($t_y > t_x$),

$$\begin{aligned} C(y-x) &= \langle O(y)\,O^{\dagger}(x)\rangle = -\left\langle\left(\overline{\psi}^{f}\Gamma\psi^{f'}\right)_y\left(\overline{\psi}^{f'}\tilde{\Gamma}\psi^{f}\right)_x\right\rangle \\ &= \mathrm{Tr}\left[\Gamma G^{f'}(y;x)\,\tilde{\Gamma}G^{f}(x;y)\right] - \delta_{ff'}\mathrm{Tr}\left[\Gamma G^{f}(y;y)\right]\mathrm{Tr}\left[\tilde{\Gamma}G^{f}(x;x)\right] \qquad (2.2.53) \end{aligned}$$

For $f \neq f'$ the second term drops. Using anti-hermiticity of the propagator we obtain

$$C(y-x) = \mathrm{Tr}\left[(\gamma_5\Gamma)\,G^{f'}(y;x)\left(\tilde{\Gamma}\gamma_5\right)G^{f\dagger}(y;x)\right]. \tag{2.2.54}$$

Thanks to γ_5-hermiticity and to translational invariance the calculation of this correlator on the computer is not significantly expensive.

2.3 Lattice methods

2.3.1 Quark field smearing

A meson interpolator of the form Eq. (2.2.50) is localised in space with the two quarks sharing the same spatial coordinate $\boldsymbol{x}$. A more realistic operator, that would create from the vacuum a state that looks more like a meson (i.e., has a better overlap with the physical meson), should instead be spread in space and adhere to the "size" of it. Then, with such smeared

operators, the excited (unwanted) states have less weight in the spectral decomposition Eq. (2.2.48), leading to a better signal. For this reason, from the local quark fields $\psi(\boldsymbol{x},t)$, so called smeared quarks are created via a smearing function S:

$$\psi^S = S\psi, \qquad \psi^S_{i\alpha}(\boldsymbol{x},t) = \sum_{zj} S_{ij}(\boldsymbol{x},\boldsymbol{z})\,\psi_{j\alpha}(\boldsymbol{z},t), \tag{2.3.1}$$

$$\overline{\psi}^S = \overline{\psi}S^\dagger, \qquad \overline{\psi}^S_{i\alpha}(\boldsymbol{x},t) = \sum_{zj} \overline{\psi}_{j\alpha}(\boldsymbol{z},t)\,S^{\dagger\mathrm{col}}_{ji}(\boldsymbol{x},\boldsymbol{z}), \tag{2.3.2}$$

with $S^{\dagger\mathrm{col}}_{ji}(\boldsymbol{x},\boldsymbol{z}) \equiv S^*_{ij}(\boldsymbol{x},\boldsymbol{z})$. In Eqs. (2.3.1) and (2.3.2) the smearing function is assumed to be spin-independent. Additionally, they are usually considered hermitian in colour and space, i.e. $S = S^\dagger$ or, for given $(\boldsymbol{x},\boldsymbol{y})$, $S^{\dagger\mathrm{col}}(\boldsymbol{x},\boldsymbol{z}) = S(\boldsymbol{z},\boldsymbol{x})$.

Technically, the smearing process is often computed iteratively, i.e., starting from the local quark field $\psi(\boldsymbol{z},t)$, n_{itr} iterations of a basic smearing algorithm are performed, resulting in the final $\psi^S(\boldsymbol{x},t)$. The number of iterations is related to the spatial distribution extent of the quark field.

A smeared mesonic operator has the form

$$O^{S_1S_2} = \overline{\psi}^{S_1,f_1}\Gamma\psi^{S_2,f_2} = \overline{\psi}^{f_1}\left(S_1^\dagger\Gamma S_2\right)\psi^{f_2} \tag{2.3.3}$$

or, more explicitly,

$$O^{S_1S_2}(x) = \overline{\psi}^{S_1,f_1}(\boldsymbol{x},t)\,\Gamma\psi^{S_2,f_2}(\boldsymbol{x},t) = \sum_{\boldsymbol{z}_1\boldsymbol{z}_2}\overline{\psi}^{f_1}(\boldsymbol{z}_1,t)\,S_1^{\dagger\mathrm{col}}(\boldsymbol{x},\boldsymbol{z}_1)\,\Gamma S_2(\boldsymbol{x},\boldsymbol{z}_2)\,\psi^{f_2}(\boldsymbol{z}_2,t). \tag{2.3.4}$$

If Γ does not contain derivative operators, the smearing functions commute with it thanks to spin-independence.

Smearing the quark-fields is equivalent to smearing the propagators at the source and at the sink:

$$\langle\psi^{S_1}\overline{\psi}^{S_2}\rangle = \langle S_1\psi\overline{\psi}S_2^\dagger\rangle = S_1\langle\psi\overline{\psi}\rangle S_2^\dagger = S_1D^{-1}S_2^\dagger. \tag{2.3.5}$$

In general, the smearing functions depend on the links U and can be constructed to be gauge covariant such that the combination Eq. (2.3.4) is gauge-invariant. The gauge links fluctuate between neighbouring lattice positions and can be smoothened to improve the signal. Typically, this is done by averaging between nearby links and this can be done

preserving gauge-invariance.

The Wuppertal smearing [22]

$$S_{\text{wupp}}(\boldsymbol{x},\boldsymbol{z}) = \frac{1}{1+6\kappa}\left(\delta_{\boldsymbol{xz}} + \kappa \sum_{j=\pm1,\pm2,\pm3} \overline{U}_j(\boldsymbol{x})\,\delta_{\boldsymbol{x}+\hat{j},\boldsymbol{z}}\right) \tag{2.3.6}$$

with APE smoothed spatial links [23] $\overline{U}_j(\boldsymbol{x})$ will be used throughout this work.

2.3.2 Stochastic sources

In Sec. (2.2.3) the difficulty of inverting a Dirac matrix was mentioned. In many cases, due to translational invariance, the calculation of a correlator requires only one column of the propagators (see e.g. Eq. (2.2.54)). In more general cases, as for the calculation of 3-point or 4-point correlators, translational invariance does not prevent us from the need of the knowledge of the whole propagator. With the present technology, the inversion of the full Dirac matrix is prohibitively expensive computationally and a cheaper approximate evaluation of the propagator is therefore required. One option is provided by stochastic source method (see e.g. [24]) which is described in this subsection.

Denoting $a = (i,\alpha,x) \in R$ as a multi-index for spin, colour and space-time, let us introduce N fields $\eta^r_a = \eta^r_{i\alpha}(x)$ with the property

$$\frac{1}{N}\sum_{r=1}^{N} \eta^r_a \eta^{r*}_b = \delta_{ab} + \epsilon_{ab}, \quad \epsilon_{ab} = \mathcal{O}\left(\frac{1}{\sqrt{N}}\right), \tag{2.3.7}$$

where $\delta_{ab} = \delta_{ij}\delta_{\alpha\beta}\delta_{xy}$. Random elements of $\mathbb{Z}_2$ satisfy this requirement and will be used throughout this thesis. More precisely, for a given point $a = (i,\alpha,x)$ and a given r, η^r_a is randomly chosen from $\{1, i, -1, -i\}$. Note that for $a = b$, the lhs of Eq. (2.3.7) is exactly one,

$$\frac{1}{N}\sum_{r=1}^{N} |\eta^r_a|^2 = \frac{1}{N}\sum_{r=1}^{N} 1 = 1, \tag{2.3.8}$$

so that ϵ_{ab} is zero for $a = b$. For $a \neq b$, each ϵ_{ab} has comparable size $\sim \mathcal{O}\left(\frac{1}{\sqrt{N}}\right)$. Given a Dirac matrix $D_{ab} = D_{i\alpha,j\beta}(y,x)$, for each r we solve

$$\sum_b D_{ab} Q^r_b = \eta^r_a, \tag{2.3.9}$$

which means

$$Q_a^r = \sum_b G_{ab}\eta_b^r. \tag{2.3.10}$$

Then,

$$\begin{aligned} \mathcal{G}_{ab} \equiv \frac{1}{N}\sum_{r=1}^{N} Q_a^r \eta_b^{r*} &= \sum_c G_{ac}\frac{1}{N}\sum_{r=1}^{N}\eta_c^r\eta_b^{r*} = \sum_c G_{ac}\delta_{cb} + \sum_c G_{ac}\epsilon_{cb} \\ &= G_{ab} + \sum_{c\neq b} G_{ac}\epsilon_{cb} \approx G_{ab}. \end{aligned} \tag{2.3.11}$$

By computing only N vector-like inversions Eq. (2.3.9) we can calculate the quantity $\frac{1}{N}\sum_{r=1}^{N} Q_a^r\eta_b^{r*}$ which is the wanted propagator G_{ab} added to a stochastic noise term which tends to zero as N increases.

Partitioning (diluting) For fixed points b (source) and a (sink), the noise term in Eq. (2.3.11) receives contributions from the value of G at any source $c \neq b$ and sink a. Due to the exponential decay of the propagator with the space-time distance, the major contributions will come from the space-time components of c that are close to those of a, including a itself. It is then advisable to remove these contributions as much as possible.

One way to achieve this is by using the partition (or dilution) technique [25]. The set of spacetime-colour-spin points is partitioned[8] $R = \cup_{m=1}^{M} R_m$ and the stochastic sources η_a^r are decomposed into fields which have support on a partition element identified by m,

$$\eta_a^r = \sum_{m=1}^{M}\eta_a^{r,m}, \qquad \eta_a^{r,m} = 0 \quad \text{if } a \notin R_m. \tag{2.3.12}$$

The fields $\eta_a^{r,m}$ are defined over the whole space R but are non-zero only for a belonging to the partition element R_m. The analogous to Eq. (2.3.7) is

$$\frac{1}{N}\sum_{r=1}^{N}\eta_a^{r,m}\eta_b^{r,m*} = \begin{cases} \delta_{ab} + \epsilon_{ab} & a,b \in R_m \\ 0 & \text{else} \end{cases}. \tag{2.3.13}$$

[8]For instance, if $a = 1, ..., 11$ then a possible partition with $M = 4$ elements is

$$a = \underbrace{1,2,3}_{m=1},\ \underbrace{4,5}_{m=2},\ \underbrace{6,7,8,9}_{m=3},\ \underbrace{10,11}_{m=4}.$$

Generalising, each number here corresponds to a point $a = (x, i, \alpha)$ on the lattice.

One example of partitioning is time-dilution with $M = N_T$ partition elements and $\eta_a^{r,m} = \eta_{i\alpha}^{r,t_0}(\boldsymbol{x},t) = \eta_{i\alpha}^{r,t_0}(\boldsymbol{x})\,\delta_{t,t_0}$: we have a stochastic field with non-zero elements $\eta_{i\alpha}^{r,t_0}(\boldsymbol{x})$ only at $t = t_0$. Another example is spin dilution ($M = 4$ partition elements), $\eta_a^{r,m} = \eta_{i\alpha}^{r,\alpha_0}(\boldsymbol{x},t) = \eta_i^{r,\alpha_0}(\boldsymbol{x},t)\,\delta_{\alpha,\alpha_0}$ or even spin-colour-time dilution ($M = 12N_T$ partition elements), $\eta_a^{r,m} = \eta_{i\alpha}^{r,\alpha_0 i_0 t_0}(\boldsymbol{x},t) = \eta^{r,\alpha_0 i_0 t_0}(\boldsymbol{x})\,\delta_{\alpha,\alpha_0}\delta_{i,i_0}\delta_{t,t_0}$. The convenience in choosing one specific way to partition the space R depends on the problem under consideration.

For fixed partition element m, the equation

$$\sum_{b\in R} D_{ab} Q_b^{r,m} = \eta_a^{r,m} \tag{2.3.14}$$

can be solved for all r, leading to $Q_b^{r,m}$. Just like Eq. (2.3.9), the indices a and b here run over the whole space, so that

$$Q_a^{r,m} = \sum_{b\in R} G_{ab}\eta_b^{r,m}. \tag{2.3.15}$$

Then, for a given m, a given $b \in R_m$ and any $a \in R$:

$$\begin{aligned} \mathcal{G}_{ab}^m = \frac{1}{N}\sum_{r=1}^{N} Q_a^{r,m}\eta_b^{r,m*} &= \sum_{c\in R_m} G_{ac}\frac{1}{N}\sum_{r=1}^{N}\eta_c^{r,m}\eta_b^{r,m*} = \sum_{c\in R_m} G_{ac}\left(\delta_{cb}+\epsilon_{cb}\right) \\ &= G_{ab} + \sum_{c\in R_m, c\neq b} G_{ac}\epsilon_{cb} \qquad\qquad a\in R, b\in R_m. \end{aligned} \tag{2.3.16}$$

Here, the sum over c runs initially over the whole R (due to Eq. (2.3.15)) but it is then restricted to R_m as $\eta_c^{r,m}$ is non-zero only in this region. From Eq. (2.3.16) we see that now the noise gets contributions only from the points lying in R_m (c.f. Eq. (2.3.11)). With only one fixed m, we have an improved estimate for the propagator G_{ab} for any sink a but for sources b only belonging to the partition element R_m. In some cases this is enough (e.g. when only timeslice-to-all propagators have to be calculated) but in order to reconstruct the full improved propagator all $N \times M$ inversions Eq. (2.3.14) have to be performed. The stochastic noise reduction due to partitioning has to justify the M fold increase of the number of inversions Eq. (2.3.14).

The one-end trick In many cases, the propagators themselves are not needed, but their combination inside spin-colour traces are. Naively, a set of stochastic fields would be required for each propagator, increasing the computational effort and the noise. A smart way to handle this for connected diagrams is to use the so called one-end trick [26], where the Kronecker deltas in Eq. (2.3.7) or Eq. (2.3.13) are appropriately inserted in the traces with

a consequent contamination of only one set of stochastic fields. The exact way how this works will be seen directly in the context of this work.

2.3.3 The variational method

The spectral decomposition formula Eq. (2.2.48) provides a way to calculate on the lattice the spectrum of the lowest lying states in the sector of non-zero overlap of the operators O_1 and O_2. As it stands, the formula is useful only if one is interested in the ground state or the first excited state, as multi-exponential fits become unreliable when higher energies and the related amplitudes are included. The variational method [27] is a very useful way to calculate excited states. Before seeing how it applies to our context, let us briefly see how it works in general.

The generalised eigenvalue problem Consider two hermitian $N \times N$ matrices C and C_0[9] and define the generalised eigenvalue problem,

$$Cv^{(i)} = \lambda^{(i)} C_0 v^{(i)} \quad i = 1, ..., N. \tag{2.3.17}$$

$\lambda^{(i)}$ and $v^{(i)}$ are the generalised eigenvalues and eigenvectors of C with respect to C_0. Since C and C_0 are hermitian, the eigenvalues are real and the eigenvectors are C_0-orthogonal,

$$\lambda^{(i)} = \lambda^{(i)*} \tag{2.3.18}$$

$$v^{(i)\dagger} C_0 v^{(j)} = \delta_{ij} f_j \tag{2.3.19}$$

Note that if $v^{(i)}$ is an eigenvector, so is $\alpha v^{(i)}$ for any complex number α. The eigenvectors can be fixed once the f_j in Eq. (2.3.19) are[10], setting them for instance to one (resulting in C_0-orthonormal eigenvectors).

Given a complex N-dimensional non-zero vector v, the (generalised) Rayleigh quotient of C and C_0 is defined as a function of v:

$$R(v) = \frac{v^\dagger C v}{v^\dagger C_0 v}. \tag{2.3.20}$$

If in particular v is an eigenvector $v^{(i)}$, the Rayleigh quotient is just the corresponding

[9] C_0 is assumed to be positive definite also.

[10] There is still a phase ambiguity $e^{i\theta_j}$, which becomes ± 1 when C and C_0 are real.

eigenvalue,

$$R\left(v^{(i)}\right)=\frac{v^{(i)\dagger}Cv^{(i)}}{v^{(i)\dagger}C_0v^{(i)}}=\lambda^{(i)}\frac{v^{(i)\dagger}C_0v^{(i)}}{v^{(i)\dagger}C_0v^{(i)}}=\lambda^{(i)}. \tag{2.3.21}$$

As the vector v is varied over the whole space $\mathbb{C}^N\setminus\{0\}$ one can show that Rayleigh quotient $R(v)$ is always bounded by the minimum and maximum eigenvalue,

$$\lambda^{\min}=R\left(v^{\min}\right)\leq R(v)\leq R\left(v^{\max}\right)=\lambda^{\max}. \tag{2.3.22}$$

Moreover, it can be shown that the Rayleigh quotient is stationary at the eigenvector positions,

$$\delta R\left(v=v^{(i)}\right)\equiv\delta\left.\frac{v^\dagger Cv}{v^\dagger C_0v}\right|_{v=v^{(i)}}=0 \tag{2.3.23}$$

Finding the vectors that make the Rayleigh quotient stationary is thus equivalent to solving the generalised eigenvalue problem Eq. (2.3.17).

Application to lattice QCD In our spectroscopic problem, instead of using one operator, a set of N operators $O_1,O_2,...O_N$ which create N linearly independent states $O_i^\dagger|0\rangle=|O_i\rangle$ are introduced. One then forms a linear combination operator

$$\Omega=\sum_{i=1}^N v_i^*O_i\qquad\qquad\Omega^\dagger=\sum_{i=1}^N v_iO_i^\dagger, \tag{2.3.24}$$

Given a fixed time $t_0<t$, we want to maximise the quantity

$$R(v)=\frac{\langle0|\Omega(t)\,\Omega^\dagger(0)\,|0\rangle}{\langle0|\Omega(t_0)\,\Omega^\dagger(0)\,|0\rangle}=\sum_n\left(\frac{|\langle0|\Omega(0)\,|n\rangle|^2}{\sum_m|\langle0|\Omega(0)\,|m\rangle|^2\,e^{-E_mt_0}}\right)e^{-E_nt} \tag{2.3.25}$$

Eq. (2.3.25) can be immediately put in Rayleigh quotient form (2.3.20),

$$R(v)=\frac{\langle0|\Omega(t)\,\Omega^\dagger(0)\,|0\rangle}{\langle0|\Omega(t_0)\,\Omega^\dagger(0)\,|0\rangle}=\frac{\sum_{i,j=1}^N v_i^*\,\langle0|O_i(t)\,O_j^\dagger(0)\,|0\rangle\,v_j}{\sum_{i,j=1}^N v_i^*\,\langle0|O_i(t_0)\,O_j^\dagger(0)\,|0\rangle\,v_j}=\frac{v^\dagger C(t)\,v}{v^\dagger C(t_0)\,v} \tag{2.3.26}$$

$C(t)$ is called the correlator matrix and has entries

$$C_{ij}(t)=\langle0|O_i(t)\,O_j^\dagger(0)\,|0\rangle=\sum_n\langle0|O_i|n\rangle\,\langle n|O_j^\dagger|0\rangle\,e^{-tE_n}\equiv\sum_n a_{in}^\dagger a_{nj}e^{-tE_n}. \tag{2.3.27}$$

where we have denoted $a_{nj}=\langle n|O_j^\dagger|0\rangle$ and $a_{in}^\dagger=\langle0|O_i|n\rangle$.

$C(t)$ is hermitian[11] and so is, of course, $C(t_0)$. Then, based on what was said in the previous paragraph, the optimal operator is found by solving the generalised eigenvalue problem

$$C(t)\, v^{(i)}(t,t_0) = \lambda^{(i)}(t,t_0)\, C(t_0)\, v^{(i)}(t,t_0) \qquad i=1,...,N \quad t>t_0\geq 0 \tag{2.3.28}$$

along with an eigenvector normalisation condition,

$$v^{(i)\dagger}(t,t_0)\, C(t_0)\, v^{(i)}(t,t_0) = 1. \tag{2.3.29}$$

For each i-th eigenvector, a different operator Ω_i is identified according to Eq. (2.3.24) and the following relations are valid in general

$$\lambda^{(i)}(t,t_0) = \langle 0|\Omega_i(t)\,\Omega_i^\dagger(0)\,|0\rangle = \sum_n \left|\langle n|\Omega_i^\dagger(0)\,|0\rangle\right|^2 e^{-E_n t}, \tag{2.3.30}$$

$$\sum_{j=1}^{N} a_{nj} v_j^{(i)} = \langle n|\Omega_i^\dagger(0)\,|0\rangle\,. \tag{2.3.31}$$

The first equation is an application of Eq. (2.3.21) to Eq. (2.3.25) , $\lambda^{(i)} = R\left(v^{(i)}\right)$, with the denominator removed due to the exact relation Eq. (2.3.29). The second equation is straightforward to see when using (2.3.24). Note that in general the eigenvectors depend on t, so a t-dependence is present also in $\langle n|\Omega_i^\dagger(0)\,|0\rangle$.

If the Hilbert space was finite, with dimensions N as the number of operators, then the $a_{nj} = \langle n|O_j^\dagger|0\rangle$ form a square matrix and inserting Eq. (2.3.27) in Eqs. (2.3.28) and (2.3.29) we get an explicit expression for Eqs. (2.3.30) and (2.3.31)

$$\lambda^{(i)}(t,t_0) = e^{-(t-t_0)E_i}, \tag{2.3.32}$$

$$\sum_{j=1}^{N} a_{nj} v_j^{(i)} = \delta_{ni} e^{i\theta_i} e^{E_i \frac{t_0}{2}}, \tag{2.3.33}$$

where θ_i is an arbitrary real number. Because of the Kronecker delta, the Ω_i operator overlaps only with the i-th state, $\left|\langle i|\Omega_i^\dagger(0)\,|0\rangle\right|^2 = e^{E_i t_0}$, leading to the simple form Eq. (2.3.32) of

[11]
$$C_{ji}^*(t) = \left(\sum_n a_{jn}^\dagger a_{ni} e^{-tE_n}\right)^* = \sum_n a_{jn}^T a_{ni}^* e^{-tE_n} = \sum_n a_{in}^\dagger a_{nj} e^{-tE_n} = C_{ij}(t)$$

Eq. (2.3.30). Eq. (2.3.33) is a matrix equation of the form $AV = K$, where V is the t-independent eigenvector matrix ($V_{ji} = v_j^{(i)}$, each column corresponds to an eigenvector) and K is diagonal. Along with Eq. (2.3.32), the energies and amplitudes can then be obtained from the eigenvalues and eigenvectors[12].

Of course the Hilbert space is not finite, but Eq. (2.3.32) is still the leading order term for the general case. In this way, the i-th state is directly accessible using the variational method as if it was a ground state for a standard one-operator analysis.

2.4 Extracting scattering data from lattice simulations

In Minkowskian quantum field theory, the S-matrix elements, expressed in terms of asymptotic states, can be accessed from correlators (in momentum space) by looking at the on-shell region. This is the content of the LSZ reduction formula. On the other hand, in an Euclidean formulation, the Euclidean correlation functions do not contain information about the S-matrix elements (apart from values at thresholds), a statement known as the Maiani-Testa no-go theorem [28]. Wick-rotating approximate Euclidean correlation functions back to Minkowski space is in principle a possible solution but it is numerically prohibitive.

2.4.1 Lüscher's method

The negativity of the Maiani-Testa theorem is based on assuming infinite volume Euclidean correlators and can be evaded when the theory is placed in a box, which is exactly the setting of Lattice QCD. The finite volume, which could initially be thought as a limitation of the lattice formulation, instead endows the Euclidean correlators with precious scattering information. The resulting discrete (and interacting) spectrum is linked to the infinite volume value of the S-matrix. This is the idea which was initiated by Lüscher [29, 30] for the simple case of s-wave scattering of spinless particles in the CM frame. Since then, several generalisations of his work were achieved, allowing for moving frames, asymmetric lattices, higher angular momenta, coupled channels. As of today, the most general result was obtained by Briceño [31], which holds for an arbitrary number of $2 \to 2$ channels, particle masses, particle spins and angular momenta. Recall the T-matrix element Eq. (1.3.5) for $2 \to 2$

[12]Note that it is not necessary to invert the eigenvector matrix to extract the amplitudes. Indeed, using the matrix form of Eq. (2.3.29), $V^\dagger C(t_0) V = \mathbb{1}$, we have $A = KV^{-1} = KV^\dagger C(t_0)$.

scattering[13]

$$\langle p'\, j'\, \sigma'_{j'}\, l'\, s' \,|T|\, p\, j\, \sigma_j\, l\, s\,\rangle = (2\pi)^4\, \delta^4\,(p-p')\, T_{j'\sigma'_j l's', j\sigma_j ls}\,(E)\,, \tag{2.4.1}$$

where due to total angular momentum symmetry, $T_{j'\sigma'_j l's', j\sigma_j ls}$ is diagonal in j (but in general not in l and s),

$$T_{j'\sigma'_j l's', j\sigma_j ls}\,(E) = \delta_{jj'}\delta_{\sigma'_j\sigma_j} T^j_{l's', ls}\,(E)\,. \tag{2.4.2}$$

Then, if E_n is an energy level extracted at finite volume L in a frame with total momentum $\boldsymbol{p}$, the quantisation condition (just one channel is considered here)

$$\det\left[T^{-1}\,(E_n) + F\,(E_n, \boldsymbol{p})\right] = 0 \tag{2.4.3}$$

is satisfied, with F being a complicated volume-dependent matrix diagonal only in the total spin s,

$$\langle\, j'\, \sigma'_{j'}\, l'\, s' \,|F|\, j\, \sigma_j\, l\, s\,\rangle = \delta_{ss'} F^s_{j'\sigma'_j l', j\sigma_j l}. \tag{2.4.4}$$

The matrix F is known and is associated with the "kinematics" at finite volume and thus depends on L (details can be found in Ref. [31]). The matrices T^{-1} and F contain all possible angular momenta labels and are therefore infinite in size. Since F is not diagonal in j, as a consequence of angular momenta mixing on the lattice, it is not possible to split the quantisation condition Eq. (2.4.3) into separate conditions for each j in an exact way. In order to turn Eq. (2.4.3) into a practical calculative tool, we note that at low energies only the lowest angular momenta give a significant contribution to the scattering matrix, Sec. (1.4.4). Based on the magnitude of the energies of the specific problem, a cutoff $j_{\max}$ should be imposed on Eq. (2.4.3) making sure that external arguments (experimental data, model calculations, etc.) show that higher angular momenta do indeed have no significant impact. The determinant equation becomes finite but it is in general still underdetermined. The situation can be improved by decomposing the vectors in Eq. (2.4.4) into irreducible spaces for the little group of the momentum $\boldsymbol{p}$ under consideration via the coefficients in Eq.

[13]The same notation of Eq. (1.3.5) is used. For the two particle system, p is the total four-momentum, j and σ_j the total angular momenta with the corresponding z-projection, l the orbital angular momentum and s the total spin. Here the energy in the CM is used, $E = \sqrt{s}$.

(2.2.44)[14]. In this basis, the F operator in Eq. (2.4.4) becomes (block-) diagonal,

$$\langle \Lambda'_{\boldsymbol{p}}\, \sigma'_{\Lambda_{\boldsymbol{p}}}\, \eta'\, l'\, s\, |F|\, \Lambda_{\boldsymbol{p}}\, \sigma_{\Lambda_{\boldsymbol{p}}}\, \eta\, l\, s \rangle = \delta_{\Lambda'_{\boldsymbol{p}}\Lambda_{\boldsymbol{p}}} \delta_{\sigma'_{\Lambda_{\boldsymbol{p}}}\sigma_{\Lambda_{\boldsymbol{p}}}} F_{l'\eta',l\eta}^{\Lambda_{\boldsymbol{p}},\sigma_{\Lambda_{\boldsymbol{p}}},s} \tag{2.4.5}$$

The quantisation condition Eq. (2.4.3) becomes therefore a determinant of block-diagonal matrices which is a product of determinants for each irreducible block. The whole product is zero and thus a separate quantisation condition for each irreducible space is identified. This procedure reduces the under-determination and will also lead, for simple cases, to a unique solution for one or more blocks.

Although very general, the Briceño relation is valid only for energies below three-particle thresholds and does not consider exponentially suppressed terms $\sim e^{-mL}$. Studies attempting to deal with the arduous problem of extending the region of application of the quantisation condition above the three-particle threshold are ongoing, see e.g. [32–34].

A simple case Let us make this more clear in the simplified case of spinless particles in s-wave. We assume that the energy is low enough such that higher partial waves are suppressed and resulting in a closed relation involving only s-waves. Also, the energy range is kept below inelastic threshold, so that only two (or one)-particle states are present with centre of mass energies E_n linked to k_n via Eq. (2.2.46),

$$\begin{aligned} E_n &= \sqrt{s_n} = \sqrt{m_1^2 + k_n^2} + \sqrt{m_2^2 + k_n^2} && (2.4.6) \\ &= \sqrt{m_1^2 + q_n^2} + \sqrt{m_2^2 + q_n^2} + \Delta E_n \qquad n = \sqrt{0}, \sqrt{1}, \sqrt{2}, \dots . && (2.4.7) \end{aligned}$$

Then, Eq. (2.4.3) reduces just to Lüscher's relation [30] and for each $k = k_n$,

$$k \cot \delta\,(k) = \frac{2}{L\sqrt{\pi}} \mathcal{Z}_{00}\left(1; \frac{L^2}{4\pi^2} k^2\right). \tag{2.4.8}$$

$\mathcal{Z}_{00}$ is the analytical continuation of the generalised zeta-function and, recall, the phase shift $\delta\,(k)$ is related to the T-matrix via Eq. (1.4.23),

$$T\,(s) = \frac{-8\pi\sqrt{s}}{k \cot \delta\,(k) - ik}. \tag{2.4.9}$$

[14]The decomposition Eq. (2.2.44) was expressed in the context of $\boldsymbol{p} = 0$ but, as mentioned in Sec. (2.2.4), it is valid in general. Note also that the general framework of Sec. (2.2.4) is being applied here for two-particle states.

Given an energy-level E_n from a lattice simulation with spatial extent L, one can calculate the rhs of Eq. (2.4.8) obtaining, from the lhs, one data point $(k_n, \delta(k_n))$ or $(s_n, T(s_n))$, with $s_n = E_n^2$. It should be clear that, although the simulation is performed at finite-volume, the information we obtain directly refers to the infinite-volume quantities ($T(s)$ or $\delta(s)$), the finite-volume theory being limited to establish the positions ($s = s_n$) at which these quantities are extracted. These positions depend on the result of the lattice simulation and cannot be known a priori but can easily be estimated by looking for instance at the non-interacting finite-volume spectrum. Multiple data points are needed in order to correctly probe the phase shift in the region of interest and to perform a fit to a modelling form. How the points are gathered from the lattice is a matter of convenience depending on the particular problem and the region of interest. Typical examples include simulating on different spatial extents, lattice geometries, moving frames, etc.

In Sections (1.4.2) and (1.4.4) we have seen that, although the T-matrix is physical in the region of scattering, $k^2 > 0$ or $\sqrt{s} \geq m_1 + m_2$, it can be analytically continued below threshold. We have also seen that the imaginary part becomes null here. This is consistent with the partial wave expression Eq. (2.4.9) where the function $k \cot \delta(k)$ remains real below threshold, where $k^2 < 0$ and $k = i|k|$ is purely imaginary. Also, the rhs of Lüscher's relation can be analytically continued, so that, the whole relation Eq. (2.4.8) is valid also below threshold. In particular, in this region, Lüscher's relation has a simple series representation

$$k \cot \delta(k) = ik + \frac{1}{L} \sum_{n=1}^{\infty} \frac{\theta_n}{\sqrt{n}} e^{-\sqrt{n}|k|L} \tag{2.4.10}$$

$$= ik + \frac{1}{L} \left(6e^{-|k|L} + \frac{12}{\sqrt{2}} e^{-\sqrt{2}|k|L} + ... \right), \tag{2.4.11}$$

where θ_n is the theta series introduced in Sec. (A.2).

A possible bound state particle at infinite-volume with mass m_B lying below threshold is also present at finite-volume with a modified mass $m_{\tilde{B}} = m_{\tilde{B}}(L)$. The corresponding energy level also satisfies Lüscher's relation Eq. (2.4.8), in particular Eq. (2.4.10), and can join the tower of levels Eqs. (2.4.6) and (2.4.7) by allowing n to assume the additional value $n = \tilde{B}$. Then $E_{\tilde{B}} = m_{\tilde{B}}$ is the mass, $k_{\tilde{B}} = i|k_{\tilde{B}}|$ the binding momentum, $q_{\tilde{B}}$ is zero and $\Delta E_{\tilde{B}} < 0$ represents the binding energy. Explicitly plugging in the solution $k = k_{\tilde{B}}$ in Eq. (2.4.10) we see that, as $L \to \infty$, the sum goes to zero, resulting in the bound state condition Eq. (1.4.28) for k_B. At the same time, the quantities $m_{\tilde{B}}$ and $\Delta E_{\tilde{B}}$ will tend to their infinite volume values m_B and ΔE_B as $L \to \infty$.

Eq. (2.4.8) can also be viewed as a set of implicit relations for $k_n(L)$, one for each n,

$$k_n(L)\cot\delta(k_n(L)) = \frac{2}{L\sqrt{\pi}}\mathcal{Z}_{00}\left(1;\frac{L^2}{4\pi^2}k_n^2(L)\right). \tag{2.4.12}$$

If the T-matrix of a two-particle system elastically scattering at infinite volume is known, Eq. (2.4.12) allows for the calculation of the volume dependence of the energies $E_n(L)$ (or $k_n(L)$) of the same system when placed in a finite volume.

2.4.2 The potential method

In Sec. (1.4.5) the partial-wave T matrix was expressed in a model-independent way in terms of a real potential $V(s)$, Eq. (1.4.40), a relation which neglects all unphysical cuts. A corresponding expression at finite volume can be constructed [35],

$$\tilde{T}(s,L) = \frac{1}{V^{-1}(s) - \tilde{G}(s,L)}. \tag{2.4.13}$$

$\tilde{T}(s,L)$ will be improperly[15] referred to as the finite-volume T-matrix. The finite-volume potential $V(s,L)$ is assumed to be equal to its infinite-volume version $V(s)$, a statement which is true up to exponentially suppressed terms, restricting all volume dependencies to the $\tilde{G}$ function. The cutoff-regularised form is obtained by simply replacing the integral Eq. (1.4.41) with a sum over discrete momenta $\boldsymbol{q} = \frac{2\pi}{L}\boldsymbol{n}$ with $\boldsymbol{n}\in\mathbb{Z}^3$,

$$\tilde{G}^c(s,\Lambda,L) = \frac{1}{L^3}\sum_{\boldsymbol{q}}^{|\boldsymbol{q}|<\Lambda} I(s,\boldsymbol{q}), \tag{2.4.14}$$

where $I(s,\boldsymbol{q})$ is again Eq. (1.4.42). The dimensional-renormalised finite-volume version of Eq. (1.4.43) is instead obtained by

$$\tilde{G}^D(s,\alpha,L) \;=\; G^D(s,\alpha) + \Delta G(s,L) \tag{2.4.15}$$

[15] No scattering happens at finite volume.

where $\Delta G(s,L)$ is the cutoff-independent regular function

$$\begin{aligned}\Delta G(s,L) &= \lim_{\Lambda\to\infty}\left(\tilde{G}^c(s,\Lambda,L)-\tilde{G}^c(s,\Lambda)\right)\\ &\equiv \lim_{\Lambda\to\infty}\left(\frac{1}{L^3}\sum_{\boldsymbol{q}}^{|\boldsymbol{q}|<\Lambda}-\int\frac{d^3q}{(2\pi)^3}\right)I(s,\boldsymbol{q})\,.\end{aligned} \tag{2.4.16}$$

Then, in either regularisations, the finite volume T-matrix Eq. (2.4.13), is written as

$$\tilde{T}(s,L)=\lim_{\Lambda\to\infty}\frac{1}{V^c(s,\Lambda)^{-1}-\tilde{G}^c(s,\Lambda,L)}=\frac{1}{V^D(s,\alpha)^{-1}-\tilde{G}^D(s,\alpha,L)} \tag{2.4.17}$$

which is the finite volume version of Eq. (1.4.45).

The finite volume T-matrix is equipped with a pole at each finite-volume energy Eq. (2.4.6) (including bound state poles), which means[16]

$$V(s_n)\,\tilde{G}(s_n,L)=1 \qquad n=\tilde{B},\sqrt{0},\sqrt{1},...\quad . \tag{2.4.18}$$

Thanks to this relation it is possible to probe the potential from the knowledge of the finite-volume spectrum. A fit to the potential can be performed and can be compared to expressions stemming from models like unitarised Chiral PT. Knowing the (fitted) potential, the bound state parameters can be extracted. Its mass (and in turn, binding momentum and binding energy) can be obtained by solving Eq. (1.4.48), the coupling g from Eq. (1.4.49) (which is realised at $s=s_B$) and finally, the compositeness parameter is $Z=g^2\left.\frac{\partial V^{-1}}{\partial s}\right|_{s=s_B}$.

Let us finally note that the infinite volume T-matrix can be accessed bypassing the fit to the potential, if this is not needed. Indeed, $V^{-1}(s_n)=\tilde{G}(s_n,L)$ from Eq. (2.4.18) can be plugged directly into Eq. (1.4.40) for each n, leading to

$$T(s_n)=\frac{1}{\Delta G(s_n,L)} \qquad n=\tilde{B},\sqrt{0},\sqrt{1},... \tag{2.4.19}$$

This relation does not require the knowledge of the $V(s)$ and is valid as long as the potential is volume-independent. It is analogous, in fact more general as shown in [35], to Lüscher's relation Eq. (2.4.8). The calculation of Eq. (2.4.16) at $s=s_n$ results directly to $T^{-1}(s_n)$, without having to consider renormalisation parameters. Then, the phase shift or the $k\cot\delta$

[16]Note that the infinite volume version of this relation, Eq. (1.4.48) contains only the bound state(s) solution, $n=B$, since the infinite tower of poles at finite volume is replaced by the physical cut.

function can be accessed using Eq. (2.4.9).

Chapter 3

DK and D^*K scattering from lattice QCD

The necessary apparatus to understand scattering processes and to treat them using lattice simulations were discussed in the previous chapters. Here, the general formalism will be applied specifically to two similar physical situations. Based on the work in [36], we will consider the scattering of a kaon and a D meson as well as a bound state which couples to this channel, the $D_{s0}^*(2317)$. In parallel, the D^*K scattering and the corresponding $D_{s1}(2460)$ will be dealt with.

An overview of the situation - both from an experimental and a lattice point of view - will be discussed in Sec. (3.1). The details of the simulation and the application of the variational method introduced in Sec. (2.3.3) to extract the energies will follow in Sec. (3.2). The latter will be used to obtain scattering information according to Sec. (2.4) and the precise way this is done for this case is presented in Sec. (3.3). The chapter ends with Sec. (3.4) which is dedicated to the calculation of the decay constants of the two bound states.

3.1 Overview of the problem

3.1.1 The physical picture

By today, all masses of the lowest lying states in the $C = S = \pm 1$ sector have been measured and are listed in Tab. (3.1). Of these, our study focuses on the $J^P = 0^+$ $D_{s0}^*(2317)$ which has the same quantum numbers of the DK scattering state and the $J^P = 1^+$ $D_{s1}(2460)$ which couples to D^*K. The former state was not seen before 2003 when the $BABAR$

J^P	State	Mass [MeV]	Width [MeV]
2^+	$D_{s2}^*(2573)$	2571.9 ± 0.8	17 ± 4
1^+	$D_{s1}(2536)$	2535.11 ± 0.06	0.92 ± 0.05
1^+	$D_{s1}(2460)$	2459.5 ± 0.6	< 3.5
0^+	$D_{s0}^*(2317)$	2317.7 ± 0.6	< 3.8
1^-	D_s^*	2112.1 ± 0.4	< 1.9
0^-	D_s	1968.30 ± 0.10	$\tau = 5.00\,(7) \times 10^{-3}$s

Table 3.1: Charmed-strange spectrum up to $J^P = 2^+$. The values are from the PDG [7].

Collaboration [37] observed the associated peak in the $D_s^+\pi_0$ invariant mass distribution. The decay to $D_s^+\pi_0$ is a strong decay, however it is isospin-violating, resulting in a small $D_{s0}^*(2317)$ width which is less than 3.8 MeV. The discovery motivated the search by the CLEO collaboration for the $D_{s1}(2460)$, which was successfully found decaying to $D_s^{*+}\pi_0$ and was announced later in the same year [38]. The identification of the two states with the quark model charm-strange $J^P = 0^+$ and 1^+ P-wave levels appeared natural but was affected by a mass puzzle. Indeed, the measured masses were surprisingly found to be few tens of MeVs below the respective DK and D^*K thresholds, in contrast with the expectations of theoretical studies which were based on a two-quark interpretation and which include quark models [39, 40] and early lattice simulations [41–44]. These studies predicted instead broad resonances which were allowed to decay to the corresponding DK and D^*K states.

In addition to the $D_{s0}^*(2317)$ and the $D_{s1}(2460)$, the other 1^+ state listed in the table, the $D_{s1}(2536)$, is also considered in this work. This particle was first seen back in 1989 by ARGUS [45] and decays mainly to D^*K either in s- or d-wave, the first being dominant, with a small width of 0.78 MeV.

From a theoretical point of view, the relatively heavy mass of the charm quark can be exploited to treat the states in Tab. (3.1) according to heavy quark effective theory. In the limit of $m_c \to \infty$, the strong interaction does not depend on the spin and the mass of the charm quark (which becomes a static colour source) and the mesons in Tab. (3.1) can be classified in terms of the spin of the strange quark. By adding this to the orbital angular momentum $l = 0, 1, ...$, we get $j^P = \frac{1}{2}^-, \frac{1}{2}^+, \frac{3}{2}^+, ...$, each value corresponding to a degenerate doublet, respectively (D_s, D_s^*), $(D_{s0}^*(2317), D_{s1}(2460))$ and $(D_{s1}(2536), D_{s2}^*(2573))$.

3.1.2 Finite volume considerations

In the previous section, the infinite volume aspects of the 0^+ and 1^+ charm-strange sectors were introduced. As discussed in Sec. (2.4), it is possible, thanks to Lüscher's formalism,

to extract infinite volume information from the finite volume energy levels which can be computed in a model independent way on the lattice. Thus, in this section the relevant finite volume spectrum will be discussed along with the computational challenges required for its extraction.

In the 0^+ channel and restricting to the CM frame, the energy levels at infinite volume corresponding to the $D_{s0}^*(2317)$ state, $|D_s\rangle$, and the continuous set of DK levels starting at threshold are replaced by the tower of levels Eq. (2.4.7). The lowest level, with $n = \tilde{D}_s$, is

$$\begin{aligned} E_{\tilde{D}_s}(L) \equiv m_{\tilde{D}_s}(L) &= \sqrt{m_K^2 + k_{\tilde{D}_s}^2} + \sqrt{m_D^2 + k_{\tilde{D}_s}^2} && (3.1.1) \\ &= m_K + m_D + \Delta E_{\tilde{D}_s}(L) && (3.1.2) \end{aligned}$$

and corresponds to the lattice Hamiltonian eigenstate $|\tilde{D}_s\rangle_L$. This level is below threshold so that the binding momentum squared and the binding energy of the D and K mesons are negative, $k_{\tilde{D}_s}^2 < 0$ and $\Delta E_{\tilde{D}_s}(L) < 0$. Above the energy Eq. (3.1.1) we find the first scattering level (Eq. (2.4.7) for $n = 0$)

$$\begin{aligned} E_0(L) &= \sqrt{m_K^2 + k_0^2} + \sqrt{m_D^2 + k_0^2} && (3.1.3) \\ &= m_K + m_D + \Delta E_0(L). && (3.1.4) \end{aligned}$$

As this level corresponds to a scattering state, the momentum squared k_0^2 and the interaction energy term $\Delta E_0(L)$ are both positive. This level is distinguished from what will be referred to as the non-interacting threshold, i.e. $E_0^{\text{free}}(L) = m_K + m_D$ - the energy level of a non-interacting system of a kaon and D meson in a box. Apart from polarisation effects, this quantity coincides with the lowest scattering state energy in the continuum. The energy of the second scattering state is

$$\begin{aligned} E_1(L) &= \sqrt{m_K^2 + k_1^2} + \sqrt{m_D^2 + k_1^2} && (3.1.5) \\ &= \sqrt{m_K^2 + \left(\frac{2\pi}{L}\boldsymbol{n}\right)^2} + \sqrt{m_D^2 + \left(-\frac{2\pi}{L}\boldsymbol{n}\right)^2} + \Delta E_1(L). && (3.1.6) \end{aligned}$$

The K and D have opposite momenta and the level is degenerate for all six values of $\boldsymbol{n} = (\pm 1, 0, 0)\,,\ (0, \pm 1, 0)\,,\ (0, 0, \pm 1)$.

Parallel considerations are valid for the 1^+ channel, which, in addition to the analogous

finite-volume versions of the $D_{s1}(2460)$ and the D^*K states, shows an additional level due to the presence of the $D_{s1}(2536)$ resonance.

The main difficulty for the lattice calculation stems from the small difference between the lowest two energy levels, the one associated to the D^*_{s0} (D_{s1}), Eq. (3.1.1), and to the threshold DK (D^*K), Eq. (3.1.3). Indeed, the previously mentioned overestimation of the D^*_{s0} mass in $\bar{c}s$ operator-based lattice simulations originated from the failure to resolve the two levels within the finite time available on the lattice. The D^*_{s0} mass was misidentified with the resulting plateaux which lies between the two energy levels; the overestimation exceeds the non-interacting DK threshold and erroneously places the D^*_{s0} above it. The importance of the employment of a variational approach founded on operators that adequately couple to the scattering state is thus evident. The most obvious way for this purpose is to include in the basis DK-like interpolators that resemble the scattering state, in addition to the standard two-quark $\bar{c}s$ operators.

Secondly, a simulation with close-to-physical pion masses is strongly advisable. The scattering state is particularly sensitive to the value of m_π due to the presence of valence light quarks in the D and K mesons and employing particularly heavy pion masses would lead to results far from physical situation.

The presence of the charm quark in this sector, which is too light for a reliable static limit approach but also too heavy to neglect discretisation effects, poses an additional issue. The heavy charm quark mass leads to possibly sizeable discretisation error terms $\mathcal{O}(am_c)$ as am_c is of order one. This term affects fine structure splittings, while spin averages are altered by milder effects $\mathcal{O}\left(a\overline{\Lambda}\right)$, with $\overline{\Lambda} \approx 500$ MeV for heavy-light systems. Lattices at several values of a generated using improved actions are preferred in order to perform the continuum-limit of the lattice results.

Less stringent conditions are instead necessary for the spatial extent of the lattice. As the connection between finite and infinite volume is well understood in the Lüscher's formalism, also moderately small volumes are considerably helpful to investigate physical properties of the system. The requirement for the volume size can be relaxed as long as exponentially suppressed terms in the Lüscher's formalism are under control.

κ_l	a(fm)	V	am_π	m_π (MeV)	Lm_π	m_K (MeV)	m_D (MeV)	m_{D^*} (MeV)	N_{conf}
0.13632	0.071	$24^3 \times 48$	0.1112 (9)	306.9 (2.5)	2.67	540(2)	1907(3)	2038(5)	2222
	0.071	$32^3 \times 64$	0.10675 (52)	294.6 (1.4)	3.42	528(1)	1902(3)	2030(5)	1453
	0.071	$40^3 \times 64$	0.10465 (38)	288.8 (1.1)	4.19	527(1)	1901(2)	2030(4)	2000
	0.071	$64^3 \times 64$	0.10487 (24)	289. (0.7)	6.70	526(1)	1898(1)	2030(2)	1463
0.13640	0.071	$48^3 \times 64$	0.05786 (55)	159.7 (1.5)	2.78	500(1)	1880(2)	2007(3)	2501
	0.071	$64^3 \times 64$	0.05425 (49)	149.7 (1.4)	3.49	497(1)	1877(1)	1996(3)	1591

Table 3.2: The six ensembles employed. Details can be found in Ref. [46].

J^P	Physical states	Two-quark op.	Four-quark op.
0^+	$D^*_{s0}(2317)$, DK	$D_s = \bar{s}\mathbb{1}c,\ \bar{s}\gamma_t c$	$DK = (\bar{u}\gamma_5 c)(\bar{s}\gamma_5 u) + \left(\bar{d}\gamma_5 c\right)(\bar{s}\gamma_5 d)$
1^+	$D_{s1}(2460)$, $D_{s1}(2536)$, D^*K	$D_s = \bar{s}\gamma_i\gamma_5 c,\ \bar{s}\gamma_t\gamma_i\gamma_5 c$	$DK = (\bar{u}\gamma_i c)(\bar{s}\gamma_5 u) + \left(\bar{d}\gamma_i c\right)(\bar{s}\gamma_5 d)$

Table 3.3: The interpolators used in the analysis.

3.2 Finite energy extraction

3.2.1 Lattice setup

The ensembles available, generated by the RQCD and QCDSF collaborations, are listed in Tab. (3.2) and can tackle some of the issues raised in the previous section. Four ensembles with $m_\pi \approx 290$ MeV and lattice length $L/a = 24, 32, 40, 64$ ($2.67 \leq Lm_\pi \leq 6.70$) are present, in addition to two ensembles with close-to-physical $m_\pi \approx 150$ MeV and $L/a = 48, 64$ ($Lm_\pi = 2.78, 3.49$). Multiple-volumes were employed in order to study the volume dependence of physical quantities and to obtain enough energy levels to probe the phase shift. An $N_f = 2$ non-perturbatively improved clover fermion action was used, with discretisation errors of order $\mathcal{O}(a^2)$. The lattice spacing is the same for all ensembles and is fairly small, $a = 0.071$ fm, corresponding to $a^{-1} = 2760$ MeV and $am_c \approx 0.5$. The strange and charm quark mass were tuned to reproduce respectively the experimental value of the combination $\sqrt{2m_K^2 - m_\pi^2} = 685.8$ MeV and the $1S$ charmonium spin average 3068.5 MeV. It is a high statistic study, with number of configurations varying from 1453 to 2501. Autocorrelations were taken into account by binning the configurations in an amount that was dependent on the particular ensemble.

3.2.2 Operator basis and the correlator matrix

Based on the statements in Sec. (3.1.2), both two-quark and four-quark interpolators are employed and are represented in Tab. (3.3). It is important to stress that the symbols

D_s and DK are just for notational convenience: both D_s and DK interpolators have the quantum numbers to create both the physical D_s and the physical DK state. For each channel, the correlator matrix has then the form

$$C(t) = \begin{pmatrix} \langle D_s(t) D_s^\dagger(0)\rangle & \langle D_s(t) (DK)^\dagger(0)\rangle \\ \langle (DK)(t) D_s^\dagger(0)\rangle & \langle (DK)(t) (DK)^\dagger(0)\rangle \end{pmatrix}. \tag{3.2.1}$$

The variational basis is enlarged by applying several smearing levels to the operators. Explicitly, for the 0^+ channel

$$\begin{aligned} D_s &= \overline{s}Ac, \\ DK &= D_u K_u + D_d K_d \\ &= (\overline{u}Bc)(\overline{s}Bu) + \left(\overline{d}Bc\right)(\overline{s}Bd), \end{aligned} \tag{3.2.2}$$

where

$$A = (\mathbb{1})^{16}, (\mathbb{1})^{60}, (\mathbb{1})^{180}, (\gamma_t)^{16}, (\gamma_t)^{60}, \tag{3.2.3}$$

$$B = (\gamma_5)^{180}. \tag{3.2.4}$$

The numbers appearing on the gamma matrices indicate the smearing level. Eqs. (3.2.2) are valid also for the 1^+ channel when replacing $\mathbb{1} \to \gamma_i\gamma_5$, $\gamma_t \to \gamma_t\gamma_i\gamma_5$ and $\gamma_5 \to \gamma_i$ in Eqs. (3.2.3) and (3.2.4). For the adjoint,

$$\begin{aligned} D_s^\dagger &= (\overline{s}Ac)^\dagger = -\overline{c}\tilde{A}s, \\ (DK)^\dagger &= (D_u K_u)^\dagger + (D_d K_d)^\dagger = K_u^\dagger D_u^\dagger + K_d^\dagger D_d^\dagger, \\ K_l^\dagger &= (\overline{s}Bl)^\dagger = -\overline{l}\tilde{B}s, \\ D_l^\dagger &= \left(\overline{l}Bc\right)^\dagger = -\overline{c}\tilde{B}l, \end{aligned}$$

with $\tilde{X} = \gamma_t X^\dagger \gamma_t$. The correlator matrix (3.2.1) is then to be viewed as a 6×6 matrix which is real and symmetric. All D_s, K and D operators are at zero momentum.

3.2.3 Wick contractions

Using the explicit formulas for the operators Eq. (3.2.2) and their adjoints, the Wick contractions of all four entries in Eq. (3.2.1) will be performed in this section. The same relations apply for both the 0^+ and 1^+ channels and the spatial index i in the latter case is

assumed fixed in the following calculations and is summed at the end. Since the valence up u and down d quarks are degenerate, the distinction between the two can be dropped once the contractions are made. The label l (light quark) will then be adopted.

In the following, the x symbol will be reserved for zero time sites, $x = (\boldsymbol{x}, 0)$. A subscript D and K to x and $\boldsymbol{x}$ is added to indicate the position of a D and K interpolator while no subscript indicates the position of the D_s interpolator. The same logic is valid for sites at timeslice t, which are indicated by $y = (\boldsymbol{y}, t)$.

The upper-left entry of Eq. (3.2.1) is the meson-meson propagation term:

$$\begin{aligned} C_{D_s,D_s'}(t) &= \langle D_s(t)\, D_s'^{\dagger}(0)\rangle = a^6 \sum_{\boldsymbol{y}\boldsymbol{x}} \langle D_s(\boldsymbol{y},t)\, D_s'^{\dagger}(\boldsymbol{x},0)\rangle \\ &= -a^6 \sum_{\boldsymbol{y}\boldsymbol{x}} \langle (\bar{s}Ac)_y \left(\bar{c}\tilde{A}'s\right)_x\rangle = a^6 \sum_{\boldsymbol{y}\boldsymbol{x}} \mathrm{Tr}\left[AG^c(y,x)\,\tilde{A}'G^s(x,y)\right]. \quad (3.2.5) \end{aligned}$$

As this is a submatrix of Eq. (3.2.1), primed indices are attached in D_s' and $\tilde{A}'$ to distinguish its off-diagonal terms.

The $DK \to D_s$ and $D_s \to DK$ entries read

$$\begin{aligned} C_{D_s,DK}(t) &= \langle D_s(t)\,(DK)^{\dagger}(0)\rangle = \langle D_s(t)\, K_u^{\dagger}(0)\, D_u^{\dagger}(0)\rangle + u \to d \\ &= 2\langle D_s(t)\, K_l^{\dagger}(0)\, D_l^{\dagger}(0)\rangle = 2a^9 \sum_{\boldsymbol{y}\boldsymbol{x}_K\boldsymbol{x}_D} \langle D_s(\boldsymbol{y},t)\, K_l^{\dagger}(\boldsymbol{x}_K,0)\, D_l^{\dagger}(\boldsymbol{x}_D,0)\rangle \\ &= 2a^9 \sum_{\boldsymbol{y}\boldsymbol{x}_K\boldsymbol{x}_D} \langle (\bar{s}Ac)_y \left(\bar{l}\tilde{B}s\right)_{x_K} \left(\bar{c}\tilde{B}l\right)_{x_D}\rangle \\ &= 2a^9 \sum_{\boldsymbol{y}\boldsymbol{x}_K\boldsymbol{x}_D} \langle (\bar{s}Ac)_y \left(\bar{c}\tilde{B}l\right)_{x_D} \left(\bar{l}\tilde{B}s\right)_{x_K}\rangle \\ &= -2a^9 \sum_{\boldsymbol{y}\boldsymbol{x}_K\boldsymbol{x}_D} \mathrm{Tr}\left[AG^c(y;x_D)\,\tilde{B}G^l(x_D;x_K)\,\tilde{B}G^s(x_K;y)\right], \quad (3.2.6) \end{aligned}$$

$$\begin{aligned}
C_{DK,D_s}(t) &= \langle (DK)(t) D_s^\dagger(0)\rangle = \langle D_u(t) K_u(t) D_s^\dagger(0)\rangle + u \to d \\
&= 2\langle D_l(t) K_l(t) D_s^\dagger(0)\rangle = 2a^9 \sum_{\boldsymbol{y}_D \boldsymbol{y}_K \boldsymbol{x}} \langle D_l(\boldsymbol{y}_D, t) K_l(\boldsymbol{y}_K, t) D_s^\dagger(\boldsymbol{x}, 0)\rangle \\
&= -2a^9 \sum_{\boldsymbol{y}_D \boldsymbol{y}_K \boldsymbol{x}} \langle \left(\bar{l}Bc\right)_{y_D} (\bar{s}Bl)_{y_K} \left(\bar{c}\tilde{A}s\right)_x \rangle \\
&= -2a^9 \sum_{\boldsymbol{y}_D \boldsymbol{y}_K \boldsymbol{x}} \langle \left(\bar{l}Bc\right)_{y_D} \left(\bar{c}\tilde{A}s\right)_x (\bar{s}Bl)_{y_K} \rangle \\
&= 2a^9 \sum_{\boldsymbol{y}_D \boldsymbol{y}_K \boldsymbol{x}} \mathrm{Tr}\left[BG^c(y_D; x)\, \tilde{A} G^s(x; y_K)\, BG^l(y_K; y_D)\right]. \qquad (3.2.7)
\end{aligned}$$

The correlator matrix is symmetric and thus computing only one of Eqs. (3.2.6) and (3.2.7) is sufficient. Nevertheless, the symmetry is valid only in the limit of infinite configurations and the two terms can be averaged for an improved signal.

The lower-right entry is more involved,

$$\begin{aligned}
C_{DK,DK}(t) &= \langle (DK)(t) (DK)^\dagger(0)\rangle \\
&= \langle \left(D_u(t) K_u(t) + D_d(t) K_d(t)\right) \left(K_u^\dagger(0) D_u^\dagger(0) + K_d^\dagger(0) D_d^\dagger(0)\right)\rangle \\
&= 2\langle D_u(t) K_u(t) K_u^\dagger(0) D_u^\dagger(0)\rangle + 2\langle D_u(t) K_u(t) K_d^\dagger(0) D_d^\dagger(0)\rangle \\
&= 2a^{12} \sum_{\boldsymbol{y}_D \boldsymbol{y}_K \boldsymbol{x}_D \boldsymbol{x}_K} \langle D_u(\boldsymbol{y}_D, t) K_u(\boldsymbol{y}_K, t) {K_u}^\dagger(\boldsymbol{x}_K, 0) D_u^\dagger(\boldsymbol{x}_D, 0)\rangle \\
&\quad + 2a^{12} \sum_{\boldsymbol{y}_D \boldsymbol{y}_K \boldsymbol{x}_D \boldsymbol{x}_K} \langle D_u(\boldsymbol{y}_D, t) K_u(\boldsymbol{y}_K, t) {K_d}^\dagger(\boldsymbol{x}_K, 0) D_d^\dagger(\boldsymbol{x}_D, 0)\rangle \\
&= 2a^{12} \sum_{\boldsymbol{y}_D \boldsymbol{y}_K \boldsymbol{x}_D \boldsymbol{x}_K} \langle (\bar{u}Bc)_{y_D} (\bar{s}Bu)_{y_K} \left(\bar{u}\tilde{B}s\right)_{x_K} \left(\bar{c}\tilde{B}u\right)_{x_D} \rangle \\
&\quad + 2a^{12} \sum_{\boldsymbol{y}_D \boldsymbol{y}_K \boldsymbol{x}_D \boldsymbol{x}_K} \langle (\bar{u}Bc)_{y_D} (\bar{s}Bu)_{y_K} \left(\bar{d}\tilde{B}s\right)_{x_K} \left(\bar{c}\tilde{B}d\right)_{x_D} \rangle .
\end{aligned}$$

The second term can be immediately contracted while the first has two contributions. We get

$$\begin{aligned}
C_{DK,DK}(t) &= \langle (DK)(t) (DK)^\dagger(0)\rangle \\
&= a^{12} \sum_{\boldsymbol{y}_D \boldsymbol{y}_K \boldsymbol{x}_D \boldsymbol{x}_K} \Big\{ 2\mathrm{Tr}\left[BG^c(y_D; x_D)\, \tilde{B} G^l(x_D; y_D)\right] \mathrm{Tr}\left[\tilde{B} G^s(x_K; y_K)\, BG^l(y_K; x_K)\right] \\
&\quad - 4\mathrm{Tr}\left[BG^c(y_D; x_D)\, \tilde{B} G^l(x_D; x_K)\, \tilde{B} G^s(x_K; y_K)\, BG^l(y_K; y_D)\right] \Big\}. \qquad (3.2.8)
\end{aligned}$$

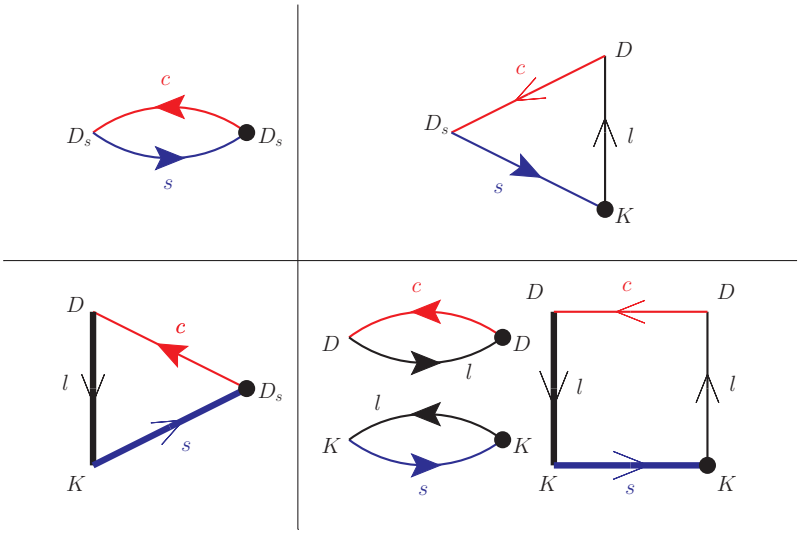

Figure 3.2.1: The Wick diagrams associated with the correlator matrix. Each line with quark q represents the corresponding propagator connecting the vertices identified by the spacetime points. Time runs from right to left. Numerical factors are understood. In terms of the text in Sec. (3.2.4), the stochastic sequential propagators are shown with open arrows and the source positions as black dots.

The traces are over the spin and colour indices and satisfy the cyclic property. The correlator matrix can thus be expressed graphically as closed oriented diagrams, Fig. (3.2.1).

3.2.4 Stochastic sources insertion

The Wick contractions performed in the previous subsection show the presence of all-to-all propagators in the box and triangular diagrams. This is the expected price to pay when two-particle operators are included in the variational basis. The problem is addressed here by the stochastic method discussed in Sec. (2.3.2). Time-spin-colour diluted noise vectors assuming values in $\mathbb{Z}_2 = \{1, i, -1, -i\}$ are introduced

$$\eta_{i\alpha}^{r,(i_0\alpha_0 t_0)}(\boldsymbol{x}, t) = \eta^{r,(i_0\alpha_0 t_0)}(\boldsymbol{x})\,\delta_{i,i_0}\delta_{\alpha,\alpha_0}\delta_{t,t_0} \tag{3.2.9}$$

and each partition element is identified by $(i_0\alpha_0 t_0)$, i.e., we have $3\cdot 4\cdot N_T$ different stochastic sources $\eta^{r,(i_0\alpha_0 t_0)}_{i\alpha}(\boldsymbol{x},t)$ which are non-zero only for $(i\alpha t)=(i_0\alpha_0 t_0)$. Explicitly, for $t=t_0$

$$\eta^{r,(i_0\alpha_0 t_0)}_{i\alpha}(\boldsymbol{x},t=t_0)=\begin{pmatrix}\eta^{r,(11t_0)}(\boldsymbol{x})\\0\\\vdots\\0\end{pmatrix},\begin{pmatrix}0\\\eta^{r,(12t_0)}(\boldsymbol{x})\\\vdots\\0\end{pmatrix},...,\begin{pmatrix}0\\0\\\vdots\\\eta^{r,(34t_0)}(\boldsymbol{x})\end{pmatrix}. \tag{3.2.10}$$

Each of the $3\cdot 4$ columns in Eq. (3.2.10) is identified by the labels $i_0\alpha_0$ while the label $i\alpha$ identifies the colour-spin components of each source. For a given Dirac matrix D, the inversions Eq. (2.3.14) can be performed,

$$\sum_{\boldsymbol{x}t_x j\beta} D_{i\alpha,j\beta}(\boldsymbol{u},t_u;\boldsymbol{x},t_x)\,Q^{r,(i_0\alpha_0 t_0)}_{j\beta}(\boldsymbol{x},t_x)=\eta^{r,(i_0\alpha_0 t_0)}_{i\alpha}(\boldsymbol{u},t_u)\,, \tag{3.2.11}$$

such that the objects Eq. (2.3.15) for each $(i_0\alpha_0 t_0)$ are obtained

$$\begin{aligned}Q^{r,(i_0\alpha_0 t_0)}_{i\alpha}(\boldsymbol{u},u_t) &= \sum_{\boldsymbol{x}x_t j\beta} G_{i\alpha,j\beta}(\boldsymbol{u},u_t;\boldsymbol{x},x_t)\,\eta^{r,(i_0\alpha_0 t_0)}_{j\beta}(\boldsymbol{x},x_t) &(3.2.12)\\ &= \sum_{\boldsymbol{x}} G_{i\alpha,i_0\alpha_0}(\boldsymbol{u},u_t;\boldsymbol{x},0)\,\eta^{r,(i_0\alpha_0 t_0)}(\boldsymbol{x})\,. &(3.2.13)\end{aligned}$$

Instead of solving Eq. (3.2.11) for each $(i_0\alpha_0 t_0)$ (and thus estimating each propagator via Eq. (2.3.16)), it is particularly useful to employ the one-end trick mentioned in Sec. (2.3.2). As it is explicitly shown in App. (A.3), all the Wick-contracted correlators of the previous subsection can be expressed in terms of the following combinations

$$\begin{aligned}Q^{q,r}(\boldsymbol{u},u_t) &= \sum_{\boldsymbol{x}} G^q(\boldsymbol{u},u_t;\boldsymbol{x},0)\,\eta^r(\boldsymbol{x})\,, \qquad u_t=0,t \quad q=l,s,c &(3.2.14)\\ S^{cl,r}(\boldsymbol{y},t) &= \sum_{\boldsymbol{x}} G^c(\boldsymbol{y},t;\boldsymbol{x},0)\,\gamma_t B^\dagger\gamma_t Q^{l,r}(\boldsymbol{x},0)\,, &(3.2.15)\\ S^{ls,r}(\boldsymbol{y},t) &= \sum_{\boldsymbol{y}'} G^l(\boldsymbol{y},t;\boldsymbol{y}'t)\,\gamma_5 B^\dagger\gamma_5 Q^{s,r}(\boldsymbol{y}',t)\,. &(3.2.16)\end{aligned}$$

These will be referred to as (stochastic) propagators. The first are just the objects Eq. (3.2.13) for $t_0=0$. This means that only the fields with $t_0=0$ are needed, such that for each $q=l,s,c$ and r only $3\cdot 4$ inversions Eq. (3.2.11) have to be performed. Eq. (3.2.14) is in spin-colour matrix form and the superscript $(i_0\alpha_0 0)$ on η is hidden. All other propagators

can be obtained sequentially, i.e., the S stochastic propagators appearing in Eqs. (3.2.15) and (3.2.16) are obtained by inversions similar to Eq. (3.2.11) using Q as a source[1]:

$$\sum_{\boldsymbol{x}t_x j\beta} D^{q'}_{i\alpha,j\beta}\left(\boldsymbol{u},t_u;\boldsymbol{x},t_x\right) S^{q'q,r,(i_0\alpha_0 t_I)}_{j\beta}\left(\boldsymbol{x},t_x\right) = \pm BQ^{qr,(i_0\alpha_0 t_I)}_{i\alpha}\left(\boldsymbol{u},t_u\right) \tag{3.2.17}$$

where $Q \propto \delta_{t_I t_u}$. The G^c propagator in Eq. (3.2.15) is needed only for $t_I = t_0 = 0$ and thus only $3 \cdot 4$ inversions (for each i_0 and α_0) are to be performed in order to obtain S^{cl}. On the contrary, in addition to the spin-colour inversions, all $t_I = t$ inversions are required for S^{ls}. This is the dominant contribution to the computational cost for the study of this channel with this method and, moreover, the cost is aggravated by the fact that each t_I inversion to obtain S^{ls} involves a light-quark.

Then, as shown in App. (A.3),

$$C_{D_s,D'_s}(t) = \frac{a^6}{N}\sum_{r\boldsymbol{y}} \mathrm{Tr}\left[(\gamma_5 A)\, Q^c\left(y;\eta^r\right)\left(\tilde{A}'\gamma_5\right) Q^{s\dagger}\left(y;\eta^r\right)\right] \tag{3.2.18}$$

$$C_{D_s,DK}(t) = -2\frac{a^9}{N}\sum_{r\boldsymbol{y}} \mathrm{Tr}\left[(\gamma_5 A)\, S^{cl}\left(y;\eta^r\right)\left(\tilde{B}\gamma_5\right) Q^{s\dagger}\left(y;\eta^r\right)\right] \tag{3.2.19}$$

$$C_{DK,D_s}(t) = 2\frac{a^9}{N}\sum_{r\boldsymbol{y}_D} \mathrm{Tr}\left[(\gamma_5 B)\, Q^c\left(y_D;\eta^r\right)\left(\tilde{A}\gamma_5\right) S^{ls\dagger}\left(y_D;\eta^r\right)\right] \tag{3.2.20}$$

$$\begin{aligned} C_{DK,DK}(t) &= 2C_D(t)\, C_K(t) - 4C_{\mathrm{box}}(t) \\ &= 2\left(\frac{a^6}{N}\sum_{r\boldsymbol{y}_D} \mathrm{Tr}\left[(\gamma_5 B)\, Q^c\left(y_D;\eta^r\right)\left(\tilde{B}\gamma_5\right) Q^{l\dagger}\left(y_D;\eta^r\right)\right]\right) \times \\ &\quad \left(\frac{a^6}{N}\sum_{r\boldsymbol{y}_K} \mathrm{Tr}\left[(\gamma_5 B)\, Q^l\left(y_K;\eta'^r\right)\left(\tilde{B}\gamma_5\right) Q^{s\dagger}\left(y_K;\eta'^r\right)\right]\right) \\ &\quad -4\frac{a^{12}}{N}\sum_{r\boldsymbol{y}_D} \mathrm{Tr}\left[(\gamma_5 B)\, S^{cl}\left(y;\eta^r\right)\left(\tilde{B}\gamma_5\right) S^{ls\dagger}\left(y_D;\eta^r\right)\right] \end{aligned} \tag{3.2.21}$$

where $y_i = (\boldsymbol{y}_i, t)$. In these expressions, the propagators Q and S are to be viewed as 12×12 matrices in spin-colour space, $Q^{r,(i_0\alpha_0 0)}_{i\alpha} \equiv Q^r_{i\alpha,i_0 a_0}$; the indices $i_0\alpha_0$ that label the partition element serve as matrix-multiplying indices in the spin-colour trace.

3.2.5 Technical implementation

This section is dedicated to more technical topics about the actual way the correlator functions in the previous subsection were obtained on the computer.

[1]The spin index α includes B, i.e. in terms of spin the rhs of Eq. (3.2.17) is $(BQ)_\alpha = \sum_{\alpha'} B_{\alpha\alpha'} Q_{\alpha'}$

Utilising only one set of stochastic sources was enough, as the stochastic error for $N = 1$ was seen to be negligible compared to the gauge error. As mentioned in App. (A.3), only spin-dilution is essential in order to recycle as many propagators as possible, although diluting also the colour was convenient.

The Wick-contractions in Sec. (3.2.3) do not explicitly show the smearing functions. As seen in Eq. (2.3.5), quark (or operator) smearing is equivalent to smearing directly the propagators such that those appearing in the Wick-contracted correlators Eqs. (3.2.5), (3.2.6), (3.2.7) and (3.2.8) are smeared both at the source and at the sink. The smearings are inherited by the stochastic propagators Q and S. In fact, inverting Eq. (3.2.11) with the smeared source $S_1\eta$ and successively smearing the result by S_2 leads to the stochastic Q in Eq. (3.2.15) in terms of the smeared propagator $G = S_2 D^{-1} S_1$. A similar argument applies for the sequential stochastic propagators S, which are obtained by the inversion Eq. (3.2.17) with a smeared $S_3 Q$ source and are successively smeared at the sink.

The smearing function used in this work is the Wuppertal-smearing Eq. (2.3.6) with APE-smoothed links and it is applied n_{itr} times to lattice objects, according to Eqs. (3.2.3) and (3.2.4). As the Wuppertal smearing is spin-independent, the smearing function can be split unevenly between the propagators. This freedom is exploited in order to minimise the number of inversions, to favour cheaper charm-quark inversions and, most importantly, calculate the expensive sequential propagator Eq. (3.2.16) only once.

The calculation of the correlator matrix required ultimately fourteen charm-quark , three strange-quark and 15+3 light-quark inversions. The fifteen inversions refer to the propagator Eq. (3.2.16) which was restricted to the interval $5 \leq t/a \leq 19$, a convenient range where the effect of excited states in the correlator have died away and where the errors are still small.

The computational time of the run, for each configuration, is determined mainly by the quark inversions but other factors have an impact. For instance, the smearing procedure itself can be time costly (especially for particular large number of iterations) and, in light of maximal efficiency, higher smeared propagators were obtained by iteratively smearing the lower ones, whenever possible.

Once all inversions and smearings were performed, the traces and the sums in Eqs. (3.2.18) (3.2.19) (3.2.20) (3.2.21) were calculated for each configuration. The $D_s - D_s$ and $D_s - DK$ diagrams were calculated for all timeslices $t/a = 0, ..., N_T - 1$ and, due to (anti)periodic boundary conditions in the temporal direction, their value at time t was averaged with those at time $N_t - t/a$ for a better signal. The $DK - D_s$ and $DK - DK$ diagrams, which contain the expensive S^{lc} propagator, were limited to the $5 \leq t/a \leq 19$

range ($4 \leq t/a \leq 17$ for the $24^3 \times 48$ ensemble). Finally, the correlator matrix was made symmetric by averaging the transposed entries.

In addition to the calculation of the correlator matrix, also the negative parity D_s and D_s^* states were simulated for every ensemble. Only two-point functions built from $\overline{c}\gamma_5 s$ and $\overline{c}\gamma_i s$ interpolators were required for the extraction of their masses. These will be displayed in Sec. (3.3.3).

This concludes the discussion regarding the computation of the correlators. Starting from the next subsection, the way how the data was analysed and linked to physical information is presented.

3.2.6 Energy results

With the correlator matrix at our disposal we can determine its eigenvalues and eigenvectors by means of the variational method discussed in Sec. (2.3.3). This is performed for each ensemble, each channel and each timeslice $6 \leq t/a \leq 19$ with the reference time $t_0 = 5$. The n-th energy level E_n can be obtained by the exponential decay of n-th eigenvalue whose leading term is Eq. (2.3.32).

Effective mass Before dealing directly with fits of the eigenvalues, a rough idea about the spectrum and the stability of the variational method can be given by computing the effective mass of the eigenvalues which tends to a constant value once the contamination from excited states have disappeared,

$$E_k\left(t + \frac{a}{2}, t_0\right) = \log \frac{\lambda_k\left(t, t_0\right)}{\lambda_k\left(t + a, t_0\right)}. \tag{3.2.22}$$

The effective masses for the lowest two eigenvalues for the 4×4 correlator matrix (discarding the operators that include γ_4) are shown in Fig. (3.2.2) for both channels. The plots show separately the $m_\pi \approx 290$ MeV and the $m_\pi \approx 150$ MeV results. It is clear that, as the volume is increased, the separation between the two levels gets smaller: as one would expect, the energy level corresponding to the scattering state decreases towards the infinite volume threshold (horizontal black line), while the level corresponding to the bound state increases to its infinite volume mass. The excited state contributions to the eigenvalues appear to fall below the noise at approximately $t/a = 12 - 14$. The error bars, obtained by the jackknife resampling method, increase with time but are still under control in the range under consideration.

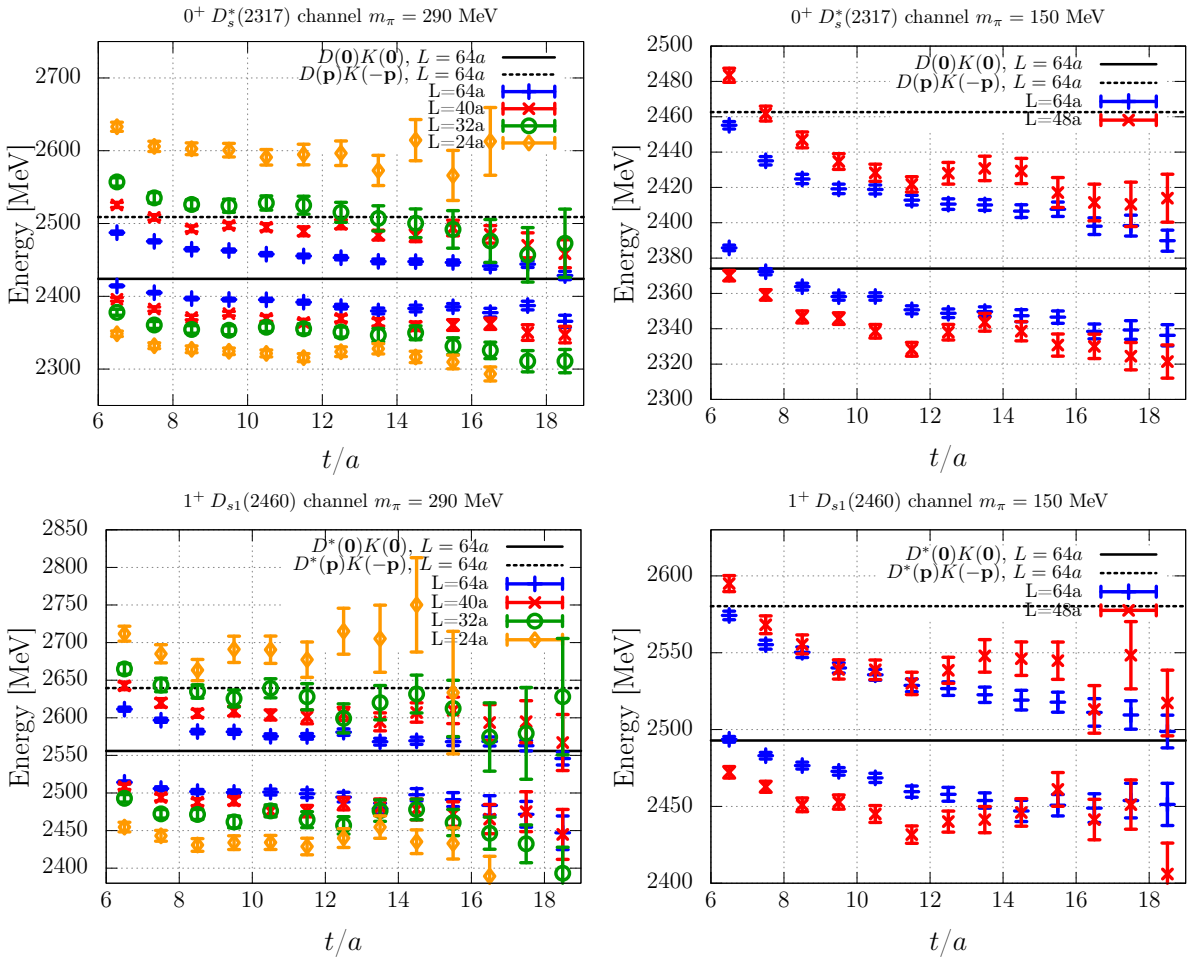

Figure 3.2.2: The effective mass of the lowest two eigenvalues for the 0^+ (top) and 1^+ (bottom) channels and for the $m_\pi = 290$ MeV (left) and $m_\pi = 150$ MeV (right) ensembles. Also shown are the non-interacting $D(\mathbf{0})K(\mathbf{0})$ and (lowest) $D(\boldsymbol{q})K(-\boldsymbol{q})$ levels for the largest spatial volume. The figure is taken from Ref. [36].

Fit The precise extraction of the energies requires a fit to the eigenvalues. Given a fitting function[2] $\lambda_\alpha(t)$ with parameters α, the fit is performed by minimising the chi-square

$$\chi^2(\alpha) = \sum_{t,t'=t_{\min}}^{t_{\max}} \left(\lambda_\alpha(t) - \lambda(t)\right) \sigma^{-1}_{tt'} \left(\lambda_\alpha(t') - \lambda(t')\right) \tag{3.2.23}$$

with respect to α. In Eq. (3.2.23), $t_{\min}$ and $t_{\max}$ indicate the fitting boundaries, $\lambda(t)$ denotes the eigenvalue data and $\sigma_{tt'}$ is the covariance matrix (expressible in terms of the eigenvalue jackknives) which takes care of correlations between different times. The fit functions which were considered are the one-exponential and two-exponential functions

$$\lambda^{(k)}_{1\text{exp}}(t,t_0) = Ae^{-E_k(t-t_0)}, \tag{3.2.24}$$

$$\lambda^{(k)}_{2\text{exp}}(t,t_0) = Ae^{-E_k(t-t_0)}\left(1+\left(\frac{1}{A}-1\right)e^{-E'_k(t-t_0)}\right). \tag{3.2.25}$$

The first is the leading term Eq. (2.3.32) for $A=1$ and can result in a reasonable χ^2/d.o.f. only for large $t_{\min}$. The amplitude parameter A was kept free to allow for any residual contamination and was checked to be close to one for large $t_{\min}$. Note that for this function, the minimisation of the χ^2 can be performed analytically in terms of the linear function $\log\lambda^{(k)}_{1\text{exp}}(t,t_0) = \log A - E_k(t-t_0)$, avoiding therefore subtleties of a numerical minimisation in the choice of suitable input parameters. The two exponential form models the contaminations of Eq. (2.3.32) in terms of a one exponential correction to Eq. (3.2.24) and can be fitted for lower times. The exact relation $\lambda^{(k)}(t=t_0,t_0)=1$, which can be immediately seen from Eq. (2.3.28), allows to reduce the number of parameters of the two exponential function from four to three, resulting in a more stable fit.

Of course, the two fitting functions should give comparable results in the corresponding region of ranges $[t_{\min}, t_{\max}]$ (different for each one) where the χ^2/d.o.f. is stable and close to one. This was always the case and it can be seen in Fig. (3.2.3) for a particular ensemble.

Discussion The variational method and the subsequent fitting was applied to each ensemble, channel and for several subsets of the interpolator basis. Also the fitting ranges $[t_{\min}, t_{\max}]$ were varied and an optimal choice was made for each case. The fitted energies are shown in Fig. (3.2.4) for both channels, for different operator bases and for the most physical ensemble $m_\pi = 150$ MeV and $L = 64a$. In both channels it is clear that, when only the D_s-like operators are included, the lowest level obtained is influenced by both the actual

[2]The reference time t_0 and the label n which identifies the eigenvalue are hidden.

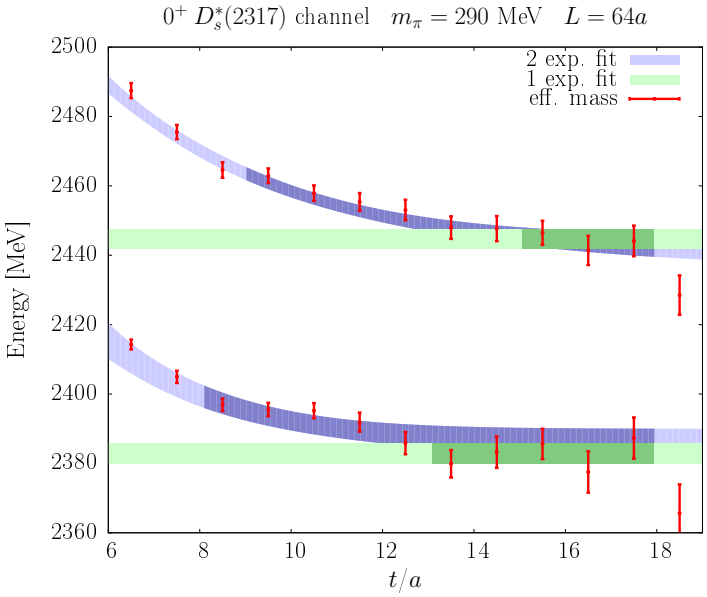

Figure 3.2.3: Comparison of the energy fits using Eqs. (3.2.24) and (3.2.25) for $k = 1, 2$ for the $m_\pi = 290$ MeV and $L = 64a$ ensemble. The darker colours indicate the fitting ranges and the widths indicate the error of Eq. (3.2.22) when using the fitted eigenvalues.

ground state and the scattering state and is correctly resolved only with the incorporation of the DK-like operators. One can note that also in the former case the position of the lowest level is below the non-interacting threshold, in agreement with a bound state interpretation, whereas some previous lattice studies placed it above.

In the 1^+ channel there is an additional level which is easily identified[3] with the $D_{s1}(2536)$. The level associated to this state is easily distinguished from that of the D^*K as it behaves differently. It has a less pronounced volume dependence and it is observed only when the $\propto \gamma_t$ interpolators are present, independently of the presence of the DK operators. This level is unaffected by the DK operators, compatible with a low coupling of the $D_{s1}(2536)$ to the D^*K state in s-wave.

The other ensembles show a similar pattern to that of Fig. (3.2.4), the main difference being that the heavy pion mass for the $m_\pi = 290$ MeV ensembles increases the D^*K scattering level which surpasses the $D_{s1}(2536)$.

Just as one does not resolve the $D(\mathbf{0})K(\mathbf{0})$ state without the four-quark operator, the next scattering state $D(\boldsymbol{q})K(-\boldsymbol{q})$ with $|\boldsymbol{q}| = \frac{2\pi}{L}$ and energy Eq. (3.1.6) is not resolved without the corresponding operator. The absence of such operator in our analysis could in

[3]Please note that a direct identification of a finite-volume level with a resonance can only make sense for resonances with particularly low coupling which implies a narrow avoided level crossing.

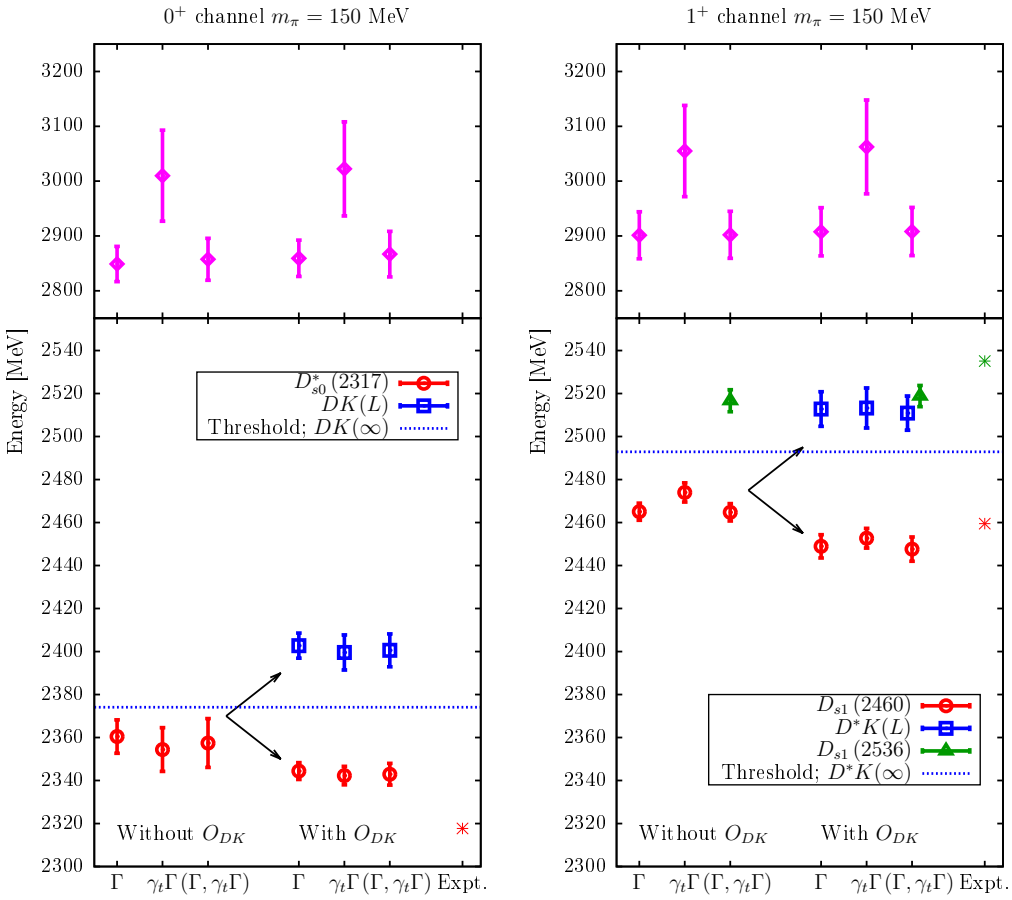

Figure 3.2.4: The fitted energy levels for the $m_\pi = 150$ MeV and $L = 64a$ ensemble for different operator bases. Here the symbol Γ identifies the operator basis according to Tab. (3.3) with $\Gamma = \mathbb{1}$ for the 0^+ channel (left plot) and $\Gamma = \gamma_i\gamma_5$ for the 1^+ (right plot). Each basis includes all smearing levels, Eq. (3.2.3), except for the combination $(\Gamma, \gamma_t\Gamma)$ in the scalar sector which discards the $(\gamma_t\Gamma)^{16}$ operator. The non-interacting threshold is shown as a dashed horizontal line.

	$J^P = 0^+$		$J^P = 1^+$		
L/a	D^*_{s0}	DK	D_{s1}	D^*K	D_{s1}
$m_\pi = 290$ MeV					
24	2318(5)	2594(13)	2435(6)	2691(16)	2549(14)
32	2352(5)	2529(5)	2469(6)	2621(14)	2540(17)
40	2362(4)	2485(6)	2477(8)	2602(6)	2574(11)
64	2382(3)	2440(5)	2496(4)	2570(3)	2552(5)
$m_\pi = 150$ MeV					
48	2332(5)	2417(6)	2440(4)	2535(4)	2533(6)
64	2344(4)	2402(6)	2449(5)	2513(8)	2519(5)

Table 3.4: The lowest energy levels in MeV for both channels. The errors are statistical and obtained by the jackknife resampling method.

principle lead to a significantly overestimated energy level for the $D(\mathbf{0})K(\mathbf{0})$ state. That this is not the case can be inferred by looking at the expected position of the $D(\boldsymbol{q})K(-\boldsymbol{q})$ level, which, due to the small size of the interaction terms in Eq. (3.1.6), is close to the related (and known) non-interacting level. The difference between the two scattering levels then ranges from approximately 85 MeV to 500 MeV according to the volume. Based on these large numbers (especially for the ensembles with smaller spatial extent) and on the results of Ref. [47] which explicitly include the $D(\boldsymbol{q})K(-\boldsymbol{q})$ operators, we can confidently conclude that this contamination is indeed small.

Finally, we summarise our final energy results in Tab. (3.4).

3.3 Connection to infinite volume

The energies which were extracted from the lattice simulation all lie around and close to the non-interacting threshold. The data points related to the D_s particle Eq. (3.1.1) and the first scattering state Eq. (3.1.3) are slightly below ($k^2 < 0$) and above ($k^2 > 0$) threshold, respectively. This is the region of the T-matrix that can be probed when using the methods of Sec. (2.4). These require the single-meson masses, m_K, m_D and m_{D^*} as an input but ignore their mild volume dependence (see Tab. (3.2)). The single-meson masses are set to be those of the largest volume $L = 64a$ of the related set of ensembles and systematics arising from this procedure will be discussed later.

The infinite-volume analysis was performed according to both the methods discussed in Sec. (2.4). Lüscher's formalism and the application of the effective range approximation is the topic of Sec. (3.3.1), while the employment of the potential method is discussed in Sec.

(3.3.2). The two methods were previously also applied to the DK and D^*K channels in Refs. [47] and [48], respectively. Finally, the results obtained are summarised and compared to experiment in Sec. (3.3.3).

3.3.1 Phase shift

As the simulation was carried out in the CM frame, the momentum k^2 which appears in Lüscher's relation Eq. (2.4.8) could be calculated by directly inverting Eq. (3.1.1) and Eq. (3.1.3). The $\mathcal{Z}_{00}$ function is then calculated by means of the formula in the appendix of Ref. [49] for data points above threshold, while the simpler Eq. (2.4.10) is used for those below threshold. The resulting $k\cot\delta\,(k)$ function is then probed and presented for both channels and pion masses in Fig. (3.3.1).

Except for the rightmost data point, we see a reasonable linear behaviour of our data, compatible with the effective range approximation Eq. (1.4.25) which is valid close to the threshold $k^2 = 0$. The fit to Eq. (1.4.25) is performed excluding the suspicious $L = 24a$ data point and the values of the scattering length and effective range are then obtained. The linear model for $k\cot\delta$ is represented by the blue and red lines in Fig. (3.3.1). In all cases, a slightly positive slope is visible, corresponding to a slightly positive r_0. Also, the value of a_0^{-1} can be read off from the intersection with the $k^2 = 0$ threshold and is always negative, compatible with the existence of the bound state. In the plot, also the curve $ik = -\sqrt{-k^2}$ is shown as a dotted curve in the left regions. By Eq. (1.4.28) and its effective range form Eq. (1.4.30), $k\cot\delta$ intersects[4] this curve at the infinite-volume binding momentum $|k_{D_s}|$, with the index D_s referring to the $D_{s0}^*\,(2317)$ bound state for the 0^+ channel and to the $D_{s1}\,(2536)$ for the 1^+. Knowing this quantity, the bound state mass m_{D_s} and binding energy ΔE_{D_s} can be obtained from the infinite-volume versions of Eq. (3.1.1) and Eq. (3.1.2) while the bound state coupling g^2, defined in Eq. (1.4.27), can be obtained from Eq. (1.4.31). All results are listed in Tab. (3.5).

As already deduced from Fig. (3.2.2), the energy levels approach the threshold as L is increased. In particular, all below-threshold $L = 64a$ data points are compatible (considering the errors) with the $ik = -\sqrt{-k^2}$ curve and, consequently, the infinite volume masses shown in Tab. (3.5) are compatible with the $L = 64a$ results of Tab. (3.4).

The pion mass plays an important role for the infinite volume results. Smaller pion masses are associated to larger (in absolute value) scattering lengths, smaller energy bindings and

[4]Note that if a_0 was positive this intersection could have not taken place.

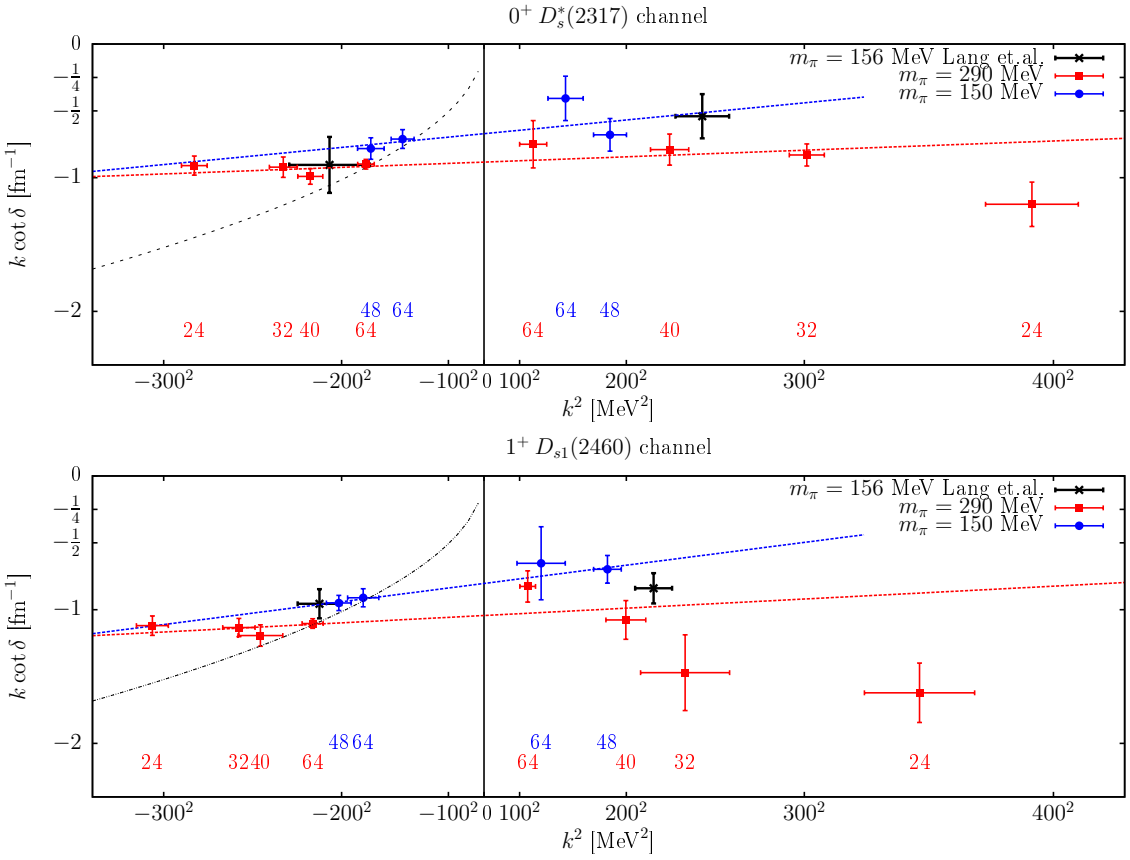

Figure 3.3.1: The real $k \cot \delta$ combination as a function of k^2 for both channels and values of m_π extracted using Lüscher's relation applied to the ground state, the left region ($k^2 < 0$), and to the first scattering state, the right region ($k^2 > 0$). The two regions are separated by the vertical line with represents the threshold $k^2 = 0$. Data from [47] are included for comparison. The blue and red lines represent the result of the fit of the data to the effective range approximation and the dotted curve in the left region represents $ik = -\sqrt{-k^2}$.

	$m_\pi = 290$ MeV	$m_\pi = 150$ MeV	Expt.
	0^+ channel		
a_0 (fm)	$-1.13\,(0.04)\,(+0.05)$	$-1.49\,(0.13)\,(-0.30)$	
r_0 (fm)	$0.08\,(0.03)\,(+0.08)$	$0.20\,(0.09)\,(+0.31)$	
$\lvert k_{D_s}\rvert$ (MeV)	$180\,(6)\,(0)$	$142\,(11)\,(-9)$	
$-\Delta E_{D_s}$ (MeV)	$40\,(3)\,(0)$	$26\,(4)\,(-3)$	$42.6\,(0.7)\,(2.0)$
m_{D_s} (MeV)	$2384\,(2)\,(-1)$	$2348\,(4)\,(+6)$	$2317.7\,(0.6)\,(2.0)$
g (GeV)	$11.9\,(0.3)\,(+0.5)$	$11.0\,(0.6)\,(+1.2)$	
	1^+ channel		
a_0 (fm)	$-0.96\,(0.05)\,(-0.04)$	$-1.24\,(0.09)\,(-0.12)$	
r_0 (fm)	$0.11\,(0.06)\,(+0.08)$	$0.27\,(0.07)\,(+0.13)$	
$\lvert k_{D_s}\rvert$ (MeV)	$219\,(7)\,(0)$	$180\,(11)\,(-3)$	
$-\Delta E_{D_s}$ (MeV)	$59\,(4)\,(0)$	$42\,(5)\,(-2)$	$42.9\,(0.7)\,(2.0)$
m_{D_s} (MeV)	$2497\,(4)\,(-1)$	$2451\,(4)\,(+1)$	$2459.5\,(0.6)\,(2.0)$
g (GeV)	$14.2\,(0.6)\,(+0.7)$	$13.8\,(0.7)\,(+1.1)$	

Table 3.5: The scattering length a_0, the effective range r_0, the binding momentum $|k_{D_s}|$, the binding energy ΔE_{D_s}, the bound state mass m_{D_s} and the bound state coupling g calculated for both channels and m_π in the setting of the effective range approximation. The first errors are statistical, the second are systematic and are obtained by repeating the analysis using only the $L = 64a$ ensemble for $m_\pi = 150$ MeV and the $L = 64a$, $40a$ ensembles for $m_\pi = 290$ MeV.

lower masses m_{D_s}. In particular, the masses of the $D_{s0}^*(2317)$ and $D_{s1}(2460)$ at $m_\pi = 150$ MeV differ considerably from their values at $m_\pi = 290$ MeV, with a difference of ~ 35 MeV and ~ 45 MeV, respectively. Such a strong pion mass dependence, not seen in the corresponding negative parity D_s and D_s^* states, makes it hard to conceive a simple charm-strange composition of these particles, favouring instead a more complicated structure involving light quarks.

Volume dependence The same information contained in Fig. (3.3.1) can be re-expressed in a convenient way that emphasises the volume dependence of the energies extracted on the lattice and their infinite-volume value. In particular, the volume dependence of the binding energy $\Delta E_{\tilde{D}_s}(L)$ in Eq. (3.1.2) and the interaction term of the first scattering state, $\Delta E_0(L)$ in Eq. (3.1.4), are displayed in the lower and upper regions of Fig. (3.3.2), respectively. Here the threshold is represented by the horizontal black line $\Delta E = 0$, to which $\Delta E_0(L)$ tends as $L \to \infty$. In this limit, the negative binding energy $\Delta E_{\tilde{D}_s}(L)$ is seen to increase towards the infinite volume value ΔE_{D_s}. It is clear from this plot that a reduction of the pion mass gives rise to a more shallow bound state. With the knowledge of the $k \cot \delta$ function in the effective range approximation it is possible to obtain the solutions $k_n(L)$ of the implicit

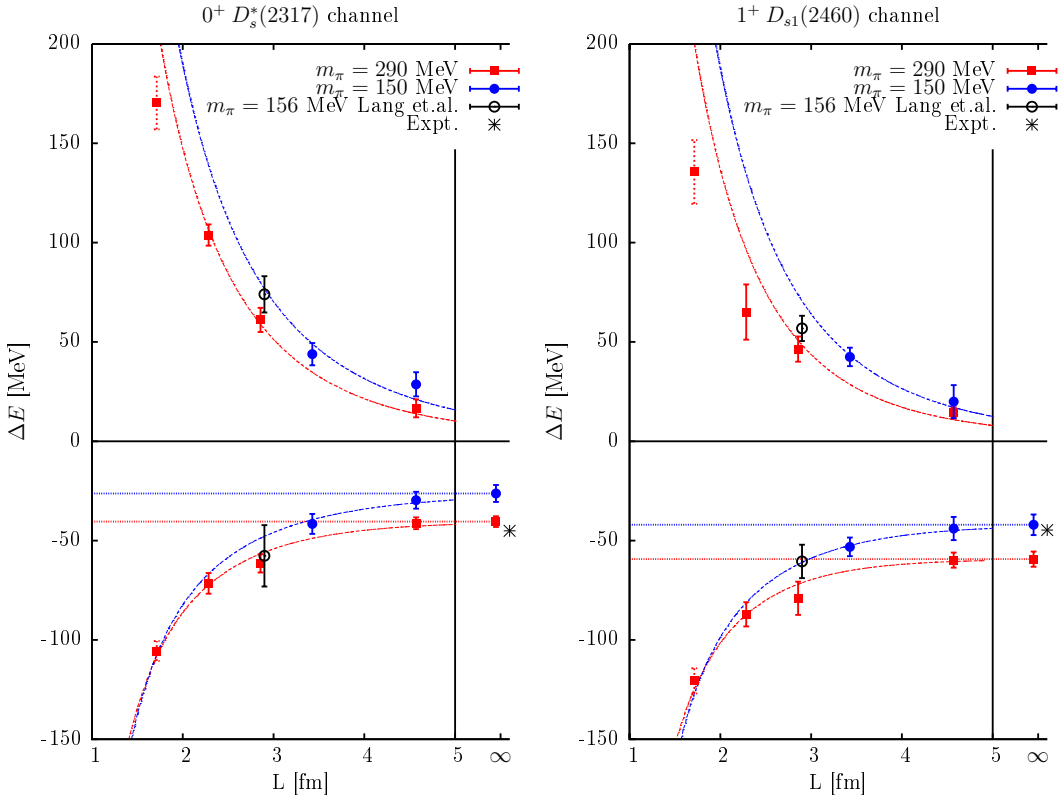

Figure 3.3.2: The splittings of the lowest two energy levels with the non-interacting threshold as a function of L. The results are compared to those of Ref. [47].

relation Eq. (2.4.12). These were plotted in Fig. (3.3.2) in terms of $\Delta E_n(L)$ for $n = D_s, 0$.

Systematics We list here the systematic errors which may have had an impact on our analysis:

- Discretisation effects are expected to be the leading contamination to our results and will be discussed in Sec. (3.3.3).

- The effect of higher partial waves is suppressed at low energies so that Lüscher's simple form Eq. (2.4.8) of the quantisation condition could have been used. This is no longer true at high energies.

- Only DK two-particle states were considered while an opening of the $D_s\eta$ and $D_s^*\eta$ channels in respectively the 0^+ and 1^+ sector is expected. The positions of the corresponding non-interacting thresholds can not be inferred from our analysis as it would have required the (expensive) calculation of the mass of the η. Nevertheless, these thresholds are expected to be located in the high energy region of Fig. (3.3.1) and do not have an impact on the lower energy points. The effect of these states should be investigated in a future work in the setting of a coupled channel analysis.

- The exponentially suppressed corrections $\sim e^{-m_\pi L}$ are not considered in Lüscher's approach and are responsible for the volume dependence of m_K, m_D and m_{D^*}. These effects are mostly notable for the $24a$ ensemble which has $Lm_\pi = 2.67$.

- The effective range approximation itself will eventually break down away from the threshold. The potential method, described in the next subsection, does not rely on the effective range approximation and consequently it is uneffected by this systematic error.

Apart from discretisation effects, all these systematics become small at lower energies, close to the threshold. The $L = 24a$ data point lies in the high energy region, the rightmost part of Fig. (3.3.1) and is therefore particularly prone to these systematics. As a consequence, this ensemble was excluded from the fit to the effective range approximation. The systematic errors, which are shown in Tab. (3.5) were estimated by repeating the fit considering only the $L = 64a$ ensemble for $m_\pi = 150$ MeV (two data points) and $L = 64a$, $40a$ for $m_\pi = 290$ MeV (four data points).

3.3.2 Potential

The potential formalism discussed in Sec. (2.4.2) is an alternative method for extracting infinite-volume information and was also employed in our work. The central equation is Eq. (2.4.18) and it was used in the dimensional-regularised form[5],

$$V\left(s_n,\alpha\right)^{-1}=\tilde{G}\left(s_n,\alpha,L\right),\qquad n=\tilde{D}_s,\sqrt{0}. \tag{3.3.1}$$

The finite-volume loop function $\tilde{G}\left(s_n,\alpha,L\right)$ was calculated using Eq. (2.4.15) for the energy levels $n=\tilde{D}_s$ and $n=\sqrt{0}$ of each ensemble. The renormalisation scale μ was set to m_D and m_{D^*} for the scalar and axialvector channels, respectively. To check consistency, the subtraction constant α was varied in five steps in the range between -0.4 and -2.2. Although the potential depends on the value of α, physical quantities should not be affected by it.

The calculation of $\tilde{G}\left(s_n,\alpha,L\right)$ requires the calculation of $\Delta G\left(s,L\right)$, Eq. (2.4.16). This is not a trivial function and its calculation is complicated by the presence of unphysical fluctuations as Λ increases. These die away in the $\Lambda\to\infty$ limit, see the left part of Fig. 2 in Ref. [50]; one may average the fluctuations over several values of Λ or, even better, introduce a smooth cutoff $\Lambda\left(\boldsymbol{q}\right)=\frac{\alpha^\tau}{a^\tau+|\boldsymbol{q}|^\tau}$ as suggested in Ref. [35]. The latter approach was chosen in our work for the values above threshold and the independence of $\Lambda\left(\boldsymbol{q}\right)I\left(s,\boldsymbol{q}\right)$ on the direction of $\boldsymbol{q}$ was exploited to transform the integral and summation parts of Eq. (2.4.16) in a one-dimensional integral and sum, respectively. The integrand contains a singularity[6] at $|\boldsymbol{q}|=k$ and thus the Cauchy's principal method is optimal for the numerical integration. For values of s below threshold we can use a simpler formula from Ref. [50], which in our case reads

$$\begin{aligned}\Delta G\left(s,L\right) &= -\frac{1}{8\pi^2}\int_0^1 dx\sum_{n=1}^{\infty}\theta_n K_0\left(L\sqrt{nf\left(s,x\right)}\right), \qquad s<s_{th},\\ f\left(s,x\right) &= x\left(x-1\right)s+xm_D^2+\left(1-x\right)m_K^2.\end{aligned}$$

K_0 is the $m=0$ modified Bessel function of the second kind and θ_n is the usual theta series in App. (A.2).

Note that we could have avoided the calculation of ΔG by employing the cutoff reg-

[5]The label D is dropped and the potential and loop functions in this section are understood to be in dimensional regularised scheme.

[6]k is related to s by Eq. (2.4.6), as usual.

ularisation instead, so that V^{-1} could have easily been obtained by calculating just Eq. (2.4.14)[7]. Nevertheless, the calculation of ΔG allows to explicitly extract the T-matrix via Eq. (2.4.19) and in turn, to access the $k\cot\delta$ function. This approach for the calculation of the $k\cot\delta$ function could then be compared to Lüscher's approach, based on Eq. (2.4.8), in order to investigate the magnitude of small effects which are present in the former approach but neglected in the latter. These turned out to be minimal (especially for the large volume ensembles) and all results quoted in the previous subsection could have been taken interchangeably from the two methods.

Another reason to employ the dimensional regularisation comes from the possibility to directly compare our potential to the explicit expression obtained from leading order heavy meson chiral perturbation theory (HMChPT) for the scalar channel [51],

$$V(s) = \frac{1}{4F_\pi^2}\left[-3s + \frac{\left(m_D^2 - m_K^2\right)^2}{s} + 2\left(m_D^2 + m_K^2\right)\right], \tag{3.3.2}$$

where F_π is the pion decay constant (with the normalisation such that it is = 92 MeV in experiment). This expression should be evaluated with the parameters of the simulation. As usual, $m_{D/K}$ are taken to be those of the $L = 64a$ ensemble of each pion mass and F_π was determined in Ref. [52], with 95.1 (3) MeV at $m_\pi = 290$ MeV and 85 (1) MeV at $m_\pi = 150$ MeV.

With these values, this function is essentially linear in the region of energies we are considering and justifies the reasonable linear behaviour that can be seen in Fig. (3.3.3) for all our data points, except for the $L = 24a$ point in the extreme right region. This modest deviation from the trend for the $L = 24a$ point was also seen for the $k\cot\delta$ data of the previous subsection and the breakdown of the effective range approximation was a plausible explanation, amongst others, for this behaviour. Yet, the same deviation is seen also in this context which does not have a corresponding breakdown. This suggests that sources of non-linearity of the potential, and in turn of our $k\cot\delta$ data, should be looked for elsewhere. Non-linear contaminations were discussed in Ref. [53], namely CDD poles [54], unphysical cuts and the influence of the $D_s\eta$ channel. The first two are shown to be negligible (see also Ref. [48]) while the last could be the responsible for the peculiar behaviour of the $L = 24a$ data point. Indeed, as discussed in Ref. [53], the effect of the new channel is to add a term $\propto G_{\eta D_s}(s)$ to the potential, where $G_{\eta D_s}(s)$ is the loop function Eq. (1.4.43) for the ηD_s system. With an estimated mass for the η, the resulting behaviour is compatible with the

[7]Of course, both regularisations were ultimately used to check consistency of the results.

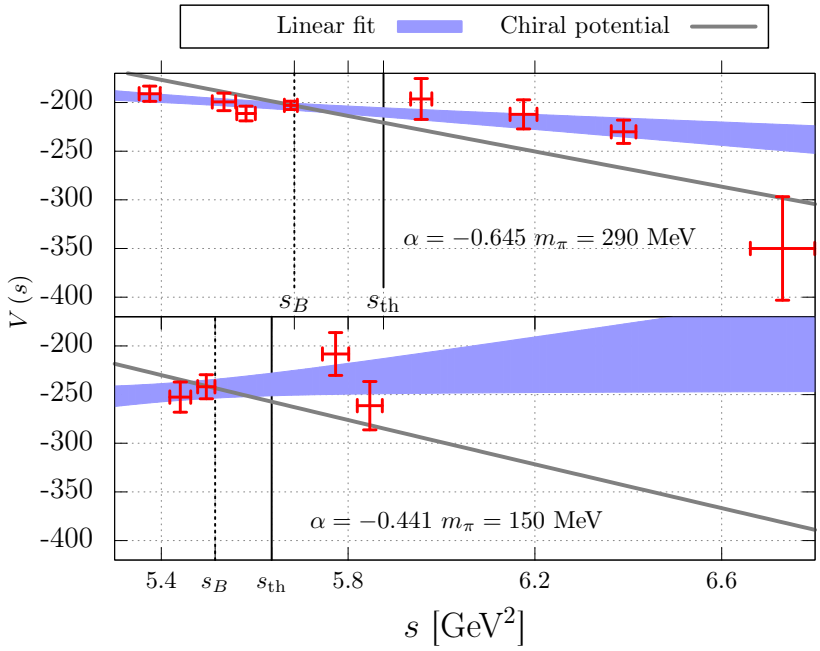

Figure 3.3.3: The potential extracted for the scalar channel and both pion masses. The subtraction constant is chosen to match the HMChPT expression (3.3.2) (shown grey) to the lowest level of the corresponding $L = 64a$ ensemble. The linear fits to the data are shown with one sigma error bars. The figure is taken from Ref. [36].

high energy region of Fig. (3.3.3) and is more evident for the 1^+ channel (not displayed), to which this discussion also applies. Together with the exponentially suppressed contributions, this could be the leading effect contaminating the potential and the $k \cot \delta$ function at higher energies but an ultimate statement can be made only when including the ηD_s (and ηD_s^*) interpolators in the simulation and performing a coupled channel analysis.

Excluding the $L = 24a$ data point, linear fits to the data are performed and the bound state mass is obtained by numerically solving Eq. (1.4.48). In turn, the coupling g^2 and compositeness $1 - Z$ are calculated from Eq. (1.4.49) and are reported in Tab. (3.6).

The independence of these results on the subtraction constant and the consistency with the previous section gives confidence in our results.

Eq. (1.4.49) tells us that the magnitude of the compositeness factor Z of the bound state can be read from the slope of the potential at $s = s_B$. Physical values $0 \leq Z \leq 1$ correspond to a negative slope, with the null slope ($Z = 0$) being the extreme case of pure DK-molecular structure. Fig. (3.3.3) shows a slightly negative slope for the $m_\pi = 290$ MeV which becomes even positive at $m_\pi = 150$ MeV but still compatible with zero due to the large size of the relative errors. As reported in Tab. (3.6), we then find a strong DK

	α	m_{D_s} (MeV)	g (GeV)	$1-Z$
Scalar				
$m_\pi = 290$ MeV	-0.4	2384(3)(0)	11.7 (0.3) (+0.7)	0.90 (0.04) (+0.10)
	-1.4	2384(2)(0)	11.7 (0.3) (+0.7)	0.90 (0.03) (+0.10)
	-2.2	2384(2)(0)	11.8 (0.3) (+0.7)	0.90 (0.03) (+0.10)
$m_\pi = 150$ MeV	-0.4	2348 (5) (+3)	11.2 (0.6) (+1.0)	1.08 (0.08) (+0.23)
	-1.4	2348 (4) (+3)	11.1 (0.6) (+1.0)	1.04 (0.08) (+0.30)
	-2.2	2348 (4) (+3)	11.1 (0.6) (+1.1)	1.04 (0.08) (+0.31)
Axialvector				
$m_\pi = 290$ MeV	-0.4	2500 (4) (-3)	14.3 (0.5) (+1.2)	1.00 (0.08) (+0.14)
	-1.4	2498 (4) (-1)	14.1 (0.5) (+1.0)	0.95 (0.07) (+0.14)
	-2.2	2497 (3) (-1)	14.0 (0.5) (+1.0)	0.94 (0.07) (+0.13)
$m_\pi = 150$ MeV	-0.4	2451 (4) (+1)	13.8 (0.6) (+0.6)	1.13 (0.08) (+0.17)
	-1.4	2451 (4) (+1)	13.8 (0.6) (+1.0)	1.14 (0.09) (+0.19)
	-2.2	2451 (4) (+1)	13.8 (0.6) (+1.0)	1.14 (0.09) (+0.19)

Table 3.6: The bound state mass, coupling and compositeness calculated with the potential method for each channel, pion mass and subtraction constant. The first errors are statistical, the second are systematic calculated as described in the caption of Tab. (3.5).

component in the wave function of the bound state, especially for light pion masses and for the axialvector channel. These values are larger than those determined in Ref. [48], who find 0.57 (21) (6) and 0.72 (13) (5) for the scalar and axialvector channel, respectively.

The quantities g and $1-Z$ can be compared to those of the HMChPT potential Eq. (3.3.2) fed with the input values of m_D, m_K and F_π of our simulation. For pion masses $m_\pi = 290$ MeV and 150 MeV, we obtain slightly lower couplings $g = 10.7$ GeV and 9.8 GeV and considerably lower factors $1-Z = 0.75$ and 0.81, respectively.

3.3.3 Final spectrum and comparison to experiment

The final charm-strange spectrum calculated in our work is now displayed in Fig. (3.3.4). The left part presents directly the masses of the D_s (0^-), D_s^* (1^-), D_{s0}^* (2317) (0^+), D_{s1} (2460) (1^+) and D_{s1} (2536) (1^+), as well as the finite-volume thresholds $m_K(L) + m_D(L)$ and $m_K(L) + m_{D^*}(L)$ (DK and D^*K).

The masses of the negative parity states, denoted in this section by m_{0^-} and m_{1^-}, show poor volume dependence and can be represented by their values extracted from the most physical ensemble, $L = 64a$ and $m_\pi = 150$ MeV. The masses of the D_{s0}^* (2317) and D_{s1} (2460), m_{0^+} and m_{1^+}, are taken from Tab. (3.5) and result from the phase shift analysis of Sec. (3.3.1) applied to the $m_\pi = 150$ MeV case. Due to its extremely low width, the D_{s1} (2536)

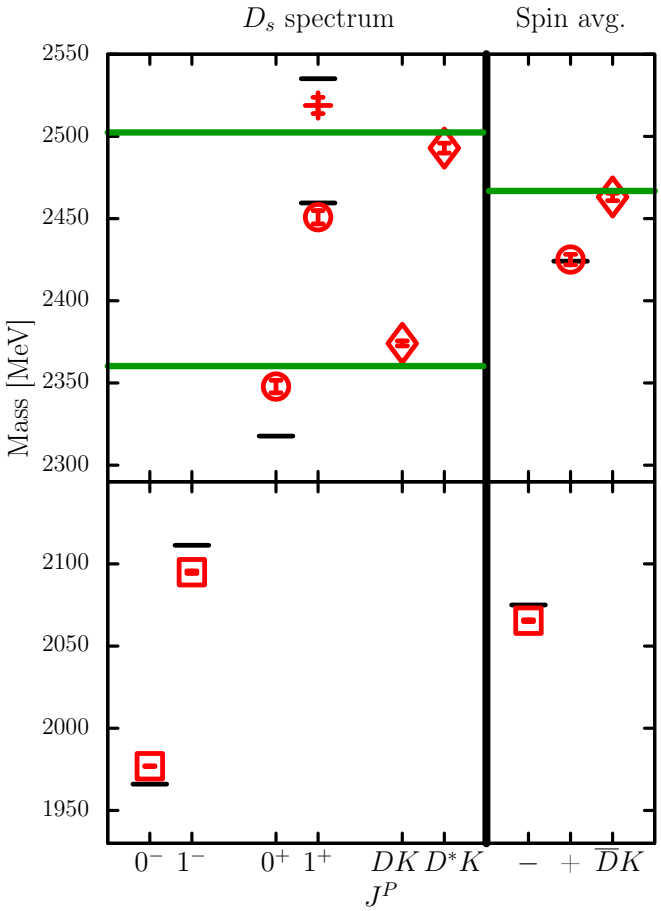

Figure 3.3.4: The final spectrum and spin averaged quantities obtained from our simulation (red labels) compared to the values from experiment (black horizontal lines). The green lines refer to the experimental thresholds. The figure is taken from [36].

		Energy (MeV)	Expt. (MeV)
D_s	m_{0^-}	1976.9 (2)	1966.0 (4)
D_s^*	m_{1^-}	2094.9 (7)	2111.3 (6)
	m_-	2065.4 (5)	2075.0 (4)
	Δm_-	118 (1)	145.3 (7)
$D_s\,(2317)$	m_{0^+}	2348 (4) (+6)	2317.7 (0.6) (2.0)
$D_{s1}\,(2460)$	m_{1^+}	2451 (4) (+1)	2459.5 (0.6) (2.0)
	m_+	2425 (4) (+2)	2424.1 (0.5) (2.0)
	Δm_+	103 (6) $\binom{+1}{-6}$	141.8 (0.9) (2.0)
$D_{s1}\,(2536)$	$m_{1'^+}$	2519 (5)	2535.1 (0.1) (2.0)

Table 3.7: Final spectrum results.

state is treated as a stable particle. Similarly to the 0^- states, its mass $m_{1'^+}$ shows an insignificant volume dependence and is also represented in the figure by the $L = 64a$ and $m_\pi = 150$ MeV ensemble.

The large number of configurations employed in our analysis enable us to achieve statistical errors smaller than 0.2% for the positive parity states and even smaller for the negative ones. At this level of accuracy the discrepancy with the experimental masses are visible, as displayed in Fig. (3.3.4). The experimental values to which we compare our results are corrected for isospin and QED effects and details can be found in Ref. [36]. The discretisation effects play the leading role in the discrepancy and, as mentioned in Sec. (3.1.2), these affect mainly hyperfine splittings while spin-averaged quantities are less altered by the finite lattice spacing. These quantities are denoted according to

	Masses		Spin averages	Hyp. splittings
Negative parity	m_{0^-}, m_{1^-}	$\Rightarrow$	$m_- = \frac{1}{4}\,(3m_{1^-} + m_{0^-})$	$\Delta m_- = m_{1^-} - m_{0^-}$
Positive parity	m_{0^+}, m_{1^+}	$\Rightarrow$	$m_+ = \frac{1}{4}\,(3m_{1^+} + m_{0^+})$	$\Delta m_+ = m_{1^+} - m_{0^+}$

and are given in Tab. (3.7). As shown in this table and in the right region of Fig. (3.3.4), both positive parity spin average m_+ and the spin-averaged thresholds are well reproduced. On the other hand, the severeness of the discretisation effects for the splittings Δm_- and Δm_+ are evident and differ from experiment respectively by 27.3 MeV and 39 MeV.

To disentangle the effect of the charm quark mass from the light and the strange quarks, the difference $m_+ - m_-$, as well as mass splittings of the two $j = \frac{1}{2}$ doublets of heavy quark theory (see Sec. (3.1.1)) are shown in Fig. (3.3.5). The mass difference is then dominated by energy scales of order $\overline{\Lambda} \sim 500$ MeV $\ll a^{-1} = 2760$ MeV. Besides the results for $m_\pi = 150$

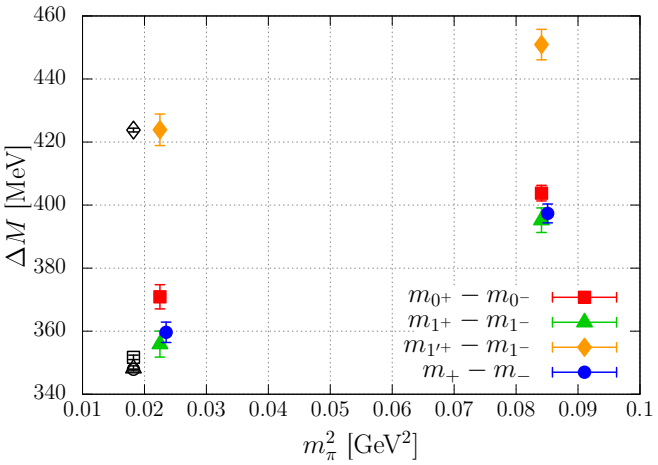

Figure 3.3.5: Mass splittings as a function of the pion mass. The errors are statistical only. The figure is from [36].

MeV, which are still slightly affected by a heavier than physical pion mass, the figure also includes corresponding results for $m_\pi = 290$ MeV and the experimental values (at $m_\pi = 135$ MeV, shown black). A crude linear extrapolation in the pion mass can be carried out, which displays, apart from a 6% difference for $m_{0^+} - m_{0^-}$, compatibility with experiment of these quantities.

3.4 Decay constants

We are interested in the matrix elements of the physical D^*_{s0} and D_{s1} with local bilinear operators. These define the scalar f_S, vector f_V, axialvector f_A and tensor f_T decay constants via the relations

$$\langle 0|\bar{s}c|D^*_{s0}(\boldsymbol{p})\rangle = f_S m_{0^+}, \tag{3.4.1}$$

$$\langle 0|\bar{s}\gamma_\mu c|D^*_{s0}(\boldsymbol{p})\rangle = f_V p_\mu, \tag{3.4.2}$$

$$\langle 0|\bar{s}\gamma_\nu\gamma_5 c|D_{s1}(\boldsymbol{p},\boldsymbol{\epsilon})\rangle = f_A m_{1^+}\epsilon_\nu, \tag{3.4.3}$$

$$\langle 0|\bar{s}\gamma_5\sigma_{\mu\nu}c|D_{s1}(\boldsymbol{p},\boldsymbol{\epsilon})\rangle = f_T\left(p_\mu\epsilon_\nu - p_\nu\epsilon_\mu\right), \tag{3.4.4}$$

where ϵ_ν are the polarisations of the spin-one D_{s1} particle. f_S and f_V are connected by the conserved vector current relation (CVC),

$$f_V = f_S \frac{m_c - m_s}{m_{0^+}}. \tag{3.4.5}$$

We set $\boldsymbol{p} = 0$, $\mu = t$ and select $\nu = i \in \{1, 2, 3\}$ (the corresponding values will be averaged), obtaining

$$\begin{aligned}
\langle 0|\overline{s}c|D^*_{s0}\rangle &= f_S m_{0^+}, && (3.4.6)\\
\langle 0|\overline{s}\gamma_t c|D^*_{s0}\rangle &= f_V m_{0^+}, && (3.4.7)\\
\langle 0|\overline{s}\gamma_i\gamma_5 c|D_{s1}(\boldsymbol{\epsilon})\rangle &= f_A m_{1^+}\epsilon_i, && (3.4.8)\\
\langle 0|\overline{s}\gamma_5\gamma_t\gamma_i c|D_{s1}(\boldsymbol{\epsilon})\rangle &= f_T m_{1^+}\epsilon_i. && (3.4.9)
\end{aligned}$$

The basic objects needed to extract the decay constats are the correlators

$$C_{Xi}(t) = \langle 0|J_X(t)\, O_i^\dagger(0)\,|0\rangle, \tag{3.4.10}$$

which were computed in addition to the correlators entering the correlator matrix. In Eq. (3.4.10) J_X are the local (unsmeared) currents, $X \in \{S, V, A, T\}$, and $O_i^\dagger(0)$ are the interpolators (see Tab. (3.3)) of the respective channel, $X = S, V$ for 0^+ and $X = A, T$ for 1^+. The calculation of the correlators Eq. (3.4.10) do not pose significant additional computational cost, as the J_X are just two-quark operators and only at the source four-quark operators can appear. Using Eq. (2.3.24), where Ω and v_i correspond to the ground state,

$$\begin{aligned}
\sum_i v_i C_{Xi}(t) &= \langle 0|J_X(t)\left(\sum_i v_i O_i^\dagger(0)\right)|0\rangle = \langle 0|J_X(t)\,\Omega^\dagger(0)\,|0\rangle\\
&= L^3\sum_n \langle 0|J_X|n\rangle\langle n|\Omega^\dagger|0\rangle\, e^{-tE_n}\\
&\approx L^3\frac{\langle 0|J_X|D_s\rangle}{\sqrt{2mL^3}}\frac{\langle D_s|\Omega^\dagger|0\rangle}{\sqrt{2mL^3}}e^{-tm}\\
&= L^3\frac{f_X^{\text{latt}} m}{\sqrt{2mL^3}}\sqrt{e^{mt_0}}e^{-tm} = f_X^{\text{latt}}\sqrt{\frac{mL^3}{2}e^{mt_0}}e^{-tm}
\end{aligned} \tag{3.4.11}$$

The states $|n\rangle$ in Sec. (2.3.3), which satisfy $\left|\langle n|\Omega^\dagger|0\rangle\right|^2 = e^{t_0 E_n}$, are normalised and therefore correspond here to $|1\rangle = \frac{1}{\sqrt{2mL^3}}|D_s\rangle$ and $\langle D_s|\Omega^\dagger|0\rangle / \sqrt{2mL^3} = e^{t_0 m/2}$, in agreement with the normalisation

$$\langle D^*_{s0}(\boldsymbol{p})\,|D^*_{s0}(\boldsymbol{p}')\rangle = 2E_{\boldsymbol{p}}L^3\delta_{\boldsymbol{p},\boldsymbol{p}'}. \tag{3.4.12}$$

The overall L^3 factor in Eqs. (3.4.11) originates from converting the $J_X(t)$ operators, defined in momentum space (at zero momentum), to coordinate space operators at $\boldsymbol{x} = 0$ (denoted again by J_X).

In Eq. (3.4.11) m refers to m_{0^+} for $X = S, V$ and to m_{1^+} for $X = A, T$ and two one-exponential simultaneous fits were performed, one for each group, to ensure consistency of the corresponding mass. The latter were compatible to those obtained from the variational analysis.

In contrast to hadron masses m, which are "physical" as they are accessed directly from one-particle states via the spectral decomposition, decay constants are related to operators which undergo renormalisation. The bare values f_X^{latt} are matched to the $\overline{\text{MS}}$ scheme,

$$f_X^{\text{ren}} = Z_X\,(1 + a\overline{m}b_X)\,f_X^{\text{latt}}, \tag{3.4.13}$$

where b_X are improvement factors and $\overline{m} = (m_c + m_s)/2$ are defined from the vector Ward identity, $2am_{c/s} = \kappa_{c/s}^{-1} - \kappa_{\text{crit}}^{-1}$. The renormalisation factors Z_X and the one loop expressions used for the b_X are taken from Ref. [46] and Refs. [55–57], respectively, and are displayed in Ref. [36].

For each ensemble, we perform the fits to Eq. (3.4.11), extract f_X^{latt}, multiply by the factors in Eq. (3.4.13) and obtain the renormalised decay constants f_X^{ren} which are displayed in Fig. (3.4.1) and in Tab. (3.8). A mild volume dependence for f_S and f_V is observed. Moreover, the decay constants at $L = 64a$ tend to decrease slightly as the pion mass is reduced. Note that the combination $f_S\,(m_c - m_s)$ in Eq. (3.4.5) is a renormalisation group invariant ($Z_S Z_m = 1$) and thus the renormalised vector decay constant can be acquired directly from the bare quantities

$$f_V^{\text{ren}} = f_S^{\text{latt}}\frac{m_c - m_s}{m_{0^+}} \tag{3.4.14}$$

without any need for renormalisation factors or improvement terms. It is also automatically $\mathcal{O}(a)$ improved (as it can be seen by using $b_S = -2b_m$). The f_V^{ren} obtained this way is shown by the black data points in Fig. (3.4.1) and is compatible with the direct determination of

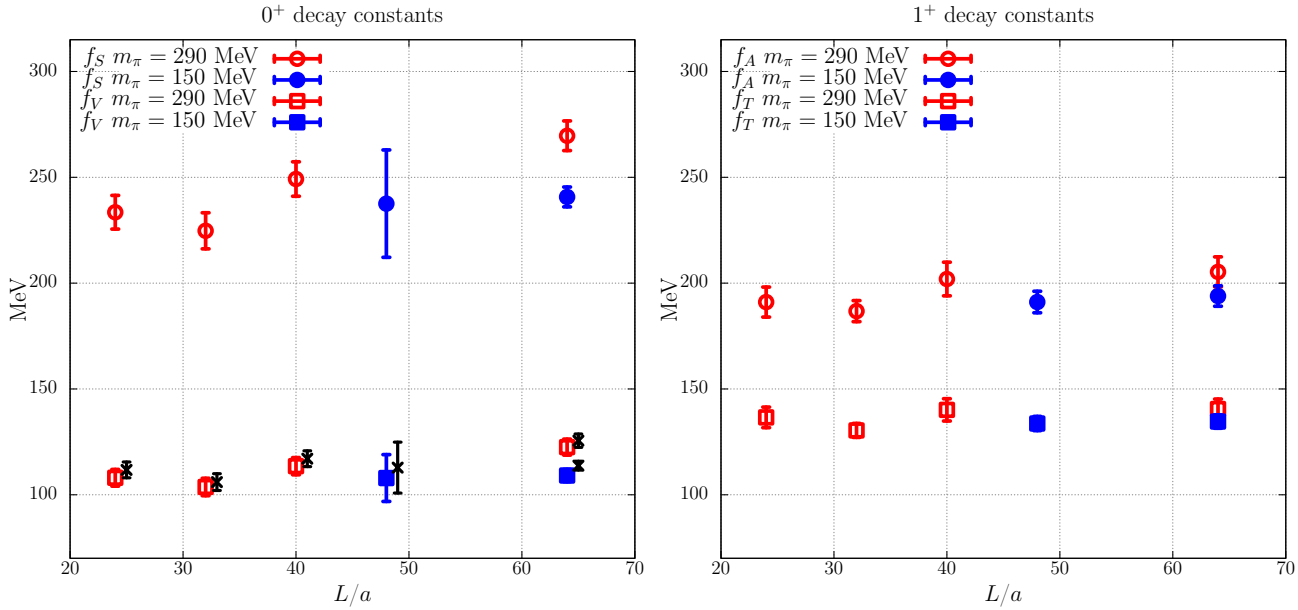

Figure 3.4.1: The renormalised decay constants calculated in this work as a function of the volume. The black points indicate f_V^{ren} as calculated from (3.4.14).

	$m_\pi = 290$ MeV				$m_\pi = 150$ MeV	
L/a	24	32	40	64	48	64
			D_{s0}^*			
f_S^{ren}	233(8)(2)	225(8)(2)	249(8)(2)	270(7)(2)	238(25)(2)	241 (4) (2) (+12) (10)
f_V^{ren}	108(3)(2)	104(4)(2)	114(3)(2)	123(3)(2)	109(11)(2)	111 (2) (2) (+05) (10)
$f_V^{CVC,\text{ren}}$	112(4)(0)	106(4)(0)	117(4)(0)	126(3)(0)	113(12)(0)	114 (2) (0) (+05) (10)
			D_{s1}			
f_A^{ren}	191(6)(4)	187(3)(4)	202(7)(4)	205(6)(4)	191(4)(4)	194 (3) (4) (+5) (10)
f_T^{ren}	137 (4) (2)	130(2)(2)	140(5)(2)	141(4)(2)	134(2)(2)	135 (2) (2) (+3) (10)

Table 3.8: The renormalised decay constants in MeV. $f_V^{CVC,\text{ren}}$ refers to the value calculated with (3.4.14). The first error is statistical, the second considers the uncertainty of the renormalisation and improvement factors. The additional errors in the last column are an estimation of finite-volume and discretisation effects, see Ref. [36] for details.

f_V^{ren} via Eq. (3.4.13). The small difference can be attributed to the $\mathcal{O}(a^2)$ discretisation effects.

The normalisation in Eqs. (3.4.1), (3.4.2), (3.4.3) and (3.4.4) are in agreement with the definition in the FLAG review [58] and in Ref. [59] of the negative parity counterpart f_{D_s}. Across this chapter, we have collected indications of a non irrelevant structure for the $D_{s0}^*(2317)$ particle more than once (strong coupling to the DK state, pion mass dependence, Weinberg's compositeness). The suppression of roughly 45% of its decay constant relative to the D_s equivalent which results from the comparison with Refs. [58] and [59], suggests a more spatially extended state and therefore, provides an additional indication of a non-ordinary meson structure[8].

In the literature it is possible to find several theoretical calculations of the decay constants we have calculated which can be useful for comparison, see Ref. [36] and references therein. These values are strongly variable according to the method used and the only lattice calculation known to us was performed by UKQCD [60]. With an $N_f = 2$ action at a single coarse lattice spacing $a = 0.10$, at a single small volume $L = 1.6$ fm and with no mention about the coupling to the threshold, they obtain the results (affected by strong uncertainties) $f_S = 340\,(110)$ and $f_V = 200\,(50)$, which are larger but consistent with ours. It will be interesting if the lattice community could provide us in the future with additional means of comparison with more realistic simulations.

[8] A larger spatial extention is generally expected for p-wave states, therefore this argument alone does not necessarily imply a molecular interpretation.

Chapter 4

$\pi\pi$ and $K\pi$ scattering

4.1 Introduction

4.1.1 Experimental overview

The elastic scattering of two pions is one of the simplest topics of QCD. Pions are spinless particles with negative intrinsic parity and form a $I = 1$ triplet (π^+, π^0, π^-) with components $I_z = 1, 0, -1$ respectively and have $S = C = B = 0$. They are the associated Goldstone bosons to the spontaneously broken $SU(2)_A$ chiral symmetry. As this symmetry is not exact, their masses are non-zero although very small with $m_{\pi^\pm} \approx 140$ MeV and $m_{\pi^0} \approx 135$ MeV. In fact, they are the lightest hadrons of the QCD spectrum. The near mass degeneracy is instead a consequence of the isospin symmetry $SU(2)_V$ which is violated only in a small amount.

Pions are one of the few truly stable particles under the strong interaction. The $\pi^\pm$ decay almost exclusively via the weak interaction to $\mu^\pm\nu_\mu$ with a branching factor of 99.99% and have a long mean lifetime of $2.6 \cdot 10^{-8}$ secs. The electromagnetic interaction is responsible for the shorter lifetime of the neutral π_0, $8 \cdot 10^{-17}$ seconds, which decays to 2γ in 99% of the times.

A system of two pions are arranged in $I = 0$, $I = 1$ and $I = 2$ multiplets. In terms of angular momenta, as for spinless particles, their total angular momentum J coincides with the orbital angular momentum of their relative motion. The parity of the system is $(-1)(-1)(-1)^J$ and thus $J^P(\pi\pi) = 0^+, 1^-, 2^+, ...$

Regarding elastic scattering of two pions, assuming perfect isospin (which will be the case here) we have three $T^{I=0,1,2}(s,t)$ scattering amplitudes and only one is independent thanks

to crossing symmetry[1].

The scattering amplitudes can be decomposed into partial waves $T^{I,J^P}(s)$ with J^P expressed as before. We consider $I = 1$ and $J^P = 1^-$. Here, one finds the ρ resonance, $\rho = (\rho^+, \rho^0, \rho^-)$, with an experimental mass of $m_\rho \approx 775$ MeV and a width $\Gamma_\rho \approx 148$ MeV.

We discuss in this chapter also $K\pi$ scattering. Kaons are spinless and have negative intrinsic parity. In terms of flavour, they are arranged in two $I = \frac{1}{2}$ multiplets (K^+, K^0) with $S = 1$ and $\left(\overline{K}^0, K^-\right)$ with $S = -1$. The masses are $m_{K^\pm} \approx 494$ MeV and $m_{K^0,\overline{K}^0} \approx 498$ MeV which are also alike due to isospin symmetry. The pion-kaon system is formed by a $I = \frac{3}{2}$ quadruplet and a $I = \frac{1}{2}$ doublet in spin-parity combinations $J^P = 0^+, 1^-, 2^+, ...$, analogously to the $\pi\pi$ system. We study $K\pi$ scattering in the $I = \frac{1}{2}$ and $J^P = 1^-$ sector which yields the strange-light analogous of the rho, the K^* resonance, with an experimental mass and decay with of $m_{K^*} \approx 896$ MeV and $\Gamma_{K^*} \approx 47$ MeV.

4.1.2 Lattice implementation

Similarly to the DK and D^*K analysis, we proceed with the extraction of the energies from the lattice and convert them to scattering information at infinite-volume via Lüscher's approach. However, there are both physical and computational differences from the DK and D^*K analysis. While in the latter Lüscher's formalism was exploited in the region around the elastic scattering threshold to extract its parameters and the properties of a nearby bound state, here we are interested to derive the mass and decay width of both ρ and K^* resonances which are located well above threshold. The flavour sector is also different, as well as the partial wave angular momentum of the infinite volume phase shift. From a computational perspective, for DK and D^*K scattering the energy data points were collected by varying the volume. For $\pi\pi$ and $K\pi$ we employ moving frames instead. To see the relevance of these, let us consider the tower of energies, Eq. (2.2.47), which are the relevant ones if the simulation was to be performed in the centre of mass frame. For two pions scattering in p-wave, the $n = 0$ threshold state in Eq. (2.2.46) is not present since a relative motion of the two pions must exist. The lowest energy level is then

$$E_1^{\text{non-inter.}}(L) = 2\sqrt{m_\pi^2 + \left(\frac{2\pi}{L}\right)^2}, \tag{4.1.1}$$

[1]See Sec. (1.3.3). All three isospin amplitudes can be obtained by the $\pi^+\pi^- \to \pi^0\pi^0$ amplitude, see e.g. Ref. [61]. With lattice simulations, we access only the physical region of a channel and since the results are spoiled by errors, the crossed channels cannot be obtained by analytical continuation. Each channel has to be determined independently.

where the small interaction term was dropped as it is not relevant for this argument. Typical simulations with $m_\pi = 270$ MeV and $L = 3$ fm imply $E_1 \sim 1$ GeV which is well above the resonance region. If this region is to be accessed via Lüscher's formalism, lattice scenarios which provide lower energy levels are to be employed. One may use twisted boundary conditions, asymmetric boxes, or, as in our case, moving frames. For instance, setting one pion to zero momentum and the other to total momentum $\boldsymbol{p} = \frac{2\pi}{L}(0,0,1)$ leads to the lowest energy

$$E_1^{\text{non-inter.}}(L) = \sqrt{m_\pi^2 + \left(\frac{2\pi}{L}\right)^2} + m_\pi \tag{4.1.2}$$

which now corresponds to $\sim$ 770 MeV with the same parameters used above. We employ ensembles with $L = 64a$ and $L = 48a$ at $m_\pi \approx 150$ MeV which are two of those used for DK scattering, Tab. (3.2). With these values, along with moving frames, $\boldsymbol{p} \propto (0,0,0)\,,\,(0,0,1)\,,\,(0,1,1)$, the resonance region can be probed for both $\pi\pi$ and $K\pi$ scattering.

For fixed frame $\boldsymbol{p} = \frac{2\pi}{L}\boldsymbol{d}$, the tower of energies is then

$$E_n^{\boldsymbol{p}} = \sqrt{m_1^2 + \boldsymbol{p}_{1,n}^2} + \sqrt{m_2^2 + \boldsymbol{p}_{2,n}^2}. \tag{4.1.3}$$

Here $m_{1/2}$ refer to the masses of either $\pi\pi$ or $K\pi$. The individual momenta $\boldsymbol{p}_{1,n}$ and $\boldsymbol{p}_{2,n}$, encompass the interaction of the mesons and are related with each other by $\boldsymbol{p}_{2,n} = \boldsymbol{p} - \boldsymbol{p}_{1,n}$. Also, the additional level due to the presence of the resonance should be added to in the tower of energies Eq. (4.1.3).

Just as for DK and D^*K, the operator basis includes four-quark operators which resemble the $\pi\pi$ and $K\pi$ as well as two-quark operators for the ρ and K^*. These are to be chosen with well-defined total momentum $\boldsymbol{p}$ and isospin according to what was mentioned previously in Sec. (4.1.1), i.e. $I = 1$ for $\rho \leftrightarrow \pi\pi$ and $I = \frac{1}{2}$ for $K^* \leftrightarrow K\pi$. The ρ is interpolated by $\overline{\psi}\gamma_i\psi$, $\overline{\psi}\gamma_i\gamma_t\psi$ and $\overline{\psi}\nabla_i\psi$ where ψ are light quarks and similarly for K^* when replacing one light quark by the strange. The four-quark operators have the form

$$\pi\pi(\boldsymbol{p}) = \frac{1}{\sqrt{2}}\left[\pi^+(\boldsymbol{q}_1)\,\pi^-(\boldsymbol{q}_2) - \pi^-(\boldsymbol{q}_1)\,\pi^+(\boldsymbol{q}_2)\right], \tag{4.1.4}$$

$$K\pi(\boldsymbol{p}) = \frac{1}{\sqrt{3}}\left[\sqrt{2}\pi^+(\boldsymbol{q}_1)\,K^-(\boldsymbol{q}_2) - \pi^0(\boldsymbol{q}_1)\,K^0(\boldsymbol{q}_2)\right], \tag{4.1.5}$$

where $\boldsymbol{p} = \boldsymbol{q}_1 + \boldsymbol{q}_2$. Finally, all operators are projected to the irreducible representation $\Lambda_{\boldsymbol{p}}$ of the little group of $\boldsymbol{p}$.

An 8×8 correlator matrix is then constructed for each frame and channel and the Wick contractions show diagrams similar to those for DK and D^*K[2]. All-to-all propagators which appear also in this case are dealt with by employing spin-diluted stochastic sources.

4.2 Results

4.2.1 Phase shifts

The fit to the eigenvalues of the correlator matrix provides for each frame and channel the lowest two energy levels, $E_n^{\boldsymbol{p}}$ in Eq. (4.1.3). These are to be converted into the centre of mass frame in order to match the phase shift $\delta(s)$ at infinite volume. The conversion is straightforward and arranged by the formula[3]

$$\sqrt{s_n^{\boldsymbol{p}}} = \sqrt{m_1^2 + \left(k_n^{\boldsymbol{p}}\right)^2} + \sqrt{m_2^2 + \left(k_n^{\boldsymbol{p}}\right)^2} = \sqrt{\left(E_n^{\boldsymbol{p}}\right)^2 - \boldsymbol{p}^2}. \tag{4.2.1}$$

As discussed in Sec. (2.4.1), the quantisation condition Eq. (2.4.3), which reduces to the formulas in Ref. [62] for this case, has to be truncated. Experiment and previous lattice studies show that we can restrict to $j \leq 1$, i.e. $\delta_j(s)$ is set to zero for $j > 1$. This leads to a one-to-one relation between the $\pi\pi$ p-wave phase shift $\delta_{j=1}^{\pi\pi}(s)$ and the energies on the lattice for every irreducible representation. For the $K\pi$ channel, mixing with $\delta_{j=0}^{K\pi}(s)$ is present only for one representation. This problem is dealt with by including a systematic error estimated by repeating the analysis with the corresponding energies removed.

The phase shift as a function of the centre of mass energy $E_{CM} = \sqrt{s}$ for both channels are displayed in Fig. (4.2.1) . The statistical errors are particularly large for the $\pi\pi$ channel as a result of the small pion mass used in the analysis. The data point shown as dashed is not considered as it is located above the four-pion threshold.

The typical resonant behaviour with a transition of the phase shift from 0 to π across its mass is seen in the figure. Fits were performed to the simple Breit-Wigner form, Eqs.

[2]An additional crossed box diagram is present for $K\pi \leftrightarrow K\pi$.

[3]Please note that on the lattice, for two or more particle states, if E_n are energies in a frame with total momentum $\boldsymbol{p}$, the transformation $E_n \to E_{CM,n} = \sqrt{E_n^2 - \boldsymbol{p}^2}$ does not identify the energy levels of the centre of mass frame, not even in the non-interacting case. Therefore, $\sqrt{s_n^{\boldsymbol{p}}}$ and $\boldsymbol{k_n^p}$ in Eq. (4.2.1) do not correspond to the energies and momenta that we would have obtained if the simulation was performed at the centre of mass frame. They are just the values at which the phase shift, which is evalutated in the continuum centre of mass frame, will be extracted via Lüscher's formula.

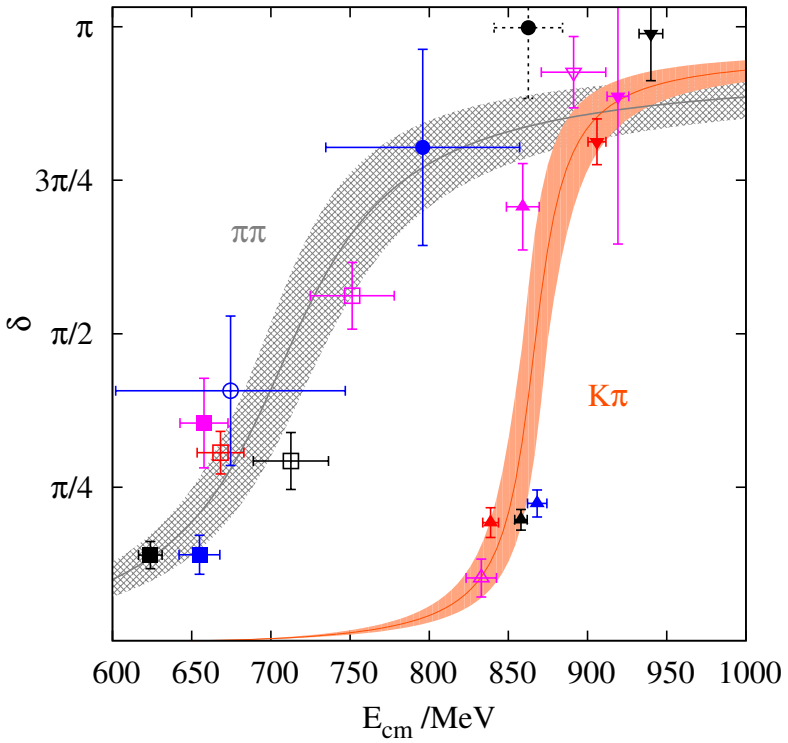

Figure 4.2.1: The p-wave phase shift for $\pi\pi \to \pi\pi$ (squares and circles data points) and $K\pi \to K\pi$ (triangles) around the resonant region. The Breit-Wigner parametrisation curves are also shown. The figure is taken from Ref. [63].

	Lattice	Expt.
	ρ	
m_ρ	716 (21) (21)	775
Γ_ρ	113 (35) (3)	148
$g_{\rho\pi\pi}$	5.64 ± 0.87	5.93
	K^*	
m_{K^*}	868 (8) (26)	896
Γ_{K^*}	30 (6) (1)	47
$g_{K^*\pi\pi}$	4.79 ± 0.49	5.39

Table 4.1: The ρ and K^* resonance parameters calculated using a Breit-Wigner parametrisation.

(1.4.39) and (1.4.38). More complex parametrisations were also accounted for but were found to be negligible compared to the dominant Breit-Wigner form.

The results for the mass, width of the resonances and the coupling to the respective channels are shown in Tab. (4.1) . Both the masses and the widths are below the corresponding physical values. The latter undershooting can be explained by noting that the pion mass is by $\sim 10\%$ above the physical value, leading to a lower phase-space for the resonances and thus, a smaller width. Couplings to the channels are instead consistent with experiment.

4.2.2 Comparison with other results

The $\pi\pi$ system is one of the most simple to simulate on the lattice and therefore it is not surprising to find in the literature a number of works carried out over the years to which compare our results. The comparison is shown in Fig. (4.2.2) which displays m_ρ as a function of m_π^2 and the coupling $g_{\rho\pi\pi}$ against m_π. A special emphasis is given in distinguishing $N_f = 2$ simulations (open symbols) from $N_f = 2 + 1$ simulations (filled symbols) in order to understand the impact of the strange quark on the results.

The coupling presents no apparent pion mass dependence in the range displayed and shows consistency with the physical value, in agreement with NNLO chiral perturbation theory [64]. The pion mass dependence of the width has therefore just a kinematical origin.

Less straightforward statements can be made for the resonance mass. A qualitative linear trend is visible, in agreement with NLO chiral perturbation theory [64, 65], but the effect of the strange quark is not clear. Using unitarised chiral perturbation theory, the authors of Ref. [66] performed an extrapolation of $N_f = 2$ lattice data both to physical pion mass and to three flavours. Their claim is that the strange quark, or the neglected $K\overline{K}$ channel, is decisive for the physical determination of the resonance mass. On the other hand, the

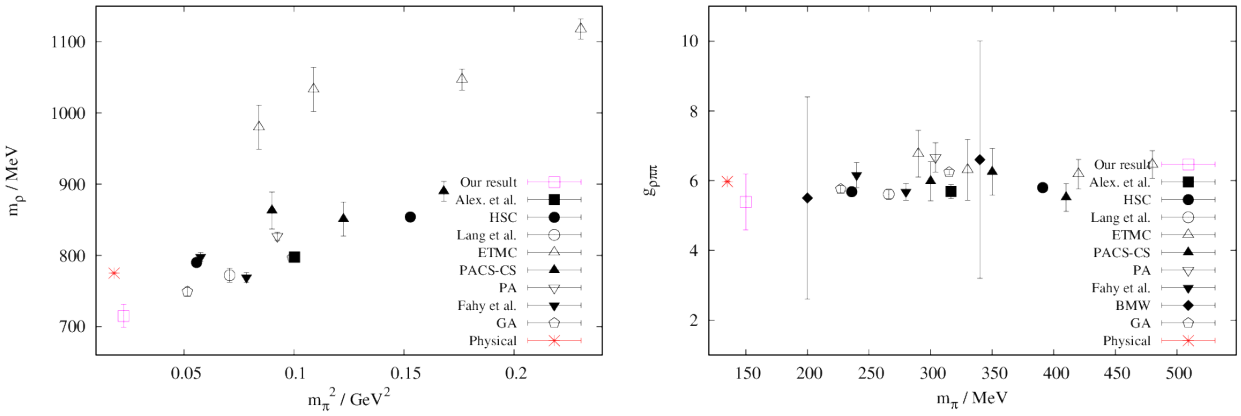

Figure 4.2.2: Our results for ρ mass and its coupling to $\pi\pi$ compared to the results of a variety of lattice calculations based on different methods and lattice parameters.

$N_f = 2 + 1$ result of Ref. [67] coincides with the $N_f = 2$ result of Ref. [68], suggesting no strange quark effect or an accidental cancellation with lattice spacing systematics. Regarding the latter, the authors of Ref. [67] suggest to replace the variables m_ρ and m_π^2 in Fig. (4.2.2), which are affected by the obviously non-universal methods for the lattice scale setting, in favour of the dimensionless am_ρ/am_N and am_π/am_N, with m_N being the nucleon mass. The resulting plot, displayed in figure 12 of their paper, shows a clear linear dependence of the $N_f = 2 + 1$ data heading towards the experimental value while the $N_f = 2$ points are distributed around the line without revealing an evident pattern. They claim that the strange quark mass plays little role in determining the value of m_ρ and associate the disparity of the $N_f = 2$ calculations with several systematics not kept under control. Of these, the only one that can be relevant in our study are due to the finite lattice spacing. If the strange quark mass truly has a negligible impact, a continuum extrapolation of the ρ mass from a multi-lattice spacing simulation, never performed in the past, should identify the experimental value also for $N_f = 2$.

Summary

We have seen how Lüscher's formalism and its extensions provide a bridge between lattice QCD and relativistic scattering theory. The finite-volume energy levels extracted from lattice simulations identify the values of the scattering T-matrix of the channel under consideration. As the T-matrix encapsulates the dynamics of the scattering process, all relevant information can be accessed, including bound states and resonances properties.

It is hence clear that the same framework can be applied to a number of systems which show different dynamical behaviour. In this work, the DK, D^*K, $\pi\pi$ and $K\pi$ channels were analysed with $J^P = 0^+, 1^+, 1^-$ and 1^-, respectively.

The first two were investigated in the region around the corresponding threshold. In this region, the T-matrix exhibits an effective range behaviour, from which the scattering length and the effective range parameters are obtained. The bound states $D^*_{s0}\,(2317)$ and $D_{s1}\,(2460)$ were found below the threshold and their masses and binding energies were calculated.

The $\pi\pi$ $(I = 1)$ and $K\pi$ $(I = \frac{1}{2})$ channels were instead investigated in the region around the ρ and the K^* resonances, respectively. Here, a clear resonant behaviour was visible and the Breit-Wigner parameters were extracted.

In all cases, the energies were extracted by employing the variational method, with a basis formed by both two-quark and four-quark operators, resembling respectively the one-particle and the scattering states. The inclusion of the four-quark operators was essential to resolve the lowest lying energy levels but came at the price of introducing sequential propagators, whose calculation increased substantially the computational effort, in particular for those ensembles with a close to physical pion mass. These were dealt with by means of the stochastic sources method.

Only one lattice spacing was employed and discretisation effects were the predominant source of systematic errors for all cases. Regarding the DK and D^*K channels, spin-averaged quantities, which suffer less from lattice artifacts, were found to be in reasonable agreement with experiment. Ambitious future work should enable a continuum-limit extrapolation

by employing ensembles with several lattice spacings while keeping the pion mass close to physical. Such analysis would allow one to understand the impact of lattice artifacts on the ρ meson's mass.

A possible way to extend the DK and D^*K analysis is to include the ηD_s and ηD_s^* interpolators in the variational basis and to perform a coupled-channel scattering analysis. This will allow one to have higher energy regions above threshold under control and to verify the impact of these states to the $D_{s0}^*(2317)$ and $D_{s1}(2460)$.

Appendix A

Appendix

A.1 Some group theory

We summarise here the notions of group theory which are relevant for relativistic scattering and for lattice QCD. For an explicit exposition of the following ideas, some of the notation is appropriate only for finite groups but can be extended also to infinite groups.

A.1.1 Cosets, orbits and little groups

Consider a group G and a subgroup H of G. The left coset of H in G with respect to a given $g \in G$ is the set

$$gH = \{\, gh \in G |\, h \in H \}\,. \tag{A.1.1}$$

The element g represents the coset gH and it belongs to it; any element of gH can serve as a representative. One can show that the left cosets partition the group and each coset has the same cardinality of H, $|gH| = |H|$. We can write G as the union of the disjoint cosets, i.e.

$$G = g_1 H \cup g_2 H ... \cup g_s H \tag{A.1.2}$$

where $\{g_1, ..., g_s\}$ are representatives of the corresponding coset and $s = \frac{|G|}{|H|}$, the number of cosets, is called the index of H in G. g_1 can be taken to be the (common) identity element of G and H so that $g_1 H = eH$ is basically H itself.

Given a $g \in G$ and a representative g_i of $g_i H$, the product $g g_i$ is of course an element of G and so it belongs necessarily to one coset. This means that there is a unique $h \in H$

(which depends on i) and a unique $\sigma_i \in \{1, 2, ..., s\}$ such that

$$g g_i = g_{\sigma_i} h, \qquad h \in H,\ \sigma_i \in \{1, 2, ..., s\}\,. \tag{A.1.3}$$

In order words, given g and g_i, there will be a unique σ_i such that the combination $g_{\sigma_i}^{-1} g g_i$ belongs to H,

$$g_{\sigma_i}^{-1} g g_i = h \in H. \tag{A.1.4}$$

This result will be useful later.

We can define an equivalence relation within each coset and define the set of all cosets

$$G/H = \{eH, g_2 H, ..., g_s H\}\,. \tag{A.1.5}$$

The subgroup H is normal if the left cosets coincide with the right cosets $Hg = \{\, hg \in G |\, h \in H\}$. In this case, G/H itself enjoys a group structure and is referred to as the quotient group.

If a group G has two subgroups H_1 and H_2 such that

1. $H_1 \cap H_2 = \{e\}$,

2. any element of $g \in G$ can be expressed as $g = h_1 h_2$ with $h_1 \in H_1$ and $h_2 \in H_2$,

3. any element of H_1 commutes with any element of H_2,

then a direct product group $H_1 \times H_2$ can be identified and it is isomorphic to G. The third condition can be traded off with the requirement that H_1 and H_2 are normal. If we relax the condition of normality for one of the subgroups, say H_2, then G is isomorphic to the semidirect product $H_1 \rtimes H_2$[1]. In both cases, the decomposition of point (2.) is unique.

Given a group G and any set X, a (left) action of G on X is defined to be a map $G \times X \to X$ which takes a point $x \in X$ and identifies a new one $gx \in X$ such that $ex = x$ and $g\,(g'x) = (gg')\,x$. If X is a vector space and G acts linearly on it, we are reduced to the definition of a (linear) representation[2]. Given $x \in X$, the orbit and the little group (or stabiliser) of x with respect to G are respectively defined as

$$\mathrm{Orb}_G\,(x) = \{\, gx \in X |\, g \in G\}\,, \tag{A.1.6}$$

$$L_G\,(x) = \{\, g \in G |\, gx = x\}\,. \tag{A.1.7}$$

[1]Note that a vertical line is added to the symbol $\times$ in the orientation of the non-normal subgroup.
[2]In this case we write $D : G \to GL\,(V)$ and replace gv by the less ambiguous $D\,(g)\,v$.

The orbit of x is the subset of X that can be reached from x under the group action. The set of all orbits partition X. A group element $g \in G$ can be visualised as an arrow connecting x to another point, gx, in the same orbit $\mathrm{Orb}_G(x)$. The little group of x is the set of elements of G that leave x invariant. The latter is easily shown to be a subgroup of G (although typically not a normal one) and, based on what addressed earlier, one can then define $G/L_G(x) = \{eL_G(x), g_2L_G(x), ..., g_sL_G(x)\}$, the set of left cosets of G with respect of $L_G(x)$. Points on the same orbit have isomorphic little groups.

The orbit-stabiliser theorem provides an important connection between orbits, little groups and cosets. Let us consider a fixed $x \in X$ and the orbit $\mathrm{Orb}_G(x)$ that it identifies. There is a bijection (one-to-one correspondence) between $\mathrm{Orb}_G(x)$ and $G/L_G(x)$, namely each point in the orbit gx identifies the left coset $gL_G(x)$. The point $x \equiv ex$ itself identifies $L_G(x) \equiv eL_G(x)$. Therefore, once x is fixed, the group elements of G can be visualised directly from the points in $\mathrm{Orb}_G(x)$, modulo the little group $L_G(x)$.

As a practical example, let us consider $SO(3)$, the group of three-dimensional proper rotations and its action on $\mathbb{R}^3$. The orbit of $\boldsymbol{x} = (0,0,r)^T$ with $r > 0$ is a the spherical surface with radius r. The little group $L_{SO(3)}(\boldsymbol{x})$ is the set of rotations in the plane orthogonal to $\boldsymbol{x}$ (i.e. the xy plane), namely

$$L_{SO(3)}(\boldsymbol{x}) = \begin{pmatrix} \cos\theta & -\sin\theta & 0 \\ \sin\theta & \cos\theta & 0 \\ 0 & 0 & 1 \end{pmatrix},$$

which is isomorphic to $SO(2)$. To another point in the same orbit, say $\boldsymbol{x}' = (r,0,0)^T$, is associated a different little group $L_{SO(3)}(\boldsymbol{x}')$ which is, however, isomorphic to $L_{SO(3)}(\boldsymbol{x})$ and to $SO(2)$.

A.1.2 Subduced and induced representations

Given a representation $D : G \to GL(V)$ of G it is straightforward to identify a representation of a subgroup H of G by just restricting the domain of definition of D to H. The representation $D|_H$ is called the representation of H subduced from the representation of G. If D is irreducible, $D|_H$ is in general not. The opposite statement is although verified, i.e., if $D|_H$ is irreducible then also D is.

Let us now consider a representation $D_H : H \to GL(W)$ of a subgroup H of G with

index $s = \frac{|G|}{|H|}$. D_H acts on vectors of W,

$$|\psi\rangle \to D_H(h)|\psi\rangle = |\psi'\rangle . \tag{A.1.8}$$

Starting from this, we want to build a representation $D_G : G \to GL(V)$ for the whole G, i.e., we want to identify a vector space V and an action D_G on it. In order to achieve this, we consider the partitioning of G in terms of cosets $g_i H$ and to each coset we create a copy W_i of the vector space W,

$$\begin{array}{ccccccccccc} G & = & g_1 H & \cup & g_2 H & \cup & ... & \cup & g_s H & & \\ V & = & W_1 & \oplus & W_2 & \oplus & ... & \oplus & W_s & \equiv & W^s \end{array} \tag{A.1.9}$$

Vectors in W_i can be expressed by $|i, \psi\rangle$ where $i = 1, ..., s$ identifies the copy and ψ labels the vectors within the copy. Taking $g_1 = e$, D_H already acts on the "first" copy in Eq. (A.1.9) and its action, Eq. (A.1.8), can be trivially cloned to any copy,

$$|i, \psi\rangle \to D_H(h)|i, \psi\rangle := |i, \psi'\rangle . \tag{A.1.10}$$

Now, consider a general $g \in G$ and a g_i associated to the i-th space. Recall from Eq. (A.1.3) that the product $g g_i$ identifies uniquely an element $h \in H$ and a representative g_{σ_i} which is, in this context, associated to the σ_i-th vector space. Therefore, we can define the action of D_G for a general $g \in G$ on the i-th space by the action of D_H via h on the σ_i-th space, namely

$$D_G(g)|i, \psi\rangle := D_H(h)|\sigma_i, \psi\rangle = |\sigma_i, \psi'\rangle . \tag{A.1.11}$$

The action is extended for a general vector in V by linearity of D_G with respect to the direct sum. It can be shown that D_G is indeed a representation for G and it is said to be induced from D_H. In summary, given $g \in G$, the induced representation D_G acts in two steps:

1. It changes the space from i to σ_i.

2. In this new space, H acts via $D_H(h)$ as usual.

The induced method is particularly useful for groups which have a semidirect product form $G = A \rtimes B$ where A is an abelian normal subgroup. In this case, all irreducible unitary representations of G can be identified by induction from a non-trivial subgroup of G. This is a fulfilling statement since physically important groups as the Euclidean group, as well as the Poincaré group happen to have this structure. As we will see explicitly for the

Poincaré group, decompositions of the form (A.1.9) are continuous for infinite groups but the underlying concept is unchanged[3].

A.1.3 The Lorentz group

The Lorentz group $O(1,3)$ is the set of all real 4×4 matrices that leaves the Minkowskian metric $\eta = \mathrm{diag}(1,-1,-1,-1)$ unchanged[4],

$$\eta = \Lambda^T \eta \Lambda. \tag{A.1.12}$$

It forms a group under matrix multiplication with identity element $\mathbb{1}_4 = \mathrm{diag}(1,1,1,1)$ and inverse elements given by the matrix inverse operation. The Lorentz group defines four-vectors $b = (b^0, \boldsymbol{b}) \in \mathbb{R}^{1,3}$ by the action $b'^\mu = \Lambda^\mu{}_v b^\nu$ which leaves the quadratic form $b^2 = \eta^{\mu\nu} b_\mu b_\nu = b^\mu b_\mu = b_\mu b^\mu = b_0^2 - |\boldsymbol{b}|^2$ invariant. Examples of four-vectors are space-time coordinates $x = (t, \boldsymbol{x})$ in Minkowski space, four-momenta $p = (p^0, \boldsymbol{p})$, electromagnetic fields $A = (A^0, \boldsymbol{A})$ etc.

The Lorentz group is a six-dimensional Lie group which is neither compact nor connected. From the definition Eq. (A.1.12) one can immediately see that $\det\Lambda = \pm 1$ and $\Lambda^0{}_0 \geq 1$ or $\Lambda^0{}_0 \leq -1$. Based on these values, four connected components are identified:

		$SO(1,3)$ Proper $\det\Lambda = 1$		Improper $\det\Lambda = -1$
$O^\uparrow(1,3)$	Orthochronus $\Lambda^0{}_0 \geq 1$	Restricted $\mathcal{L} = SO^\uparrow(1,3)$	$\xrightarrow{P}$	
		$\downarrow PT$	$\searrow T$	$\downarrow PT$
	Non-orthochronus $\Lambda^0{}_0 \leq -1$		$\xrightarrow{P}$	

The component which contains the identity is called the restricted Lorentz group and will be denoted here by $\mathcal{L} = SO^\uparrow(1,3)$. A general Lorentz transformation can be accessed by multiplying any element $\Lambda \in \mathcal{L}$ with an element of the group of components

$$O(1,3)/SO^\uparrow(1,3) = \{1, P, T, PT\} \cong \mathbb{Z}_2 \times \mathbb{Z}_2 \tag{A.1.13}$$

[3]Technically the corresponding Ws are fibers of vector bundles with an orbit of G (or left cosets) as base manifold.

[4]In components, $\mathrm{diag}(1,-1,-1,-1) = \eta^{\mu\nu} = (\Lambda^T)^\mu{}_\rho \, \eta^{\rho\sigma} \Lambda_\sigma{}^\nu \equiv \eta^{\rho\sigma} \Lambda_\rho{}^\mu \Lambda_\sigma{}^\nu$.

where $P \equiv \eta = \mathrm{diag}\,(1,-1,-1,-1)$ and $T = \mathrm{diag}\,(-1,1,1,1)$ are the space and time inversions respectively.

Let us focus now on the restricted Lorentz group $\mathcal{L} = SO^{\uparrow}(1,3)$. It is connected but not simply connected and its (simply connected) universal cover is the group $\overline{\mathcal{L}} = SL(2,\mathbb{C})$ with $SL(2,\mathbb{C})/\mathbb{Z}_2 \cong \mathcal{L}$. Each element in $\mathcal{L}$ can be expressed in terms of its Lie algebra via antisymmetric elements $M^{\mu\nu} = -M^{\nu\mu}$

$$\Lambda(\omega) = e^{-\frac{i}{2}\omega_{\mu\nu}M^{\mu\nu}}, \tag{A.1.14}$$

$$[M^{\mu\nu}, M^{\rho\sigma}] = i\left(\eta^{\mu\sigma}M^{\nu\rho} + \eta^{\nu\rho}M^{\mu\sigma} - \eta^{\mu\rho}M^{\nu\sigma} - \eta^{\nu\sigma}M^{\mu\rho}\right). \tag{A.1.15}$$

Alternatively, defining

$$J^1 = M^{23}, \quad J^2 = M^{31}, \quad J^3 = M^{12},$$
$$K^1 = M^{01}, \quad K^2 = M^{02}, \quad K^3 = M^{03},$$

a general $\Lambda \in \mathcal{L}$ is parametrised in terms of the angular momentum $\boldsymbol{J}$ and boosts $\boldsymbol{K}$

$$\Lambda(\boldsymbol{\phi}, \boldsymbol{w}) = e^{-i(\boldsymbol{\phi}\cdot\boldsymbol{J} + \boldsymbol{w}\cdot\boldsymbol{K})} \tag{A.1.16}$$

with

$$\left[J^i, J^j\right] = i\epsilon^{ijk}J^k, \quad \left[K^i, K^j\right] = -i\epsilon^{ijk}J^k, \quad \left[J^i, K^j\right] = i\epsilon^{ijk}K^k. \tag{A.1.17}$$

We see that the algebra $[J^i, J^j]$ is closed, therefore $SO(3)$ rotations form a subgroup of $\mathcal{L}$.

Orbits Let us now look at how the space of four-momenta $p = (p^0, \boldsymbol{p}) \in \mathbb{R}^{1,3}$ is partitioned via orbits under the action of the restricted Lorentz group $\mathcal{L}$[5]. Since any $\Lambda \in \mathcal{L}$ does not change the value of p^2 and the sign p^0, the Minkowski space is parametrised in terms of surfaces, hyperboloids and cones, of constant values of these variables. Denoting $m^2 = p^2 =$

[5]We use four-momenta variables for a direct connection to the representations of the Poincaré group but, of course, all following statements apply also for Minkowski space-time variables $x = (t, \boldsymbol{x})$.

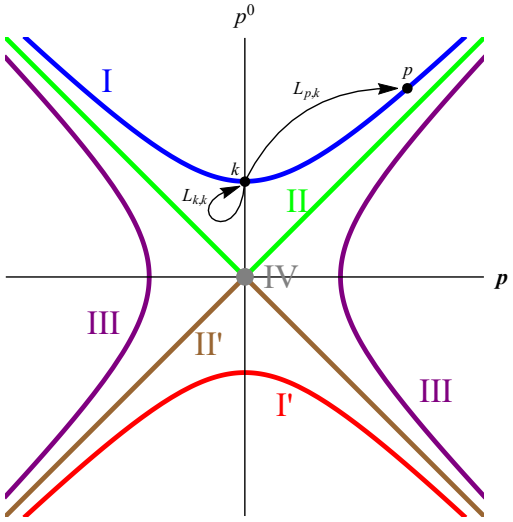

Figure A.1.1: Orbit representatives of the Lorentz group for each class. The three-dimensional $\boldsymbol{p}$ is collapsed to one-dimension for illustration.

$p_0^2 - |\boldsymbol{p}|^2$, the orbits are arranged according to six distinct classes[6],

Class	Description	p^2	sgn (p_0)	Standard k	Little group
I	Forward hyperboloid	$m^2 > 0$	$p^0 > 0$	$(m, \mathbf{0})$	$SO(3)$
I'	Backward hyperboloid	$m^2 > 0$	$p^0 < 0$	$(-m, \mathbf{0})$	$SO(3)$
II	Forward light cone	$m^2 = 0$	$p^0 > 0$	$(\kappa, 0, 0, \kappa)$	$E(2)$
II'	Backward light cone	$m^2 = 0$	$p^0 < 0$	$(-\kappa, 0, 0, \kappa)$	$E(2)$
III	Spacelike hyperboloid	$m^2 \equiv -\kappa^2 < 0$		$(0, 0, 0, \kappa)$	$SO(1,2)$
IV	Null vector	$p = 0$		$(0, \mathbf{0})$	$SO^{\uparrow}(1,3)$

which can be visualised in Fig. (A.1.1). Only elements belonging to the same orbit can be connected by a restricted Lorentz transformation. The table shows also a "standard" vector belonging to the corresponding class.

Let us consider one of these, $k = (m, \mathbf{0})^T$ (shown in the figure) which generates the orbit $\mathrm{Orb}_{\mathcal{L}}(k)$ belonging to class I. The little group $L_{\mathcal{L}}(k)$ of k, i.e. the subgroup of $\mathcal{L}$ of elements $L_{k,k}$ which leaves k invariant, $k \to k = L_{k,k}k$, is clearly the $SO(3)$-isomorphic group of three

[6]Note that the same orbit classification is valid for the more general $O^{\uparrow}(1,3)$ which includes improper transformations. On the other hand, for $SO(1,3)$ and for the full Lorentz group $O(1,3)$, the possibility of time reflections merge the orbits I I' to $I \cup I'$ and II II' to $II \cup II'$, resulting in just four distinct classes.

dimensional rotations in the subspace orthogonal to k,

$$L_{k,k} = \begin{pmatrix} 1 & 0 \\ 0 & \boldsymbol{R} \end{pmatrix}.$$

Now, any $p \in \mathrm{Orb}_{\mathcal{L}}(k)$ can be identified by a so called Wigner boost $L_{p,k} \in \mathcal{L}$, $p = L_{p,k}k$. Just as there is a $SO(3)$ "degeneracy" in connecting $k \to k$, there is a similar one connecting $k \to p$. Indeed, if $p = L_{p,k}k$, then also $L_{p,k}L_{k,k}$ for any $L_{k,k} \in L_{\mathcal{L}}(k)$ identifies p,

$$(L_{p,k}L_{k,k})\, k = L_{p,k}\,(L_{k,k}k) = L_{p,k}k = p.$$

As discussed in Sec. (A.1.1) in general, each $p \in \mathrm{Orb}_{\mathcal{L}}(k)$ identifies uniquely a left coset $L_{p,k}L_{\mathcal{L}}(k) \in \mathcal{L}/L_{\mathcal{L}}(k)$ of the restricted Lorentz group with respect to $L_{\mathcal{L}}(k)$ with representative $L_{p,k}$. The restricted Lorentz group is decomposed into left cosets $L_{p,k}L_{\mathcal{L}}(k)$ represented by elements $L_{p,k}$ labelled by p varying in the orbit of the fixed k[7]. Moreover, given any $\Lambda \in \mathcal{L}$ and a coset representative $L_{p,k}$, the unique decomposition (A.1.3) reads

$$\Lambda L_{p,k} = L_{\Lambda p,k}L_{k,k} \tag{A.1.18}$$

or, in other words, $L^{-1}_{\Lambda p,k}\Lambda L_{p,k}$ belongs to the little group[8] $L_{\mathcal{L}}(k)$ and is called Wigner rotation.

Since little groups in the same orbit are isomorphic, these results are independent on the choice of the standard vector k in the same orbit. For a different orbit class, analogous considerations are valid. We obtain a different little group (see the table above) and partition the restricted Lorentz group in terms of cosets corresponding to this little group. For the trivial case of $p = (0,0,0,0)$, any element in $\mathcal{L}$ leaves the null vector unchanged and the little group is trivially $\mathcal{L}$ itself.

We finally note that these considerations apply also to $SL(2,\mathbb{C})$, the universal cover of the restricted Lorentz group. The orbit classification is unchanged and the little groups are the universal covers of the corresponding little groups for $\mathcal{L}$. For instance, $L_{SL(2,\mathbb{C})}\left(k = (m,\mathbf{0})^T\right) \cong SU(2)$.

[7]Note the analogy with the notation in (A.1.1), $i \longleftrightarrow p$ and $g_i \longleftrightarrow L_{p,k}$.

[8]Indeed, when applying $L^{-1}_{\Lambda p,k}\Lambda L_{p,k}$ on k we have $k \xrightarrow{L_{p,k}} p \xrightarrow{\Lambda} \Lambda p \xrightarrow{L_{k,\Lambda p}} k$.

Finite-dimensional representations Eq. (A.1.18) is the equation which is at the base of the induction method for generating infinite-dimensional representations of $\mathcal{L}$ from those of $L_G(k)$. Nevertheless, for $\mathcal{L}$ these turn out to be reducible and Eq. (A.1.18) will be used for the Poincaré group. For completeness, we state here instead that the finite-dimensional irreducible representations of the restricted Lorentz group, or more precisely of its double cover $SL(2,\mathbb{C})$, are identified by a pair of integers and semi-integers, $(j_1, j_2) \quad j_{1/2} = 0, \frac{1}{2}, 1, \frac{3}{2}, ...$ with dimension $(2j_1+1)(2j_2+1)$. This follows directly from the fact that the algebra Eq. (A.1.17) can be decomposed in two independent $SU(2)$ subalgebras. The finite-dimensional representations determine the transformation properties of the components of relativistic fields which live in the corresponding vector space. The lowest-dimensional representations and the related relativistic fields are listed in the following table.

Field	Representation	Dimension	Spin	Examples
Scalar	$(0,0)$	1	0	Pions, Higgs
Weyl left-handed spinor	$\left(\frac{1}{2},0\right)$	2	1/2	Neutrinos
Weyl right-handed spinor	$\left(0,\frac{1}{2}\right)$	2	1/2	Anti-neutrinos
Dirac	$\left(\frac{1}{2},0\right)\oplus\left(0,\frac{1}{2}\right)$	4	1/2	leptons, nucleons
Vector	$\left(\frac{1}{2},\frac{1}{2}\right)$	4	1	Gauge fields: $\gamma\, Z\, W^{\pm}\, g$
Rarita-Schwinger	$\left(1,\frac{1}{2}\right)$	6	3/2	
Spin 2 field	$(1,1)$	9	2	Graviton

A.1.4 The Poincaré group and its unitary irreducible representations

The Poincaré group (or the inhomogeneous Lorentz group) is the generalisation of the Lorentz group which includes translations. Formally it is the semidirect product $\mathbb{R}^{1,3} \rtimes O(1,3)$ of two of its subgroups, the abelian four-dimensional translation group and the Lorentz group. The elements of the Poincaré group are denoted by the couple $g = (a, \Lambda)$ where $a \in \mathbb{R}^4$ and Λ satisfies Eq. (A.1.12). The group law is defined by

$$(a_2, \Lambda_2)(a_1, \Lambda_1) = (\Lambda_2 a_1 + a_2, \Lambda_2 \Lambda_1) \tag{A.1.19}$$

with identity element $(0, \mathbb{1}_4)$ and inverse $(a,\Lambda)^{-1} = (-\Lambda^{-1}a, \Lambda^{-1})$. Each element can be written uniquely as $(a,\Lambda) = (a, \mathbb{1}_4)(0,\Lambda)$. The Poincaré group is the group of isometries on Minkowski space, i.e., the action on a four-vector $x = (x^0, \boldsymbol{x})$, given by $x \to x' = \Lambda x + a$, preserves distances $(x-y)^2$. The Lorentz group is the little group of the Poincaré group at the origin.

Just as the Lorentz group, the Poincaré group is not compact and is formed by the analogous four connected components. The component connected to the identity (with $\det\Lambda = 1, \Lambda^0{}_0 \geq 1$) is called the restricted Poincaré group and is denoted here by $\mathcal{P} = \mathbb{R}^{1,3} \rtimes \mathcal{L} = \mathbb{R}^{1,3} \rtimes SO^{\uparrow}(1,3)$. $\mathcal{P}$ is not simply-connected and has universal cover $\overline{\mathcal{P}} = \mathbb{R}^{1,3} \rtimes SL(2,\mathbb{C})$.

Elements of $\mathcal{P}$ can be expressed via its Lie algebra

$$(a, \Lambda(\omega)) = e^{ia_\mu P^\mu} e^{-\frac{i}{2}\omega_{\mu\nu}M^{\mu\nu}} \tag{A.1.20}$$

with

$$[P^\mu, P^\nu] = 0, \qquad [P^\mu, M^{\rho\sigma}] = i\left(\eta^{\mu\rho}P^\sigma - \eta^{\mu\sigma}P^\rho\right), \tag{A.1.21}$$

in addition to Eq. (A.1.15). The P^μ are the generators of the space-time translations. Similarly Eq. (A.1.16) generalises to

$$(a, \Lambda(\boldsymbol{\phi}, \boldsymbol{w})) = e^{ia_\mu P^\mu} e^{-i(\boldsymbol{\phi}\cdot\boldsymbol{J} + \boldsymbol{w}\cdot\boldsymbol{K})} \tag{A.1.22}$$

with algebra

$$\begin{array}{lll} [J^i, J^j] = i\epsilon^{ijk}J^k & [K^i, K^j] = -i\epsilon^{ijk}J^k & [J^i, K^j] = i\epsilon^{ijk}K^k \\ [J^i, P^j] = i\epsilon^{ijk}P^k & [K^i, P^j] = -i\delta^{ij}P^0 & [P^i, P^j] = 0 \\ [J^i, P^0] = 0 & [K^i, P^0] = -iP^i & [P^i, P^0] = 0 \end{array} \tag{A.1.23}$$

We also define the Pauli-Lyubanski vector

$$W_\mu(P) = \frac{1}{2}\epsilon_{\mu\nu\lambda\sigma}M^{\nu\lambda}P^\sigma, \tag{A.1.24}$$

which satisfies orthogonality and commutation with P^μ,

$$W_\mu(P)\,P^\mu = 0 \tag{A.1.25}$$

$$[W^\mu(P), P^\nu] = 0 \tag{A.1.26}$$

$$[W^\mu(P), W^\nu(P)] = i\epsilon^{\mu\nu\rho\sigma}W_\rho(P)\,P_\sigma \tag{A.1.27}$$

The quantities $P^2 = P_\mu P^\mu$ and $W^2 = W_\mu(P) W^\mu(P)$ are Casimir invariants for the Poincaré group. Moreover, for a four-vector $k \neq 0$, the independent components of $W_\mu(k)$ are the generators of the little group of $\mathcal{L}$ with respect to k,

$$L_{k,k}(b) = e^{-ib_c W^c(k)}. \tag{A.1.28}$$

This can be seen by expressing the condition $\Lambda k = k$ in terms of the generators in (A.1.14).

Unitary irreducible representations The non-compactness of the Poincaré group implies that its unitary irreducible representations have infinite dimensionality. We have mentioned at the end of Sec. (A.1.2) the important result that for this group all such representations can be obtained by induction from some subgroup. The construction and classification using the induction method was accomplished by Wigner [69]. We will follow the procedure outlined in Sec. (A.1.2) for the construction of the representations of the universal cover $\overline{\mathcal{P}} = \mathbb{R}^{1,3} \rtimes SL(2,\mathbb{C})$.

The first step is to identify a subgroup of $\overline{\mathcal{P}}$ and one of its representations. Given a standard vector $k = (k_0, \boldsymbol{k})$, this is chosen to be the group $H = \mathbb{R}^{1,3} \rtimes L_{\overline{\mathcal{L}}}(k)$, the semidirect product of translations with the little group of k with respect to $\overline{\mathcal{L}}$. Irreducible representations of this subgroup are known. For the translation group we select the (unidimensional) representation $e^{ia_\mu P^\mu}|k\rangle = e^{ia_\mu k^\mu}|k\rangle$; for the little group, we take any of its irreducible representations with label s and express it in terms of (A.1.28),

$$D^{(s)}(\Lambda_{k,k}) \equiv D^{(s)}(\Lambda_{k,k}(b)) = e^{-ib_c W^c(k)}, \tag{A.1.29}$$

where the $W^c(k)$ satisfy the k-dependent Lie algebra corresponding to Eq. (A.1.27). Then, for $(a, \Lambda_{k,k}) \in H$, the action of H on a vector space W_k (analogous to the $W \equiv W_1$ in Sec. (A.1.2)) is written as

$$|k,\sigma\rangle \to D_H(a,\Lambda_{k,k})|k,\psi\rangle = e^{ika} D^{(s)}(\Lambda_{k,k})|k,\psi\rangle = e^{ika}|k,\psi'\rangle. \tag{A.1.30}$$

The dimensionality of W_k is given by the the dimensionality of the irreducible representation $D^{(s)}$ of $L_{\overline{\mathcal{L}}}(k)$ considered.

The second step is to create copies of W_k, one for each left coset of $\overline{\mathcal{P}} = \mathbb{R}^{1,3} \rtimes SL(2,\mathbb{C})$ with respect to $H = \mathbb{R}^{1,3} \rtimes L_{\overline{\mathcal{L}}}(k)$. These are the same of those of the Lorentz group with

respect to $L_{\overline{\mathcal{L}}}(k)$[9], already discussed in Sec. (A.1.3), each represented by some $L_{p,k} \in \overline{\mathcal{L}}$ identified uniquely by a $p \in \mathrm{Orb}_{\overline{\mathcal{L}}}(k)$. For each p, we create a copy W_p of W_k and, according to Eqs. (A.1.11) and (A.1.18), the Poincaré group action $D_{\overline{\mathcal{P}}} \equiv U$ on W_p is given by the action of H on $W_{\Lambda p}$,

$$|p,\psi\rangle \to U(a,\Lambda)\,|p,\psi\rangle = e^{i(\Lambda p)a} D^{(s)}(\Lambda_{k,k})\,|\Lambda p,\psi\rangle = e^{i(\Lambda p)a}\,|\Lambda p,\psi'\rangle\,, \tag{A.1.31}$$

where $\Lambda_{k,k} = L^{-1}_{\Lambda p,k}\Lambda L_{p,k} \in L_{\overline{\mathcal{L}}}(k)$. If the representation $L_{\overline{\mathcal{L}}}(k)$ is irreducible, this construction identifies an irreducible representation of $\overline{\mathcal{P}}$ for each orbit and for each value of s. These are parametrised in terms of the eigenvalues of the Casimir operators W^2 and $P^2 = m^2\mathbb{1}$, and by the sign of p^0.

In particular, for orbits in class I with standard vector $k = (m, \mathbf{0})$, the Pauli-Lyubanski vectors in (A.1.29) become simply $W^0 = 0$ and $\boldsymbol{W} = m\boldsymbol{J}$ with algebra (A.1.27) that reduces to the algebra of $SU(2)$, reflecting the isomorphism $L_{\overline{\mathcal{L}}}(k) \cong SU(2)$. Then, the label $s \in \left\{0, \frac{1}{2}, 1, \frac{3}{2}...\right\}$ refers to the eigenvalues of $W^2 = -m^2J^2 = -m^2 s(s+1)$ and $\dim W_k = 2s+1$. We have an irreducible representation for each couple (m,s) on the full space $V_{(m,s)}$ on which a complete set of commuting operators $\{P^2, W^2, \boldsymbol{P}, \Sigma\}$ act,

$$\begin{aligned}
P^2\,|\,m\,s\,;\,p\,\sigma\,\rangle &= m^2\,|\,m\,s\,;\,p\,\sigma\,\rangle && \text{(A.1.32)}\\
W^2\,|\,m\,s\,;\,p\,\sigma\,\rangle &= -m^2 s(s+1)\,|\,m\,s\,;\,p\,\sigma\,\rangle && \text{(A.1.33)}\\
P_\mu\,|\,m\,s\,;\,p\,\sigma\,\rangle &= p_\mu\,|\,m\,s\,;\,p\,\sigma\,\rangle && \text{(A.1.34)}\\
\Sigma\,|\,m\,s\,;\,p\,\sigma\,\rangle &= \sigma\,|\,m\,s\,;\,p\,\sigma\,\rangle && \text{(A.1.35)}\\
U(a,\Lambda)\,|\,m\,s\,;\,p\,\sigma\,\rangle &= e^{i(\Lambda p)a}\sum_{\sigma'=-s}^{s} D^{(s)}_{\sigma'\sigma}\left(L^{-1}_{\Lambda p,k}\Lambda L_{p,k}\right)|\,m\,s\,;\,\Lambda p\,\sigma'\,\rangle && \text{(A.1.36)}
\end{aligned}$$

where $p^2 = m^2 > 0$ and $p^0 > 0$. The operator Σ with eigenvalues $\sigma = -s, ..., s$ is a P-dependent relativistic generalisation of the spin. It depends on the particular choice of the representatives of the cosets. In the so-called standard basis it reduces to $W_3/m = J_3$ in the $k = (m, \mathbf{0})$ subspace. In the helicity basis, $\Sigma = \frac{\boldsymbol{J}\cdot\boldsymbol{P}}{|\boldsymbol{P}|}$.

The expressions above constitute the foundations of relativistic quantum field theory. Using group theoretical arguments alone, and more precisely, investigating the consequences of the preservation of isometries of Minkowski space-time, a natural connection between special relativity and quantum mechanics is created. Indeed, a quantum mechanical interpretation

[9] $\overline{\mathcal{P}}/H = \mathbb{R}^{1,3} \rtimes SL(2,\mathbb{C})/\mathbb{R}^{1,3} \rtimes L_{\overline{\mathcal{L}}}(k) \equiv SL(2,\mathbb{C})/L_{\overline{\mathcal{L}}}(k)$

stems from the identification of the Hamiltonian with the P^0 generator of the Poincaré group with eigenvalue $E_{\boldsymbol{p}} = \sqrt{m^2 + |\boldsymbol{p}|^2}$ and from the definition of a scalar product

$$\begin{aligned} \langle\, m\, s\,;\, p\,\sigma \,|\, m\, s\,;\, p'\,\sigma'\,\rangle &= (2\pi)^4\, \delta^{(4)}\,(p - p')\, \delta_{\sigma\sigma'} && \text{(A.1.37)} \\ &\equiv 2E_{\boldsymbol{p}}\,(2\pi)^3\, \delta^{(3)}\,(\boldsymbol{p} - \boldsymbol{p}')\, \delta_{\sigma\sigma'}, && \text{(A.1.38)} \end{aligned}$$

which promotes $V_{(m,s)}$ to an Hilbert space. A relativistic particle interpretation is straightforward. The value $p^2 = m^2 > 0$ is identified with the mass of the particle and s is its spin. Using (A.1.38) we can write the general state of a particle with mass m and spin s, called a one-particle state,

$$|\psi\rangle = \sum_{\sigma=-s}^{s} \int \frac{d^3p}{(2\pi)^3\, 2E_{\boldsymbol{p}}} \psi_\sigma\,(\boldsymbol{p})\,|\, m\, s\,;\, \boldsymbol{p}\,\sigma\,\rangle\,, \qquad \text{(A.1.39)}$$

where $\psi_\sigma\,(\boldsymbol{p}) = \langle\, \boldsymbol{p}\,\sigma\,|\psi\rangle$ is the particle's (momentum) wave function. Massless particles appear also in this framework in a natural way, i.e. from the representations $s^{\pm} = 0, \frac{1}{2}^{\pm}, 1^{\pm}, ...$ of the Euclidean group $\overline{E}\,(2)$ identified with the spin s and a sign which refers to helicities $\pm s$. Other representations, e.g. those associated to the orbit class III (tachyonic), have no present physical interpretation.

The irreducible basis of $\overline{\mathcal{P}}$ provide, by tensor products, all possible scattering states which form a basis of the whole Hilbert space of any relativistic quantum theory.

A.2 Space-time discretisation

In this appendix the definition of a discretised space-time is given and the notation used throughout the thesis is settled.

Let us start by introducing a four-dimensional space-time box discretised such that, given a non-zero lattice spacing a with spacelike dimensions $[a] = -1$ and four numbers N_μ, $\mu = 1, 2, 3, 4$, we have the set of space-time points

$$\Lambda = \{\, x = (x_1, x_2, x_3, x_4) |\, x_\mu = n_\mu a\,,\; n_\mu = 0, ..., N_\mu - 1\}\,. \qquad \text{(A.2.1)}$$

A given lattice point is thus identified by four-dimensional integers:

$$x = (x_1, x_2, x_3, x_4) = (n_1 a, n_2 a, n_3 a, n_4 a) = (n_1, n_2, n_3, n_4)\, a = na. \qquad \text{(A.2.2)}$$

The lattice extent for all spatial directions is assumed to be the same, $N_1 = N_2 = N_3 \equiv N_L$,

while the time extent is denoted by $N_4 = N_T$. The physical dimensions of the box are $L = N_L a$ and $T = N_T a$, resulting in a volume $L^3 \times T$. Vector notation for space indices is also used:

$$x = (\boldsymbol{x}, t) = (\boldsymbol{n}a, n_t a) = (\boldsymbol{n}, n_t)\, a = na. \tag{A.2.3}$$

The range of n is such that $n_i = 0, ..., N_i \equiv N_L$ and $n_4 = 0, ..., N_4 \equiv N_T$. Elementary directions are identified by

$$\hat{1} = (a, 0, 0, 0)\,, \qquad \hat{2} = (0, a, 0, 0)\,, \qquad \hat{3} = (0, 0, a, 0)\,, \qquad \hat{4} = (0, 0, 0, a)\,,$$

such that

$$x = n_1\hat{1} + n_2\hat{2} + n_3\hat{3} + n_4\hat{4}. \tag{A.2.4}$$

All eight neighbouring points of x are reached by $x \pm \hat{\mu}$ as μ varies from one to four.

Functions can be defined on the lattice, $f(x) = f(na)$. If f has a canonical dimension of $a^{[f]}$, a dimensionless quantity can be introduced as $\hat{f}(n) = a^{-[f]} f(an)$.

Periodic boundary conditions are assumed, i.e., for a function f,

$$f(x + \hat{\mu} N_\mu) = f(x)\,. \tag{A.2.5}$$

For some functions the periodic boundary conditions are reserved only for spatial directions. Derivatives in the direction μ and Laplacians are defined by

$$\partial_\mu f(x) = \frac{f(x + \hat{\mu}) - f(x - \hat{\mu})}{2a}, \tag{A.2.6}$$

$$\Box f(x) = \sum_\mu \frac{f(x + \hat{\mu}) + f(x - \hat{\mu}) - 2f(x)}{a^2}. \tag{A.2.7}$$

Integrals in the continuum are replaced on the lattice by

$$\int d^4x f(x) \to a^4 \sum_x f(x) \equiv a^4 \sum_n f(na)\,. \tag{A.2.8}$$

Momentum space To the space-time set of points (A.2.2) and to the periodic boundary conditions (A.2.5) is associated the momentum space

$$\tilde{\Lambda} = \left\{ p = (p_1, p_2, p_3, p_4) \middle|\, p_\mu = \frac{2\pi}{aN_\mu} k_\mu\,,\ k_\mu = -\frac{N_\mu}{2} + 1, ..., 0, ..., \frac{N_\mu}{2} \right\}. \tag{A.2.9}$$

We can thus write

$$p = (p_1, p_2, p_3, p_4) = \left(\frac{2\pi}{L}k_1, \frac{2\pi}{L}k_2, \frac{2\pi}{L}k_3, \frac{2\pi}{T}k_4\right) \equiv (\boldsymbol{p}, k_4) = \left(\frac{2\pi}{L}\boldsymbol{k}, \frac{2\pi}{T}\right). \tag{A.2.10}$$

The momentum in direction μ increases by steps of $\frac{2\pi}{aN_\mu}$ and is limited in the region $-\frac{\pi}{a} + \frac{2\pi}{aN_\mu} \leq p_\mu \leq \frac{\pi}{a}$. The finite lattice spacing introduces a cutoff in momentum space. As a gets smaller and smaller, the distance between space-time points gets smaller (and so does the total volume) while the distance between momenta points gets larger and larger and the cutoff is extended. On the other hand, for fixed a and for increasing lattice extent $aN_\mu \to \infty$, spacetime becomes an infinite grid and momentum space becomes continuous but is still restricted in a box by the cutoff $\frac{\pi}{a}$.

On the 3d-lattice, the modulus of $\boldsymbol{k}$ assumes values $|\boldsymbol{k}| = \sqrt{k_1^2 + k_2^2 + k_3^2} = \sqrt{0}, \sqrt{1}, \sqrt{2}, ..., \sqrt{m}, ...$. There are $\theta_m = 1, 6, 12, 8, 6, 24, ...$ vectors for each $|\boldsymbol{k}| = \sqrt{m}$, θ_m being the Theta series of a simple cubic lattice.

Given a space-time point x and a four-momentum point p, the scalar product is dimensionless:

$$p \cdot x = (\boldsymbol{p}, p_4) \cdot (\boldsymbol{x}, x_4) = \boldsymbol{p} \cdot \boldsymbol{x} + p_4 x_4 = \frac{2\pi}{N_L}\boldsymbol{k} \cdot \boldsymbol{n} + \frac{2\pi}{N_T}k_4 n_4.$$

In particular, for $x = \hat{\mu}$:

$$p \cdot \hat{\mu} = p_\mu a. \tag{A.2.11}$$

From the Dirac delta identity in the continuum, the corresponding on the lattice is obtained,

$$\int d^3x e^{i\boldsymbol{p}\cdot\boldsymbol{x}} = (2\pi)^3 \delta^3(\boldsymbol{p}) \tag{A.2.12}$$

$$a^3 \sum_{\boldsymbol{x}} e^{i\boldsymbol{p}\cdot\boldsymbol{x}} = L^3 \delta^3_{\boldsymbol{p},\boldsymbol{0}} \tag{A.2.13}$$

Note that, while δ^3 carries the inverse of the dimension of its variable (cubed), the corresponding Kronecker delta is dimensionless. With (A.2.13), the 3D Fourier transform of a function f and its inverse can be defined for a given t

$$\tilde{f}(\boldsymbol{p}, t) = \alpha a^3 \sum_{\boldsymbol{x}} e^{-i\boldsymbol{p}\cdot\boldsymbol{x}} f(\boldsymbol{x}, t), \tag{A.2.14}$$

$$f(\boldsymbol{x}, t) = \frac{1}{\alpha}\frac{1}{L^3}\sum_{\boldsymbol{p}} e^{i\boldsymbol{p}\cdot\boldsymbol{x}} \tilde{f}(\boldsymbol{p}, t). \tag{A.2.15}$$

The value of α is arbitrary and will be set to one in this work. The analogous relation holds

for the 4-dimensional case with functions $f(x)$ and $\tilde{f}(p)$.

A.3 Evaluation of the $D_s \longleftrightarrow DK$ diagrams

In Sec. (3.2.3) the Wick contractions for the four entries of the correlator matrix (3.2.1) were performed, resulting in Eqs. (3.2.5), (3.2.6), (3.2.7) and (3.2.8). In this appendix, by means of the one-end trick, the correlators are expressed in terms of the stochastic propagators (3.2.14), (3.2.15) and (3.2.16) which are directly obtainable by numerical inversions on the computer. The derivation is based on the insertion of the spin-colour-time diluted stochastic sources Eq. (3.2.9) at time $t_0 = 0$ whose non-zero components satisfy

$$\frac{1}{N}\sum_{r=1}^{N}\eta^{r}(\boldsymbol{z})\,\eta^{r*}(\boldsymbol{x}) \approx \delta_{\boldsymbol{z},\boldsymbol{x}}. \tag{A.3.1}$$

In light of full spin-colour dilution, the stochastic sources at each space point are pure c-numbers. The advantage of diluting the spin is that the $\eta^{r}(\boldsymbol{z})$ can be moved at will in the traces, such that the resulting stochastic propagators Q (3.2.5) do not depend on the gamma matrices that appear at the vertices of the diagrams. This allows for extensive recycling of the Qs.

The following expressions rely on the γ_5-hermiticity of the propagators, on the cycle nature of the trace, as well as its additivity which allows to insert sums inside it:

$$\begin{aligned}
\mathrm{Tr}\left[A_1A_2A_3...A_n\right] &= \mathrm{Tr}\left[A_2A_3...A_nA_1\right] = \mathrm{Tr}\left[A_3...A_nA_1A_2\right] = ... && \text{(A.3.2)}\\
\sum_{i=1}^{n}\mathrm{Tr}\left[A_iB\right] &= \mathrm{Tr}\left[A_1B\right] + ... + \mathrm{Tr}\left[A_nB\right] = \mathrm{Tr}\left[A_1B + ... + A_nB\right] \\
&= \mathrm{Tr}\left[\left(A_1 + ... + A_n\right)B\right] = \mathrm{Tr}\left[\left(\sum_{i=1}^{n}A_i\right)B\right]. && \text{(A.3.3)}
\end{aligned}$$

The spacetime notation of Sec. (3.2.3) will be retained, i.e. $x_i = (\boldsymbol{x}_i, 0)$, $y_i = (\boldsymbol{y}_i, t)$, as well as $z_i = (\boldsymbol{z}_i, 0)$.

The most simple correlator is (3.2.5) and, inserting the Kronecker delta (A.3.1), we have

$$
\begin{aligned}
C_{D_s,D_s'}(t) &= a^6 \sum_{\boldsymbol{yx}} \mathrm{Tr}\left[A G^c(y;x)\, \tilde{A}' \gamma_5 G^{s\dagger}(y;x)\, \gamma_5 \right] \\
&= a^6 \sum_{\boldsymbol{yxz}} \mathrm{Tr}\left[\gamma_5 A G^c(y;x)\, \delta_{\boldsymbol{xz}} \tilde{A}' \gamma_5 G^{s\dagger}(y;z) \right] \\
&= \frac{a^6}{N} \sum_{r\boldsymbol{yxz}} \mathrm{Tr}\left[\gamma_5 A G^c(y;x)\, \eta^r(\boldsymbol{x})\, \eta^{r*}(\boldsymbol{z})\, \tilde{A}' \gamma_5 G^{s\dagger}(y;z) \right] \\
&= \frac{a^6}{N} \sum_{r\boldsymbol{y}} \mathrm{Tr}\left[\gamma_5 A \left(\sum_{\boldsymbol{x}} G^c(y;x)\, \eta^r(\boldsymbol{x}) \right) \tilde{A}' \gamma_5 \left(\sum_{\boldsymbol{z}} G^s(y;z)\, \eta^r(\boldsymbol{z}) \right)^{\dagger} \right] \\
&= \frac{a^6}{N} \sum_{r\boldsymbol{y}} \mathrm{Tr}\left[(\gamma_5 A)\, Q^c(y;\eta^r) \left(\tilde{A}' \gamma_5 \right) Q^{s\dagger}(y;\eta^r) \right].
\end{aligned}
$$

Although the $D_s - D_s$ correlator can be calculated by the traditional one-to-all propagators, for consistency and for better recycling of the propagators, also this correlator is treated stochastically.

The off-diagonal terms (3.2.6) and (3.2.7) are

$$
\begin{aligned}
C_{D_s,DK}(t) &= -2a^9 \sum_{\boldsymbol{y x}_K \boldsymbol{x}_D} \mathrm{Tr}\left[A G^c(y;x_D)\, \tilde{B} G^l(x_D;x_K)\, \tilde{B} \gamma_5 G^{s\dagger}(y;x_K)\, \gamma_5 \right] \\
&= -2a^9 \sum_{\boldsymbol{y x}_K \boldsymbol{x}_D \boldsymbol{z}_K} \mathrm{Tr}\left[\gamma_5 A G^c(y;x_D)\, \tilde{B} G^l(x_D;x_K)\, \delta_{\boldsymbol{x}_K \boldsymbol{z}_K} \tilde{B} \gamma_5 G^{s\dagger}(y;z_K) \right] \\
&= \frac{-2a^9}{N} \sum_{r\boldsymbol{y x}_K \boldsymbol{x}_D \boldsymbol{z}_K} \mathrm{Tr}\left[\gamma_5 A G^c(y;x_D)\, \tilde{B} G^l(x_D;x_K)\, \eta^r(\boldsymbol{x}_K)\, \eta^{r*}(\boldsymbol{z}_K)\, \tilde{B} \gamma_5 G^{s\dagger}(y;z_K) \right] \\
&= \frac{-2a^9}{N} \sum_{r\boldsymbol{y x}_D} \mathrm{Tr}\left[\gamma_5 A G^c(y;x_D)\, \tilde{B} \left(\sum_{\boldsymbol{x}_K} G^l(x_D;x_K)\, \eta^r(\boldsymbol{x}_K) \right) \tilde{B} \gamma_5 \left(\sum_{\boldsymbol{z}_K} G^s(y;z_K)\, \eta^r(\boldsymbol{z}_K) \right)^{\dagger} \right] \\
&= \frac{-2a^9}{N} \sum_{r\boldsymbol{y}} \mathrm{Tr}\left[\gamma_5 A \left\{ \sum_{\boldsymbol{x}_D} G^c(y;x_D)\, \tilde{B} Q^l(x_D;\eta^r) \right\} \tilde{B} \gamma_5 Q^{s\dagger}(y;\eta^r) \right] \\
&= \frac{-2a^9}{N} \sum_{r\boldsymbol{y}} \mathrm{Tr}\left[(\gamma_5 A)\, S^{cl}(y;\eta^r) \left(\tilde{B} \gamma_5 \right) Q^{s\dagger}(y;\eta^r) \right],
\end{aligned}
$$

$$
\begin{aligned}
C_{DK,D_s}(t) &= 2a^9 \sum_{\boldsymbol{y}_D \boldsymbol{y}_K \boldsymbol{x}} \mathrm{Tr}\left[BG^c(y_D;x)\,\tilde{A}\gamma_5 G^{s\dagger}(y_K;x)\,\gamma_5 B\gamma_5 G^{l\dagger}(y_D;y_K)\,\gamma_5 \right] \\
&= 2a^9 \sum_{\boldsymbol{y}_D \boldsymbol{y}_K \boldsymbol{x}\boldsymbol{z}} \mathrm{Tr}\left[\gamma_5 BG^c(y_D;x)\,\delta_{\boldsymbol{x},\boldsymbol{z}}\tilde{A}\gamma_5 G^{s\dagger}(y_K;z)\,\gamma_5 B\gamma_5 G^{l\dagger}(y_D;y_K) \right] \\
&= \frac{2a^9}{N} \sum_{r\boldsymbol{y}_D \boldsymbol{y}_K \boldsymbol{x}\boldsymbol{z}} \mathrm{Tr}\left[\gamma_5 BG^c(y_D;x)\,\eta^r(\boldsymbol{x})\,\eta^{r*}(\boldsymbol{z})\,\tilde{A}\gamma_5 G^{s\dagger}(y_K;z)\,\gamma_5 B\gamma_5 G^{l\dagger}(y_D;y_K) \right] \\
&= \frac{2a^9}{N} \sum_{r\boldsymbol{y}_D \boldsymbol{y}_K \boldsymbol{x}\boldsymbol{z}} \mathrm{Tr}\left[\gamma_5 BG^c(y_D;x)\,\eta^r(\boldsymbol{x})\,\tilde{A}\gamma_5 \left(G^l(y_D;y_K)\,\gamma_5 B^\dagger \gamma_5 G^s(y_K;z)\,\eta^r(\boldsymbol{z}) \right)^\dagger \right] \\
&= \frac{2a^9}{N} \sum_{r\boldsymbol{y}_D} \mathrm{Tr}\left[\gamma_5 B \left(\sum_{\boldsymbol{x}} G^c(y_D;x)\,\eta^r(\boldsymbol{x}) \right) \tilde{A}\gamma_5 \left(\sum_{\boldsymbol{y}_K} G^l(y_D;y_K)\,\gamma_5 B^\dagger \gamma_5 \sum_{\boldsymbol{z}} G^s(y_K;z)\,\eta^r(\boldsymbol{z}) \right)^\dagger \right] \\
&= \frac{2a^9}{N} \sum_{r\boldsymbol{y}_D} \mathrm{Tr}\left[\gamma_5 BQ^c(y_D;\eta^r)\,\tilde{A}\gamma_5 \left(\sum_{\boldsymbol{y}_K} G^l(y_D;y_K)\,\gamma_5 B^\dagger \gamma_5 Q^s(y_K;\eta^r) \right)^\dagger \right] \\
&= \frac{2a^9}{N} \sum_{r\boldsymbol{y}_D} \mathrm{Tr}\left[(\gamma_5 B)\,Q^c(y_D;\eta^r)\left(\tilde{A}\gamma_5\right) S^{ls\dagger}(y_D;\eta^r) \right].
\end{aligned}
$$

The $DK - DK$ entry has a disconnected and a box contribution with the following form,

$$
C_{DK,DK}(t) = 2C_D(t)\,C_K(t) - 4C_{box}(t).
$$

The $C_D(t)$ correlator is

$$
\begin{aligned}
C_D(t) &= a^6 \sum_{\boldsymbol{y}_D \boldsymbol{x}_D} \mathrm{Tr}\left[BG^c(y_D;x_D)\,\tilde{B}\gamma_5 G^{l\dagger}(y_D;x_D)\,\gamma_5 \right] \\
&= a^6 \sum_{\boldsymbol{y}_D \boldsymbol{x}_D \boldsymbol{z}_D} \mathrm{Tr}\left[\gamma_5 BG^c(y_D;x_D)\,\delta_{\boldsymbol{x}_D \boldsymbol{z}_D}\tilde{B}\gamma_5 G^{l\dagger}(y_D;z_D) \right] \\
&= \frac{a^6}{N} \sum_{r\boldsymbol{y}_D \boldsymbol{x}_D \boldsymbol{z}_D} \mathrm{Tr}\left[\gamma_5 BG^c(y_D;x_D)\,\eta_D^{rD}(\boldsymbol{x}_D)\,\eta_D^{rD*}(\boldsymbol{z}_D)\,\tilde{B}\gamma_5 G^{l\dagger}(y_D;z_D) \right] \\
&= \frac{a^6}{N} \sum_{r\boldsymbol{y}_D} \mathrm{Tr}\left[\gamma_5 B \left(\sum_{\boldsymbol{x}_D} G^c(y_D;x_D)\,\eta_D^{rD}(\boldsymbol{x}_D) \right) \tilde{B}\gamma_5 \left(\sum_{\boldsymbol{z}_D} G^l(y_D;z_D)\,\eta_D^{rD}(\boldsymbol{z}_D) \right)^\dagger \right] \\
&= \frac{a^6}{N} \sum_{r\boldsymbol{y}_D} \mathrm{Tr}\left[(\gamma_5 B)\,Q^c(y_D;\eta^r)\left(\tilde{B}\gamma_5\right) Q^{l\dagger}(y_D;\eta^r) \right].
\end{aligned}
$$

The kaon correlator is obtained by simply substituting $(c,l) \to (l,s)$:

$$
C_K(t) = \frac{a^6}{N} \sum_{r\boldsymbol{y}_K} \mathrm{Tr}\left[(\gamma_5 B)\,Q^l(y_K;\eta^r)\left(\tilde{B}\gamma_5\right) Q^{s\dagger}(y_K;\eta^r) \right].
$$

Please note that two different stochastic sources are required for the disconnected part, i.e., two separate sources η_D^r and η_K^r should be generated. Finally, the box diagram reads,

$$
\begin{aligned}
C_{box}(t) &= a^{12} \sum_{\boldsymbol{y}_D \boldsymbol{y}_K \boldsymbol{x}_D \boldsymbol{x}_K} \mathrm{Tr}\left[B G^c(y_D; x_D) \tilde{B} G^l(x_D; x_K) \tilde{B} \gamma_5 G^{s\dagger}(y_K; x_K) \gamma_5 B \gamma_5 G^{l\dagger}(y_D; y_K) \gamma_5 \right] \\
&= a^{12} \sum_{\boldsymbol{y}_D \boldsymbol{y}_K \boldsymbol{x}_D \boldsymbol{x}_K \boldsymbol{z}_K} \mathrm{Tr}\left[\gamma_5 B G^c(y_D; x_D) \tilde{B} G^l(x_D; x_K) \delta_{\boldsymbol{x}_K \boldsymbol{z}_K} \tilde{B} \gamma_5 G^{s\dagger}(y_K; z_K) \gamma_5 B \gamma_5 G^{l\dagger}(y_D; y_K) \right] \\
&= \frac{a^{12}}{N} \sum_{\boldsymbol{y}_D \boldsymbol{y}_K \boldsymbol{x}_D \boldsymbol{x}_K \boldsymbol{z}_K} \mathrm{Tr}\left[\gamma_5 B G^c(y_D; x_D) \tilde{B} G^l(x_D; x_K) \eta^r(\boldsymbol{x}_K) \eta^{r*}(\boldsymbol{z}_K) \tilde{B} \gamma_5 G^{s\dagger}(y_K; z_K) \gamma_5 B \gamma_5 G^{l\dagger}(y_D; y_K) \right] \\
&= \frac{a^{12}}{N} \sum_{\boldsymbol{y}_D \boldsymbol{y}_K \boldsymbol{x}_D \boldsymbol{x}_K \boldsymbol{z}_K} \mathrm{Tr}\left[\gamma_5 B G^c(y_D; x_D) \tilde{B} G^l(x_D; x_K) \eta^r(\boldsymbol{x}_K) \tilde{B} \gamma_5 \left(G^l(y_D; y_K) \gamma_5 B^\dagger \gamma_5 G^s(y_K; z_K) \eta^r(\boldsymbol{z}_K) \right)^\dagger \right] \\
&= \frac{a^{12}}{N} \sum_{r \boldsymbol{y}_D} \mathrm{Tr}\left[\gamma_5 B \left(\sum_{\boldsymbol{x}_D} G^c(y_D; x_D) \tilde{B} \left(\sum_{\boldsymbol{x}_K} G^l(x_D; x_K) \eta^r(\boldsymbol{x}_K) \right) \right) \right. \\
&\quad \left. \times \tilde{B} \gamma_5 \left(\sum_{\boldsymbol{y}_K} G^l(y_D; y_K) \gamma_5 B^\dagger \gamma_5 \left(\sum_{\boldsymbol{z}_K} G^s(y_K; z_K) \eta^r(\boldsymbol{z}_K) \right) \right)^\dagger \right] \\
&= \frac{a^{12}}{N} \sum_{r \boldsymbol{y}_D} \mathrm{Tr}\left[\gamma_5 B \left(\sum_{\boldsymbol{x}_D} G^c(y_D; x_D) \tilde{B} Q^l(x_D; \eta^r) \right) \tilde{B} \gamma_5 \left(\sum_{\boldsymbol{y}_K} G^l(y_D; y_K) \gamma_5 B^\dagger \gamma_5 Q^s(y_K; \eta^r) \right)^\dagger \right] \\
&= \frac{a^{12}}{N} \sum_{r \boldsymbol{y}_D} \mathrm{Tr}\left[(\gamma_5 B) S^{cl}(y; \eta^r) \left(\tilde{B} \gamma_5 \right) S^{ls\dagger}(y_D; \eta^r) \right].
\end{aligned}
$$

Bibliography

[1] P. Roman. *Introduction to quantum field theory*. Wiley, 1969.

[2] Novozhilov. *Introduction to elementary particle theory*. Oxford,New York: Pergamon Press, 1975. ISBN: 0-08-017954-1.

[3] Alan Martin. *Elementary particle theory*. Amsterdam: North-Holland Pub. Co, 1970. ISBN: 0720401577.

[4] Hugh Burkhardt. *Dispersion relation dynamics. A phenomenological introduction to S-matrix theory*. Amsterdam,London: North-Holland Pub. Co, 1969. ISBN: 0720401488.

[5] S. Weinberg. *The Quantum Theory of Fields*. The Quantum Theory of Fields 3 Volume Hardback Set v. 1. Cambridge University Press, 1995. ISBN: 9780521550017.

[6] T. W. B. Kibble. "Kinematics of General Scattering Processes and the Mandelstam Representation". In: *Phys. Rev.* 117 (4 Feb. 1960), pp. 1159–1162. DOI: 10.1103/PhysRev.117.1159. URL: https://link.aps.org/doi/10.1103/PhysRev.117.1159.

[7] C. Patrignani and Particle Data Group. "Review of Particle Physics". In: *Chinese Physics C* 40.10 (2016), p. 100001. URL: http://stacks.iop.org/1674-1137/40/i=10/a=100001.

[8] Geoffrey F. Chew and Stanley Mandelstam. "Theory of low-energy pion pion interactions". In: *Phys. Rev.* 119 (1960), pp. 467–477. DOI: 10.1103/PhysRev.119.467.

[9] J. A. Oller and E. Oset. "N/D". In: *Phys. Rev. D* 60 (7 Sept. 1999), p. 074023. DOI: 10.1103/PhysRevD.60.074023. URL: https://link.aps.org/doi/10.1103/PhysRevD.60.074023.

[10] J. A. Oller, E. Oset and J. R. Peláez. "Erratum: Meson-meson interactions in a nonperturbative chiral approach [Phys. Rev. D 59, 074001 (1999)]". In: *Phys. Rev. D* 75 (9 May 2007), p. 099903. DOI: 10.1103/PhysRevD.75.099903. URL: https://link.aps.org/doi/10.1103/PhysRevD.75.099903.

[11] J. A. Oller, E. Oset and J. R. Peláez. "Meson-meson interactions in a nonperturbative chiral approach". In: *Phys. Rev. D* 59 (7 Feb. 1999), p. 074001. DOI: 10.1103/PhysRevD.59.074001. URL: https://link.aps.org/doi/10.1103/PhysRevD.59.074001.

[12] D. Gamermann et al. "Couplings in coupled channels versus wave functions: Application to the $X(3872)$ resonance". In: *Phys. Rev. D* 81 (1 Jan. 2010), p. 014029. DOI: 10.1103/PhysRevD.81.014029. URL: https://link.aps.org/doi/10.1103/PhysRevD.81.014029.

[13] Tetsuo Hyodo. "Structure and compositeness of hadron resonances". In: *Int. J. Mod. Phys.* A28 (2013), p. 1330045. DOI: 10.1142/S0217751X13300457. arXiv: 1310.1176 [hep-ph].

[14] Steven Weinberg. "Evidence That the Deuteron Is Not an Elementary Particle". In: *Phys. Rev.* 137 (3B Feb. 1965), B672–B678. DOI: 10.1103/PhysRev.137.B672. URL: https://link.aps.org/doi/10.1103/PhysRev.137.B672.

[15] Kenneth G. Wilson. "Confinement of Quarks". In: *Phys. Rev.* D10 (1974). [,45(1974)], pp. 2445–2459. DOI: 10.1103/PhysRevD.10.2445.

[16] K. Symanzik. "Continuum Limit and Improved Action in Lattice Theories. 1. Principles and phi**4 Theory". In: *Nucl. Phys.* B226 (1983), pp. 187–204. DOI: 10.1016/0550-3213(83)90468-6.

[17] Rainer Sommer. "Non-perturbative QCD: Renormalization, O(a)-improvement and matching to Heavy Quark Effective Theory". In: *Workshop on Perspectives in Lattice QCD Nara, Japan, October 31-November 11, 2005*. 2006. arXiv: hep-lat/0611020 [hep-lat].

[18] Konrad Osterwalder and Robert Schrader. "Axioms for Euclidean Green's Functions. 2." In: *Commun. Math. Phys.* 42 (1975), p. 281. DOI: 10.1007/BF01608978.

[19] K Osterwalder and E Seiler. "Gauge field theories on a lattice". In: *Annals of Physics* 110.2 (1978), pp. 440–471. ISSN: 0003-4916. DOI: https://doi.org/10.1016/0003-4916(78)90039-8. URL: http://www.sciencedirect.com/science/article/pii/0003491678900398.

[20] M. LÃŒscher. "Construction of a selfadjoint, strictly positive transfer matrix for euclidean lattice gauge theories". In: *Comm. Math. Phys.* 54.3 (1977), pp. 283–292. URL: https://projecteuclid.org:443/euclid.cmp/1103900872.

[21] David C. Moore and George Tamminga Fleming. "Angular momentum on the lattice: The Case of non-zero linear momentum". In: *Phys. Rev.* D73 (2006). [Erratum: Phys. Rev.D74,079905(2006)], p. 014504. DOI: 10.1103/PhysRevD.73.014504,10.1103/PhysRevD.74.079905. arXiv: hep-lat/0507018 [hep-lat].

[22] S. Gusken. "A Study of smearing techniques for hadron correlation functions". In: *Nucl. Phys. Proc. Suppl.* 17 (1990), pp. 361–364. DOI: 10.1016/0920-5632(90)90273-W.

[23] M. Albanese et al. "Glueball Masses and String Tension in Lattice QCD". In: *Phys. Lett.* B192 (1987), pp. 163–169. DOI: 10.1016/0370-2693(87)91160-9.

[24] Shao-Jing Dong and Keh-Fei Liu. "Stochastic estimation with Z(2) noise". In: *Phys. Lett.* B328 (1994), pp. 130–136. DOI: 10.1016/0370-2693(94)90440-5. arXiv: hep-lat/9308015 [hep-lat].

[25] Shannon Bernardson, Paul McCarty and Chris Thron. "Monte Carlo methods for estimating linear combinations of inverse matrix entries in lattice QCD". In: *Computer Physics Communications* 78.3 (1994), pp. 256–264. ISSN: 0010-4655. DOI: https://doi.org/10.1016/0010-4655(94)90004-3. URL: http://www.sciencedirect.com/science/article/pii/0010465594900043.

[26] M. Foster and C. Michael. "Quark mass dependence of hadron masses from lattice QCD". In: *Phys. Rev. D* 59 (7 Feb. 1999), p. 074503. DOI: 10.1103/PhysRevD.59.074503. URL: https://link.aps.org/doi/10.1103/PhysRevD.59.074503.

[27] Martin Lüscher and Ulli Wolff. "How to calculate The elastic scattering matrix in two-dimensional quantum field theories by numerical simulation". In: *Nucl. Phys.* B339 (1990), pp. 222–252. DOI: 10.1016/0550-3213(90)90540-T.

[28] L. Maiani and M. Testa. "Final state interactions from Euclidean correlation functions". In: *Phys. Lett.* B245 (1990), pp. 585–590. DOI: 10.1016/0370-2693(90)90695-3.

[29] M. Luscher. "Volume Dependence of the Energy Spectrum in Massive Quantum Field Theories. 2. Scattering States". In: *Commun. Math. Phys.* 105 (1986), pp. 153–188. DOI: 10.1007/BF01211097.

[30] Martin Lüscher. "Two particle states on a torus and their relation to the scattering matrix". In: *Nucl. Phys.* B354 (1991), pp. 531–578. DOI: 10.1016/0550-3213(91)90366-6.

[31] Raul A. Briceno. "Two-particle multichannel systems in a finite volume with arbitrary spin". In: *Phys. Rev.* D89.7 (2014), p. 074507. DOI: 10.1103/PhysRevD.89.074507. arXiv: 1401.3312 [hep-lat].

[32] Raúl A. Briceño and Zohreh Davoudi. "Three-particle scattering amplitudes from a finite volume formalism". In: *Phys. Rev. D* 87 (9 May 2013), p. 094507. DOI: 10.1103/PhysRevD.87.094507. URL: https://link.aps.org/doi/10.1103/PhysRevD.87.094507.

[33] Maxwell T. Hansen and Stephen R. Sharpe. "Relativistic, model-independent, three-particle quantization condition". In: *Phys. Rev. D* 90 (11 Dec. 2014), p. 116003. DOI: 10.1103/PhysRevD.90.116003. URL: https://link.aps.org/doi/10.1103/PhysRevD.90.116003.

[34] Ulf-G. Meißner, Guillermo Ríos and Akaki Rusetsky. "Spectrum of Three-Body Bound States in a Finite Volume". In: *Phys. Rev. Lett.* 114 (9 Mar. 2015), p. 091602. DOI: 10.1103/PhysRevLett.114.091602. URL: https://link.aps.org/doi/10.1103/PhysRevLett.114.091602.

[35] M. Doring et al. "Unitarized Chiral Perturbation Theory in a finite volume: Scalar meson sector". In: *Eur. Phys. J.* A47 (2011), p. 139. DOI: 10.1140/epja/i2011-11139-7. arXiv: 1107.3988 [hep-lat].

[36] Gunnar S. Bali et al. "Masses and decay constants of the $D_{s0}^*(2317)$ and $D_{s1}(2460)$ from $N_f = 2$ lattice QCD close to the physical point". In: *Phys. Rev. D* 96 (7 Oct. 2017), p. 074501. DOI: 10.1103/PhysRevD.96.074501. URL: https://link.aps.org/doi/10.1103/PhysRevD.96.074501.

[37] B. Aubert et al. "Observation of a narrow meson decaying to $D_s^+\pi^0$ at a mass of 2.32-GeV/c^2". In: *Phys. Rev. Lett.* 90 (2003), p. 242001. DOI: 10.1103/PhysRevLett.90.242001. arXiv: hep-ex/0304021 [hep-ex].

[38] D. Besson et al. "Observation of a narrow resonance of mass 2.46-GeV/c**2 in the D*(s)+ pi0 final state, and confirmation of the D*(sJ)(2317)". In: *AIP Conf. Proc.* 698 (2004). [,497(2003)], pp. 497–502. DOI: 10.1063/1.1664286. arXiv: hep-ex/0305017 [hep-ex].

[39] Stephen Godfrey and Nathan Isgur. "Mesons in a relativized quark model with chromodynamics". In: *Phys. Rev. D* 32 (1 July 1985), pp. 189–231. DOI: 10.1103/PhysRevD.32.189. URL: https://link.aps.org/doi/10.1103/PhysRevD.32.189.

[40] Stephen Godfrey and Richard Kokoski. "Properties of P-wave mesons with one heavy quark". In: *Phys. Rev. D* 43 (5 Mar. 1991), pp. 1679–1687. DOI: 10.1103/PhysRevD.43.1679. URL: https://link.aps.org/doi/10.1103/PhysRevD.43.1679.

[41] Randy Lewis and R. M. Woloshyn. "S". In: *Phys. Rev. D* 62 (11 Nov. 2000), p. 114507. DOI: 10.1103/PhysRevD.62.114507. URL: https://link.aps.org/doi/10.1103/PhysRevD.62.114507.

[42] Joachim Hein et al. "Scaling of the B and D meson spectrum in lattice QCD". In: *Phys. Rev. D* 62 (7 Aug. 2000), p. 074503. DOI: 10.1103/PhysRevD.62.074503. URL: https://link.aps.org/doi/10.1103/PhysRevD.62.074503.

[43] Gunnar S. Bali. "$D_{\mathrm{sJ}}^{+}(2317)$:". In: *Phys. Rev. D* 68 (7 Oct. 2003), p. 071501. DOI: 10.1103/PhysRevD.68.071501. URL: https://link.aps.org/doi/10.1103/PhysRevD.68.071501.

[44] A Dougall et al. "The spectrum of Ds mesons from lattice QCD". In: *Physics Letters B* 569.1 (2003), pp. 41–44. ISSN: 0370-2693. DOI: https://doi.org/10.1016/j.physletb.2003.07.017. URL: http://www.sciencedirect.com/science/article/pii/S0370269303010372.

[45] H. Albrecht et al. "Observation of a New Charmed - Strange Meson". In: *Phys. Lett.* B230 (1989), p. 162. DOI: 10.1016/0370-2693(89)91672-9.

[46] Gunnar S. Bali et al. "Nucleon isovector couplings from $N_f = 2$ lattice QCD". In: *Phys. Rev. D* 91 (5 Mar. 2015), p. 054501. DOI: 10.1103/PhysRevD.91.054501. URL: https://link.aps.org/doi/10.1103/PhysRevD.91.054501.

[47] C. B. Lang et al. "D_s". In: *Phys. Rev. D* 90 (3 Aug. 2014), p. 034510. DOI: 10.1103/PhysRevD.90.034510. URL: https://link.aps.org/doi/10.1103/PhysRevD.90.034510.

[48] A. MartÃnez Torres et al. "Reanalysis of lattice QCD spectra leading to the $D_{s0}^{*}(2317)$ and $D_{s1}^{*}(2460)$". In: *JHEP* 05 (2015), p. 153. DOI: 10.1007/JHEP05(2015)153. arXiv: 1412.1706 [hep-lat].

[49] T. Yamazaki et al. "$I = 2\pi\pi$". In: *Phys. Rev. D* 70 (7 Oct. 2004), p. 074513. DOI: 10.1103/PhysRevD.70.074513. URL: https://link.aps.org/doi/10.1103/PhysRevD.70.074513.

[50] Li-Sheng Geng et al. "S". In: *Phys. Rev. D* 92 (1 July 2015), p. 014029. DOI: 10.1103/PhysRevD.92.014029. URL: https://link.aps.org/doi/10.1103/PhysRevD.92.014029.

[51] E. E. Kolomeitsev and M. F. M. Lutz. "On Heavy light meson resonances and chiral symmetry". In: *Phys. Lett.* B582 (2004), pp. 39–48. DOI: 10.1016/j.physletb.2003.10.118. arXiv: hep-ph/0307133 [hep-ph].

[52] Gunnar S. Bali et al. "Nucleon isovector couplings from $N_f = 2$ lattice QCD". In: *Phys. Rev. D* 91 (5 Mar. 2015), p. 054501. DOI: 10.1103/PhysRevD.91.054501. URL: https://link.aps.org/doi/10.1103/PhysRevD.91.054501.

[53] Miguel Albaladejo, Marina Nielsen and Eulogio Oset. "$D_{s0}^{*\pm}(2317)$ and KD scattering from B_s^0 decay". In: *Phys. Lett.* B746 (2015), pp. 305–310. DOI: 10.1016/j.physletb.2015.05.019. arXiv: 1501.03455 [hep-ph].

[54] L. Castillejo, R. H. Dalitz and F. J. Dyson. "Low's Scattering Equation for the Charged and Neutral Scalar Theories". In: *Phys. Rev.* 101 (1 Jan. 1956), pp. 453–458. DOI: 10.1103/PhysRev.101.453. URL: https://link.aps.org/doi/10.1103/PhysRev.101.453.

[55] Stefan Sint and Peter Weisz. "Further results on O(a) improved lattice QCD to one loop order of perturbation theory". In: *Nucl. Phys.* B502 (1997), pp. 251–268. DOI: 10.1016/S0550-3213(97)00372-6. arXiv: hep-lat/9704001 [hep-lat].

[56] Yusuke Taniguchi and Akira Ukawa. "Perturbative calculation of improvement coefficients to $O(g^2a)$ for bilinear quark operators in lattice QCD". In: *Phys. Rev. D* 58 (11 Oct. 1998), p. 114503. DOI: 10.1103/PhysRevD.58.114503. URL: https://link.aps.org/doi/10.1103/PhysRevD.58.114503.

[57] S. Capitani et al. "Renormalization and off-shell improvement in lattice perturbation theory". In: *Nucl. Phys.* B593 (2001), pp. 183–228. DOI: 10.1016/S0550-3213(00)00590-3. arXiv: hep-lat/0007004 [hep-lat].

[58] S. Aoki et al. "Review of lattice results concerning low-energy particle physics". In: *Eur. Phys. J.* C77.2 (2017), p. 112. DOI: 10.1140/epjc/s10052-016-4509-7. arXiv: 1607.00299 [hep-lat].

[59] Jochen Heitger et al. "Charm quark mass and D-meson decay constants from two-flavour lattice QCD". In: *PoS* LATTICE2013 (2014), p. 475. arXiv: 1312.7693 [hep-lat].

[60] G. Herdoiza, C. McNeile and C. Michael. "Decay constants of P-wave heavy-light mesons from unquenched lattice QCD". In: *Phys. Rev. D* 74 (1 July 2006), p. 014510. DOI: 10.1103/PhysRevD.74.014510. URL: https://link.aps.org/doi/10.1103/PhysRevD.74.014510.

[61] A. Gómez Nicola and J. R. Peláez. "Meson-meson scattering within one-loop chiral perturbation theory and its unitarization". In: *Phys. Rev. D* 65 (5 Jan. 2002), p. 054009. DOI: 10.1103/PhysRevD.65.054009. URL: https://link.aps.org/doi/10.1103/PhysRevD.65.054009.

[62] M. Gockeler et al. "Scattering phases for meson and baryon resonances on general moving-frame lattices". In: *Phys. Rev.* D86 (2012), p. 094513. DOI: 10.1103/PhysRevD.86.094513. arXiv: 1206.4141 [hep-lat].

[63] Gunnar S. Bali et al. "ρ and K^* resonances on the lattice at nearly physical quark masses and $N_f = 2$". In: *Phys. Rev.* D93.5 (2016), p. 054509. DOI: 10.1103/PhysRevD.93.054509. arXiv: 1512.08678 [hep-lat].

[64] J. R. Pelaez and G. Rios. "Chiral extrapolation of light resonances from one and two-loop unitarized Chiral Perturbation Theory versus lattice results". In: *Phys. Rev.* D82 (2010), p. 114002. DOI: 10.1103/PhysRevD.82.114002. arXiv: 1010.6008 [hep-ph].

[65] C. Hanhart, J. R. Pelaez and G. Rios. "Quark mass dependence of the rho and sigma from dispersion relations and Chiral Perturbation Theory". In: *Phys. Rev. Lett.* 100 (2008), p. 152001. DOI: 10.1103/PhysRevLett.100.152001. arXiv: 0801.2871 [hep-ph].

[66] B. Hu et al. "Two-flavor Simulations of the $\rho(770)$ and the Role of the $K\bar{K}$ Channel". In: *Phys. Rev. Lett.* 117.12 (2016), p. 122001. DOI: 10.1103/PhysRevLett.117.122001. arXiv: 1605.04823 [hep-lat].

[67] Constantia Alexandrou et al. "P". In: *Phys. Rev. D* 96 (3 Aug. 2017), p. 034525. DOI: 10.1103/PhysRevD.96.034525. URL: https://link.aps.org/doi/10.1103/PhysRevD.96.034525.

[68] Dehua Guo et al. "Rho resonance parameters from lattice QCD". In: *Phys. Rev. D* 94 (3 Aug. 2016), p. 034501. DOI: 10.1103/PhysRevD.94.034501. URL: https://link.aps.org/doi/10.1103/PhysRevD.94.034501.

[69] E. Wigner. “On Unitary Representations of the Inhomogeneous Lorentz Group”. In: *Annals of Mathematics* 40.1 (1939), pp. 149–204. ISSN: 0003486X. URL: http://www.jstor.org/stable/1968551.